Review Article

Viswanathan S. Saji*

Carbon nanostructure-based superhydrophobic surfaces and coatings

https://doi.org/10.1515/ntrev-2021-0039
received May 26, 2021; accepted June 8, 2021

Abstract: Research and development on superhydrophobic carbon nanostructures and their nanocomposites have high industrial significance. Here, a comprehensive review of the topic is provided. Reported works on superhydrophobic surfaces and coatings of carbon nanotubes, nanofibres, nanospheres/nanothorns/others, nanodiamond, fullerene and their various nanocomposites with metals, ceramics, and polymers are described. Superhydrophobic nanostructured carbon soot, graphitic carbon, and others are also presented. The section on superhydrophobic graphene is presented concisely at the end. Reports in different application areas, including anti-corrosion, anti-icing, oil separation, anti-biofouling, and sensors, are discussed separately. Superoleophobic and superamphiphobic surfaces are also discussed.

Keywords: carbon nanomaterial, superhydrophobic, carbon nanotube, graphene, anti-corrosion, oil separation

1 Introduction

Carbon nanostructures and their composites continued to attract colossal research attention, owing to their outstanding chemical, physical, mechanical, and electrical properties [1–3]. The discovery of fullerenes in 1985 (1996 Nobel Prize in Chemistry) [4], carbon nanotubes (CNTs) in 1993 [5,6], and graphene (GR) in 2004 (2010 Nobel Prize in Physics) [7,8] led to a mammoth increase of research outputs in this area. The most investigated candidates are CNTs and GR [2,3,9–13].

* **Corresponding author: Viswanathan S. Saji,** Interdisciplinary Research Center for Advanced Materials, King Fahd University of Petroleum & Minerals, Dhahran 31261, Saudi Arabia,
e-mail: saji.viswanathan@kfupm.edu.sa, tel: +966-13-860-1187, fax: +966-13-860-3996

The research realm of superhydrophobic (SHPC) surfaces (water contact angle [CA] > 150°) [14–18] has enticed substantial scientific curiosity owed to their impending real-world applications [19–21]. The extreme water repellency of SHPC surfaces is credited to the confined air layer at the surface/water interface [18–25]. Typically, the superhydrophobicity (SHPY) could be achieved *via* proper optimization of the surface roughness (micro/nano-hierarchical surface structuring) and the surface energy (low SE) [20,21,24]. Low sliding angle (SA < 5°) and contact angle hysteresis (CAH < 10°) deliver added self-cleaning properties [19–21,25]. Precise fundamentals of SHPY [19–21,26–32] and details of basic surface wettability theories [22,23,33–35] are described elsewhere.

Carbon nanomaterials (CNMs) are typically hydrophobic [10,11]. SEs of CNTs could be at the range of 27–45.3 mJ/m^2 [12]. SEs of chemically exfoliated GR and graphene oxide (GO) have shown to be 46.7 and 62.1 mJ/m^2, in that order, while that of normal graphite flake was ~54.8 mJ/m^2 [13]. The higher surface roughness, nano/micro-hierarchical surface structures (nanoscale CNMs and their microscale aggregates), surface reduction processes (removal of hydrophilic surface groups), additional low SE treatments all could boost the hydrophobicity.

A significantly higher number of reports are available on SHPC carbon nanostructure (CNS)-based surfaces and coatings. Hitherto, no comprehensive review is available on the topic. Most of the published reviews focused on GR. Chen *et al.* in 2013 [36] and Wang *et al.* in 2015 [37] reviewed SHPC GR. Gupta *et al.* reviewed various CNMs in oil separation application [38]. Liu *et al.* [39], Khan *et al.* [40], and Li *et al.* [41] provided good accounts of photo-reduced, chemical vapour deposited, and laser-structured GR, respectively. Jishnu *et al.* reviewed GR-based SHPC anti-corrosion coatings [42], whereas Sharma *et al.* provided a short account of CNT-based corrosion-resistant coatings [43]. Recent advances in laser-fabricated GR surfaces have been reviewed by Ma *et al.* [44]. A few recent reviews described SHPC CNSs as a part [10,45,46]. A considerably higher number of recent reports are available in this area. Hence, we made a systematic approach to comprehensively present the entire domain's available

information under one roof. Single and multicomponent (with metals, ceramics, and polymers) SHPC surfaces and coatings based on CNTs, carbon nanofibres (CNFs), carbon nanospheres/thorns/others, nanodiamonds, fullerenes, nanoscale carbon soot/graphitic carbon/others, as well as GR are presented. Due to the available reviews, detailed descriptions of GR-based materials were not attempted; however, the literature carefully covered and presented concisely. Four application areas, *viz.*, anti-corrosion, oil-separation, anti-icing, and anti-biofouling, are highlighted; other applications are briefly mentioned.

2 Carbon nanostructure-based superhydrophobic surfaces

Nearly 45% of the reports fall under GR, followed by CNTs (~32%) (Figure 1a). The most investigated application area is oil separation, and the second most is the anti-corrosion coatings (Figure 1b and c).

2.1 CNTs

SHPY was observed for both aligned and non-aligned CNT films, with and without an additional low SE component/modification. Typically, composite formation with polymers and ceramics help overcome the long-term durability issues of SHPC CNT surfaces [47–49].

2.1.1 Aligned carbon nanotube (ACNT) arrays

ACNTs have attracted significant research attention owing to their unique surface topography [50,51]. The surface roughness of vertically ACNTs (VACNTs) could be finely

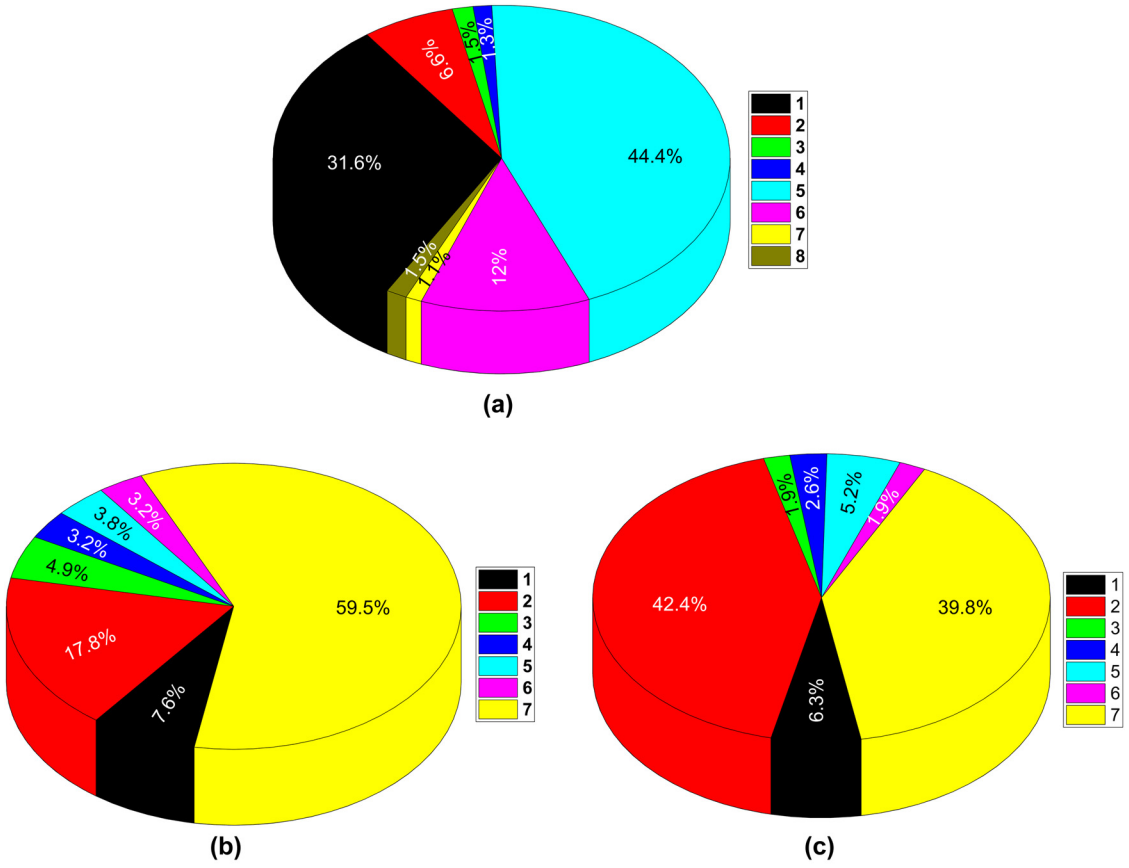

Figure 1: (a) Pie chart showing the extent of works reported with different CNS-based SHPC surfaces: (1) CNTs, (2) CNFs, (3) carbon nano/microspheres, (4) carbon nanothorn/onion/others, (5) GR, (6) nanoscale carbon soot/graphitic carbon/others, (7) nanodiamond, and (8) fullerene. (b and c) Pie charts on works reported on (b) CNTs and (c) GR in different applications: (1) anti-corrosion, (2) oil separation, (3) anti-icing, (4) biomedical/anti-biofouling, (5) sensor, (6) others, and (7) fabrication/mechanism (no specific application studies). Both single and multi-component (with metals/ceramics/polymers) SHPC surfaces considered. Works reported on SOPC and SAPC systems are also included (Source: SciFinder/Various sources).

tuned by adjusting their diameter and interspace distance [52–57]. Until 2006, the SHPY was reported for VACNTs only [58–62].

Chemical vapour deposition (CVD)-fabricated 3D anisotropic ACNT film on the patterned Si template (with quadrate pillar array) displayed both SHPY and superhydrophilicity (SHLY) at varying structural parameters of the template. The SHPY of the as-formed CNT arrays was attributed to the vertically aligned organization and the copious fraction of trapped air. The as-formed arrays with pillar space of 20, 15, 10, and 6 μm have shown CAs of ~22.1°, 142.9°, 25.5°, and 10°, respectively. The corresponding CAs of the surfaces after a vinyltrimethoxysilane modification were 21.2°, 153.3°, 27.2°, and 20.8° [63]. Lau *et al.* showed that a thin layer of polytetrafluoroethylene (PTFE) coating on VACNT forest could avoid the potential droplet seeping into the CNT's voids down to the microscopic level and created a stable SHPC surface with advancing and receding CAs of 170° and 160°, respectively. CVD was employed to deposit both the CNT array and the PTFE coating [52]. Wang *et al.* studied SHPY under dynamic conditions and observed that the droplet bounces off several times on an array with a CA of 163°, whereas for an array with a CA of 140°, the drop remained pinned [56]. For microfluidics applications, Qu *et al.* reported a variety of SHPC ordered CNT polyhedron structures with a CA of up to 162° *via* CVD (~850°C) inside the microchannels of patterned SiO_2 substrate, where the confined space was decisive in the realization of polyhedral structures with hexa/hepta/octagonal cross-sections. CNT's self-ordering and the high-temperature deposition yielded SHPY where no low SE treatment was used [64]. Lu *et al.* showed that micropatterning of MWCNTs enhances hydrophobicity. They employed a laser pruning technique to make SHPC parallel microwall arrays from VA-MWCNTs. The optimal SHPC surface consisted of micro-wall arrays with a width of ~13 μm and a channel width of ~50 μm [65]. Ramos *et al.* showed that CO_2 laser treatment could re-establish superhydrophilic (SHPL) VACNT surface to SHPC by decreasing the polar components (oxygen terminations on the surface) due to the high local heating rate. The microwave (MW) plasma CVD-deposited VACNT film was initially pretreated with oxygen plasma to convert to SHPL and then subjected to the laser treatment [66]. Lepore *et al.* compared SHPY of cabbage leaf and CVD-grown VACNT carpet and showed that cabbage-like morphologies could be helpful to achieve better SHPY for nanofluidic applications [67]. Hierarchical CNT assembly fabricated on a Si micro-pillar array displayed slippery SHPY (CA of ~155° and SA of ~5°) with excellent durability against water ingression. The corresponding CNTs grown on planar Si wafer lose the SHPY once exposed to tiny water droplets [68]. Aligned crystalline carboxyl-functionalized MWCNTs grown on SiC cellular skeleton (ceramic pillars with ~700 μm porous microchannels and ~250 μm diameter) by catalyst CVD displayed long-term stability against water-droplet ingression [69].

To enhance the surface durability against water-ingression and surface tension-assisted tie-up, *various surface treatments* for SHPC VACNT forests were investigated. In an earlier study, Journet *et al.* proposed a thiol modification for CVD-grown (planar Si substrate, 750°C) CNT forests. The surface first covered with a thin sputtered Au layer and subsequently, thiol-modified (CA ~ 164 ± 2°) [70]. Studies on liquid flow slippage over SHPC thiol-modified VACNT forests (CVD, microchannels) disclosed that the slip lengths varied linearly with the lateral roughness scale [71]. Santhagopalan *et al.* showed that a high-voltage electrophoretic deposited (EPD) and low SE PTFE-coated VACNT film displayed a CA of ~160° [72]. Jeong *et al.* employed a simple contact transfer micropatterning technique to fabricate VACNT micro-pillar arrays with different inter-pillar spacings extending from 45 to 160 μm (width ~65 μm) (Figure 2a–c). A thin hydrophobic CVD silicone layer coating was helpful to enhance the SHPC robustness, even under pressurized conditions. The CAs of the as-fabricated VACNT arrays (without silicon coating) displayed a steady decrease, whereas the CAs of silicone-coated arrays were stable regardless of the droplet volume (Figure 2d). The CAs of the VACNTs gradually increased with the increase of the inter-pillar spacing, reaching a maximum for 160 μm spaced sample (CA of 168 ± 0.3°, CAH of 2.64 ± 0.4°, and SA ~ 5°) [73]. Sojoudi *et al.* have shown that the top-gathering and elastocapillary densification of the porous CNTs could be prohibited by conformal deposition (CVD, 80°C) of an ultrathin film of poly(1*H*,1*H*,2*H*,2*H*-perfluorodecylacrylate) [74]. Yung *et al.* investigated CF_4 plasma modification on VACNTs using CVD (800°C) to fabricate ultra-low reflectance SHPC surface [75].

Aria and Gharib showed that SHPC CNT arrays could be made by exposing hydrophilic CNT arrays to a suitable *vacuum annealing* (*via* removal of oxygenated hydrophilic groups). Alternate vacuum pyrolysis and UV/ozone treatments allowed easy switching of ACNT arrays between SHPY and SHLY [76]. The authors in a later work studied droplet-impact dynamics of SHPC CNT arrays and revealed that no droplet pinning happened during a wide range of critical Weber number (W_n) [57]. Babu *et al.* showed that SHPC VACNTs could be fabricated *via* water-assisted CVD by a regrowth process (by a second-time catalyst-assisted

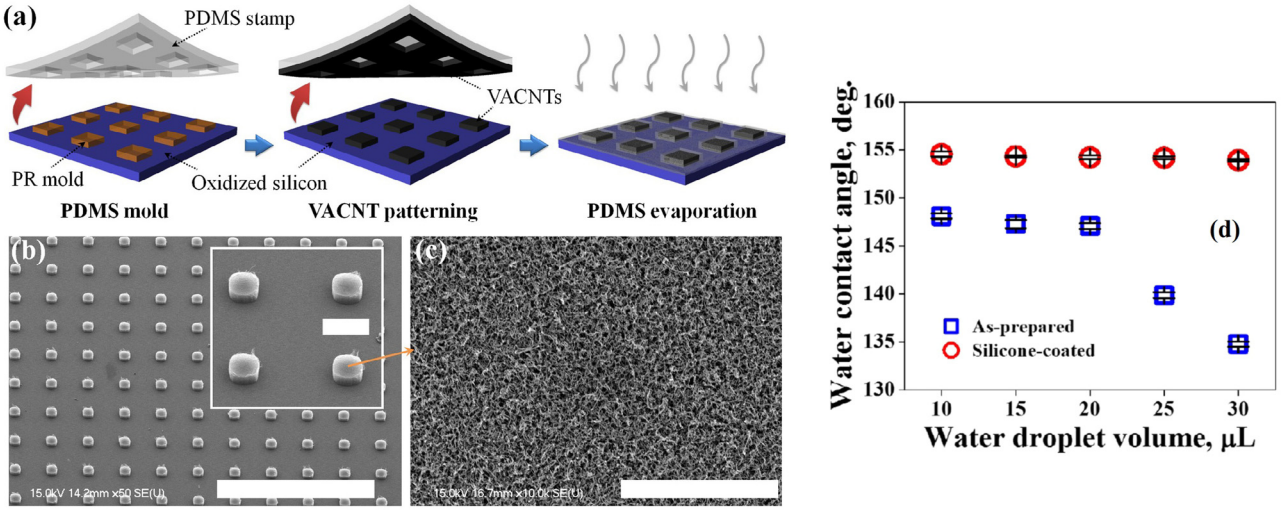

Figure 2: (a) Scheme showing fabrication steps of hierarchical VACNT SHPC surface. (b) SEM image of the CNT micro-pillar arrays. Scale bars correspond to 1 mm and 100 μm (inset). (c) Enlarged view of the pillar top. (d) CA variation with water-droplet volume [73]. Reproduced with permission from ref. [73]; © 2014 Elsevier Ltd.

deposition). The regrown CNTs displayed high CA (due to increased surface roughness); however, the CAH was ~60° (attributed to the surface hydrophilic groups). A subsequent vacuum annealing (350°C) or polydimethylsiloxane (PDMS) modification could further increase the CA with a significant CAH reduction (Figure 3). Both the high-temperature annealing and the low SE treatment were helpful to eliminate the hydrophilic groups [77]. Later, the authors confirmed a flat continuous reflecting air layer at the VACNT surface a few moments after submerging in water [78]. Hsiao *et al.* fabricated SHPC and self-cleaning CNT forest on a quartz surface by CVD at 850°C (CA ~ 154°). The lower CA (~115°) obtained for a higher temperature (950°C) processed sample was attributed to the widened outer tube diameters [79].

Several studies reported *composites of ACNTs with other CNSs*. Maziar *et al.* synthesized self-assembled ACNT/carbon-nanosphere hybrid film. Here, the ACNT array was first fabricated by CVD (800°C), and then amorphous carbon nanospheres were deposited by cathodic vacuum arc (negative substrate bias of 100 V). The wettability was closely related to the size of the deposited nanospheres. Increasing the deposition time increased the spheres' size, decreased the air gaps between the CNTs, and lowered the surface hydrophobicity [80]. SHPC CNT arrays capped with amorphous carbon NPs were fabricated by

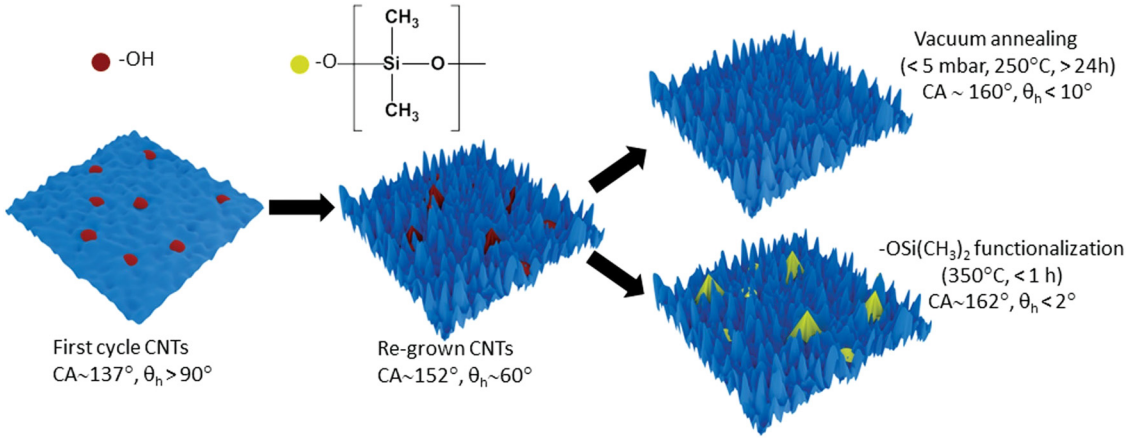

Figure 3: Schematic of the process. The regrowth CVD process increased the roughness of the CNT surface. Hydrophilic groups in the regrown CNTs are removed by either vacuum annealing or silane modification (θ_h corresponds to CAH) [77]. Reproduced with permission from ref. [77]; © 2014 WILEY-VCH Verlag GmbH & Co. KGaA, Weinheim.

plasma immersion ion implantation (PII, 800°C). The CA of unprocessed CNT forests was ~0°, whereas the nanocomposite displayed a CA of ~180°. The excellent SHPY was attributed to the unique overhang structure in which drops could penetrate only under a higher hydrostatic pressure [81]. Han *et al.* synthesized CNT forests (CVD, 800°C) and then processed them by Ar PII so that the graphitic sidewalls of CNTs were partly shattered and sphere-shaped amorphous carbon NPs were shaped on top. The surface displayed a CA of ~160° and an SA of ~5°. Their electrowetting studies explored slippery–sticky transformation with applied potentials [82].

Huang *et al.* demonstrated SHPC ZnO-coated CNTs (CA ~ 159°) where ZnO thin film was deposited (by cathodic vacuum arc) on CVD-made ACNTs. Contrary to the bare CNT surface, the coated surface showed no water ingression even after an extended period [83]. A report is available on room temperature EPD-made CNT-Ni and CNT-Zn. The study showed that CAs of the nanocomposite could be adjusted from 60° to >150° by altering the EPD voltage from 50 V to 250–550 V. The SHPY was attributed to the combined effect of the multi-scale roughness and the low SE attributed to the adsorbed hydrocarbon groups [84].

Most of these studies categorically showed that SHPC VACNT arrays suffer from long-term durability issues due to the potential water ingression. A subsequent low SE surface coating or a desirable composite formation could alleviate the shortcoming to the desired extent.

2.1.2 CNTs (non-aligned)

Randomly laid CNT films would deliver a more accessible and cost-effective method for developing SHPC coatings [62,85–193]. Many fabrication techniques, including CVD, vacuum filtration, spray coating, and drop coating, were reported. Typically, as-purchased pristine CNTs or low SE-modified CNTs are used.

Xu *et al.* reported SHPC non-aligned CNT coating (drop coated on glass) by using alkyl ($COOC_{18}H_{37}$)*n*)-modified MWCNTs. The CAs of alkyl-modified, carboxylic-functionalized, and as-purchased MWCNTs were 155° (SA > 5°), 63°, and 39°, respectively. The SHPY was attributed to the double-structured surface roughness and the low SE grafted alkyl chains [62]. Hong *et al.* prepared SHPC CNT powder by low-pressure NF_3 glow-discharge plasma. The fluorinated CNTs with very low SE (0.12 mJ/m^2) displayed CAs at the range of 153–158° for polyethylene glycol (PEG), glycerol, and water. The corresponding untreated CNT powder was SHPL (CA ~ 0°) [85,86]. SHPC MWCNTs were derived *via* a three-step procedure involving oxidation, cycloaddition, and silane modification. The study showed that incorporating fluorosilane-coated CNTs in polymers or textiles in small proportions could render them SHPC [119]. Hsieh *et al.* employed catalytic CVD to decorate CNTs on a carbon fabric. The resulted two-tier roughness along with a spin-coated perfluoroalkyl top coating yielded CA and CAH of 169.5° and 4.7°, respectively [120]. Zhang and Resasco demonstrated dramatic changes in hydrophobicity with different types of SWCNT films made on Si wafers, namely, random network (grass), vertically aligned (forest), and bundled (pillars). The CNT pillars prepared under optimized conditions exhibited the best SHPY with a CA of ~160°, which is attributed to the typical nano/microscale surface roughness [88].

Sunny *et al.* have grown CNTs on acid-etched steel by CVD (750°C), and subsequently, a thin layer of PDMS (0.5 g of Sylgard in 1 mL of xylene) was spin coated and dried at 70°C (to facilitate PDMS cross-linking). The coating improved the abrasion resistance of the surface while the SHPY and the conductivity were unaffected [127]. Li *et al.* described a highly flexible SHPC (CA of ~155°) carpet structure composed of long (~300 μm), roughly aligned, and pure cup-stacked CNTs synthesized by catalytic CVD at 850°C [89]. Wang *et al.* developed a one-step template-free CVD approach, and the fabricated CNT film effectively avoided the capillary-induced liquid spreading. The SHPC surface displayed excellent air exposure and chemical durability (Figure 4) [93]. Recently, Yin *et al.* made SHPC CNT film composed of short CNT strands *via* CVD at 700°C. The fraction of the water/air contact area was calculated to be 95.7%, demonstrating a significant extent of the air pocket existed. The surface showed excellent durability during 4 weeks of wettability test and superb chemical robustness over a wider pH range (0–14) [94]. A few earlier studies attempted CNT only-coatings on steel meshes by CVD [90,91].

Several works employed *vacuum filtering*. Wu *et al.* used a mixture of 0.1 g of MWCNTs with the desired amount of stearic acid (STA) in 80 mL of deionized water. The mixture was further diluted with water (5 mL diluted to 100 mL), CH_3COOH (1 mL) was added, vacuum filtrated, and dried (70°C) to obtain the SHPC MWCNT hybrid [95]. A film fabricated from octadecylamine (ODA) (~14%) functionalized MWCNTs by vacuum filtration (MWCNT–ODA dispersion was sieved through a filter paper, peeled off, and dried at 60°C) exhibited a CA of 165° and an electrical conductivity of 860 S/m [96]. Chen *et al.* reported MWCNT/SWCNT hybrid film with a CA of 152° and an SA of 2°. CVD-made MWCNTs were ultrasonically dispersed in EtOH (25 mg/mL) and vacuum

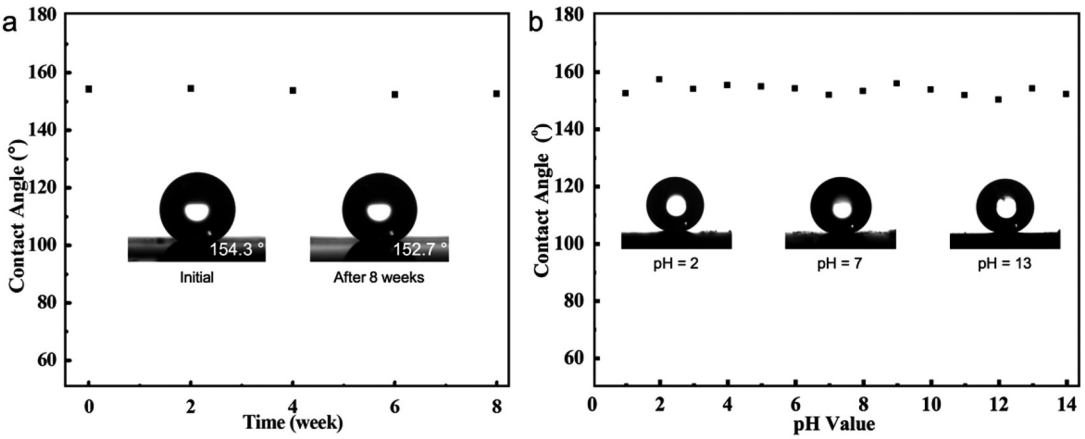

Figure 4: CAs of the SHPC CNT film during (a) air (~60% humidity) and (b) corrosive liquid exposure [93]. Reproduced with permission from ref. [93]; © 2017 American Chemical Society.

filtrated through an SWCNT film, dried at 80°C, and annealed at 700°C. The MWCNTs do not detach from the SWCNTs during bending or twisting studies, displaying a firm hybrid structure [97]. Su *et al.* reported layer-by-layer (LbL) SHPC CNT film by vacuum-assembling multilayer carboxylated/aminated MWCNTs, followed by transferring onto ethylene-vinyl acetate (EVA) copolymer and modifying with ODA [99]. An ultrathin nanocomposite was fabricated on polyethylene *via* LbL self-assembly of aminated-MWCNTs (nucleophilic) and polyacrylic acid (PAA) or Gantrez (electrophilic). Ionic assembly of aminated-MWCNT/PAA or covalent assembly of aminated-MWCNT/Gantrez resulted in SHPY. A five-times covalent LbL-deposited surface showed a CA of 165° and an SA of >5°, whereas the corresponding ionic LbL film resulted in CA ~ 155° with water pinning [98]. Kakade *et al.* reported electrowetting transition (from SHPC to hydrophilic) in MWCNTs buckypaper fabricated by ozonolysis and vacuum filtration [87].

Spray-coated SHPC CNTs were widely investigated. Yang *et al.* showed that simple spray-coated MWCNT film (as-purchased, 20 mg, dispersed in 10 mL of chloroform) on Cu displayed SHPY (CA ~ 155°, SA ~ 3.1°) without any chemical modification. SHPC–SHPL transition was also demonstrated *via* alternating UV irradiation and dark storage [100]. The authors in a later work showed that SHPC spray-coated film changed to SHPL after heating at 300°C, and the transition was attributed to the change of electronic structure of CNTs [101]. Li *et al.* also reported SHPC spray-coated CNT film without any low SE polymer coating (CA ~ 160° and SA ~ 3°). As-purchased CNTs (20 mg) dispersed in 10 mL of EtOH were used, and the coating was dried at room temperature. The reversible switchable transition between high and low water adhesion was presented by alternating heat treatment and UV illumination [102]. An extremely durable SHPC coating (CA 153.1 ± 2° and SA < 5°) was fabricated by spraying an aqueous dispersion of CNTs and perfluoroalkoxy resin [131]. Yoon *et al.* reported a two-step process where CNT solution was first spray coated on stainless steel (SS), and subsequently, a PTFE suspension (water-based, 60% w/w PTFE) was spin coated. A coating annealed at 360°C displayed a CA of 154.6 ± 6° [124]. Wang *et al.* reported spray-coated and pressure-proof flexible CNT/silane coating where PDMS and as-purchased MWCNTs were used. First, the substrate was spin coated with a solution of 0.1 g of PDMS and 0.01 g of curing agent in 10 mL of toluene or *n*-hexane. Subsequently, MWCNT/EtOH suspension was spray coated, and the surface heated at ~90°C and oven-cured at 150°C. The coated Al foil displayed high CAs even after subjecting to uniaxial pressing under 3.56–32 ksi pressure. The film displayed excellent chemical (pH 1–14) and aggressive-air-exposure (2 weeks) durability [103]. Zhu *et al.* fabricated SHPC coating by spraying MWCNT dispersion (0.2 g in 30 mL acetone + formic acid) followed by a subsequent fluorination step. The spray-coated sample was oven-dried (120°C) and placed in a sealed desiccator (having ~0.1 mL of fluorosilane) under vacuum for the surface fluorination. The study also showed that a thermal treatment (400°C) could retain the damaged (due to mechanical abrasion) SHPY. However, annealing above 400°C resulted in the loss of SHPY due to fluorosilane degradation [104]. Ogihara *et al.* demonstrated three types of dispersions, namely, CNT/EtOH, dodecyl-functionalized-CNT/EtOH, and CNT/trimethylsiloxysilicate (TMSS)/EtOH. With the unmodified CNTs, the aggregation due to π–π interaction

reduced the hydrophobicity, whereas the dodecyl functionalization screened the π–π interaction. The TMSS performed like glue, barred CNTs from aggregation, and lowered the required CNTs for the SHPY [105]. A hot/cold water-repelling superamphiphobic (SAPC) surface was fabricated by spray coating a suspension of MWCNTs, prepared *via* hydrolytic condensation of tetraethoxysilane (TEOS) and perfluorodecyltrichlorosilane (PFTS). The introduction of PFTS was beneficial for enhancing the coating's durability, whereas the TEOS addition was helpful to reduce the SE. Representative SEM images of the SAPC coating displayed a random cross-linked network structure with two-tier roughness composed of modified MWCNTs (Figure 5b–d). At 1 mg/mL of CNTs, the fluorosilane wrapped most of the CNTs resulting in lower surface roughness. As the concentration increased to 2 and 4 mg/mL, the fraction of exposed CNTs increased with an associated enhancement of micro/nanoscale roughness resulting in superior superamphiphobicity (SAPY) (Figure 5e). The wettability varied considerably with the CNT's diameter (Figure 5f) [106].

The authors also reported a transparent, hot liquid-repelling durable SAPC coating from a suspension of polysiloxane-modified MWCNTs in toluene, followed by calcination to form SiO_2 nanotubes (SNTs) and subsequent PFTS modification. The SNT/PFTS coating presented high chemical and mechanical durability during liquid immersion (in water, toluene, EtOH, and 1M HCl), UV light exposure, and water jetting tests [107]. Wang *et al.* reported spray-coated SHPC coating with enhanced wear resistance from an aqueous dispersion containing CNTs and PTFE. Thin film fabricated on Si (CA of 154.1 ± 2° and SA < 2°) retained the SHPY even after 500 times of abrasion test under 50 g/cm^2 [134]. Belsanti *et al.* fabricated SHPC film *via* spraying CNT suspension on Al alloy for anti-corrosion application [118]. A flexible, SHPC (CA of 165 ± 2°) and transparent (>70%) PDMS/CNT strain sensor was fabricated by spray coating CNT solution onto the PDMS nanowrinkle substrate [109].

Li *et al.* presented an approach to creating an SHPC surface from hierarchically combined polystyrene (PS) microspheres and CNTs. First, a monolayer of PS colloidal crystals was spin coated on a glass substrate and dried at 130°C; subsequently, Au layer was sputter coated, and the sample was dipped into 0.1 M mercaptoethylamine solution to facilitate linking of –COOH-terminated CNTs on the PS spheres (CNT solution was drop coated on the modified colloidal layer). The surface was then immersion coated with EtOH solution of 20 mM PFTS and dried at 120°C. The CA before and after the PFTS modification was ~33° and 165°, respectively. The CA decreased to 158° after 5 days of continuous immersion in water; however, no significant change was observed during long-term air exposure studies [110]. Meng and Park employed as-

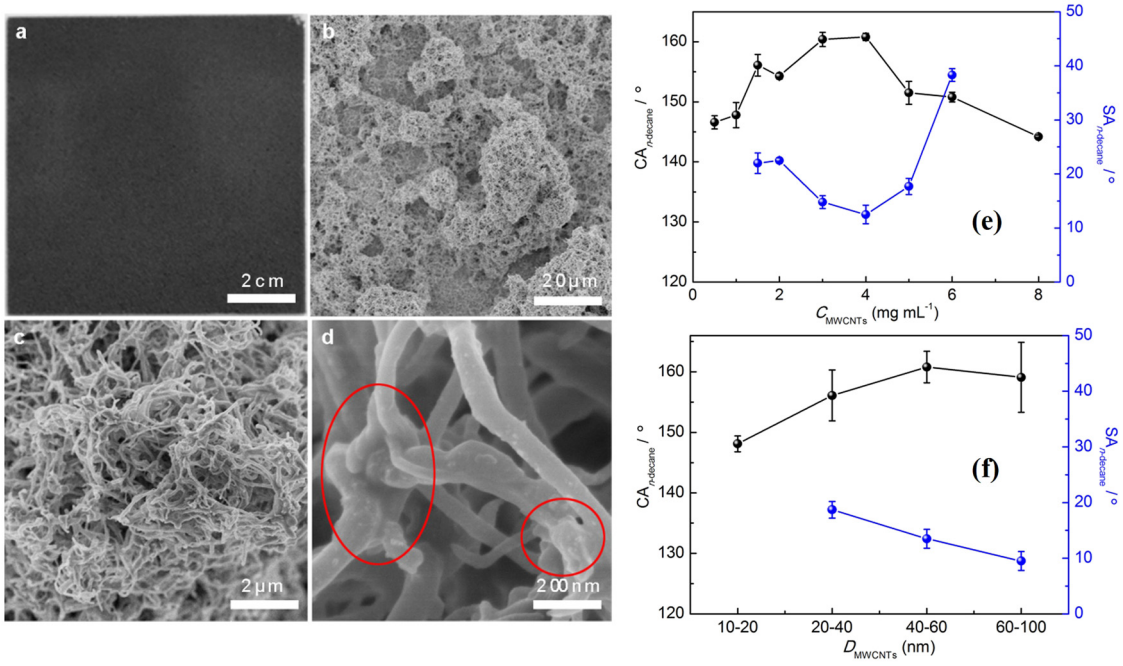

Figure 5: (a) Digital and (b–d) SEM images of the MWCNT-based composite SAPC coating. (e and f) CAs and SAs of *n*-decane on the spray-coated surface as a function of (e) concentration and (f) diameter of MWCNTs [106]. Reproduced with permission from ref. [106]; © 2017 Elsevier Inc.

purchased and functionalized MWCNTs (by refluxing in H_2O_2), which was first dispersed in $CHCl_3$ (0.5 mg/mL) and further mixed with a fluoropolymer (1 wt%), and *dip coated* on glass. A seven-time dip-coated film with 10:3 (v/v) MWCNT/fluoropolymer displayed the highest CA of 160.2°, along with 83.5% transmittance and 1.38 × 10^4 Ω/sq sheet resistance [121]. Dispersions of CNTs, GR, and carbon black (CB) in water/organic solvents were investigated as water-repellent agents for hydrophilic wood by simple drop/dip coating [114].

Several works made use of laser in getting patterned/transparent SHPC surfaces. Kinoshita *et al.* achieved SHPC/SHPL micropatterning on CNT film using a laser-assisted process where the areas exposed to hyperthermal F-atom and O-atom beams, respectively, became SHPC and SHPL [111]. To obtain high transparent SHPC patterned CNT clusters, femtosecond laser micro-machining was employed by Tang *et al.* [112].

Li *et al.* hot-pressed raw MWCNTs (1,500°C, 3 min, 30 MPa, vacuum, spark plasma sintering) and the polished sample was subsequently dipped into a commercial aqueous PTFE latex (1 s, ultrasonication) and heated at 310°C for 20 min. The bulk composite (CNTs, tiny PTFE particles, and air) having nanometre-scale grains showed CA >160°. The CA of the bare PTFE was ~114° [113].

Rajiv *et al.* reported long-term-durable SHPC MWCNT–CNF composite coatings on fibre-reinforced polymer (FRP) sheets. The supercritical fluid processing method was used to reduce the composite flaws and the CNT's aggregation. The composite layer displayed better SHPY (CA ~ 171.6° and SA ~ 2.7°) than a corresponding coating made by physical mixing (160° and 7.12°, respectively) [115].

2.1.3 As filler in organic coatings/composites with polymers

Several works employed CNTs as fillers in the polymer matrix to enhance mechanical durability. The incorporated CNTs could also provide the required hierarchical surface roughness for the SHPY. The CA and SA of the composite coating could be fine-tuned by regulating the aspect ratio or concentration of the CNTs. Their inclusion could also provide additional functionalities, such as conductivity, photothermal effect, EMI shielding, and self-cleaning.

2.1.3.1 With F/Si polymers

Other than the previous section's works, there are many reports on CNTs with F/Si polymers. Several works focused on *CNT–PDMS systems*. Zhang *et al.* reported an SHPC coating *via* spraying CNT/PDMS/toluene suspension, followed by curing at 120°C [133]. Caffrey and Gupta reported a method of fabricating electrically conductive SHPC coating with a micro-textured surface by adding CNT fillers to the PDMS matrix and duplicating the surface texture using a master. The surface displayed CA >160°, without any additional modification. A MWCNT loading of 4.4 wt% improved the conductivity by a factor $>10^{11}$ over the pure PDMS [129]. Park *et al.* have developed a conducting SHPC film with improved adhesion by using a zirco-aluminate coupling agent. Here, CNTs were first dispersed in $CHCl_3$ and then in triton-x surfactant. Subsequently, SiO_2 NPs (10 vol%) were added, dispersed, sonicated, and then PDMS and curing agents were added, sonicated, and the dispersion was used for spray coating. High CAs and low SAs were obtained until 25 vol% of CNTs [135]. An SHPC flexible film with a sandwich-like structure consisting of PDMS, MWCNTs, and a thermoplastic elastomer was fabricated by spray coating of the elastomer on the top side of the MWCNT sheet and PDMS modification on the bottom side. The top elastomer layer glued free MWCNTs together, the middle MWCNT layer formed a web-like conductive network, whereas the PDMS layer acted both as a glue and a low SE component. Maximum CA (169.4°) and minimum SA (2.7°) were obtained when the PDMS concentration was 1.5 wt%. The loss of SHPY at a PDMS concentration of >4 wt% was attributed to the thick coating formed and the buried MWCNTs [137]. Jung *et al.* proposed a highly reliable SHPC surface where CNTs were firmly immobilized on a PDMS/adhesive multilayer. The exposed CNTs at the lower surface of the layer helped to enhance the coating/substrate adhesion, whereas those exposed on the top surface contributed to SHPY. A CNT loading of 2.5 wt% was found to be essential for the SHPY. Tape tests showed that the SHPC surface was robust against adhesive material's induced damages. The surface well preserved the SHPY even at 300°C (Figure 6a). Until 200°C, the SA remained < 2°, while at 300°C, it becomes ~3.7°. The CA of the bare PDMS sheet (116° at 20°C) displayed an obvious decline with the rise of temperature (~100° at 300°C). Even at 10,000 kPa, the CA of the SHPC composite coating was reduced by ~8° only (Figure 6b). The surface also presented excellent durability during bending, adhesion, water jet, and chemical tests [139]. Han *et al.* fabricated SHPC surface on a flexible substrate *via* screen printing with a paste of PDMS–PEG copolymer and MWCNTs. Superior SHPY with >1,000 S/m of conductivity was attained at 25 wt% of PDMS–PEG [143].

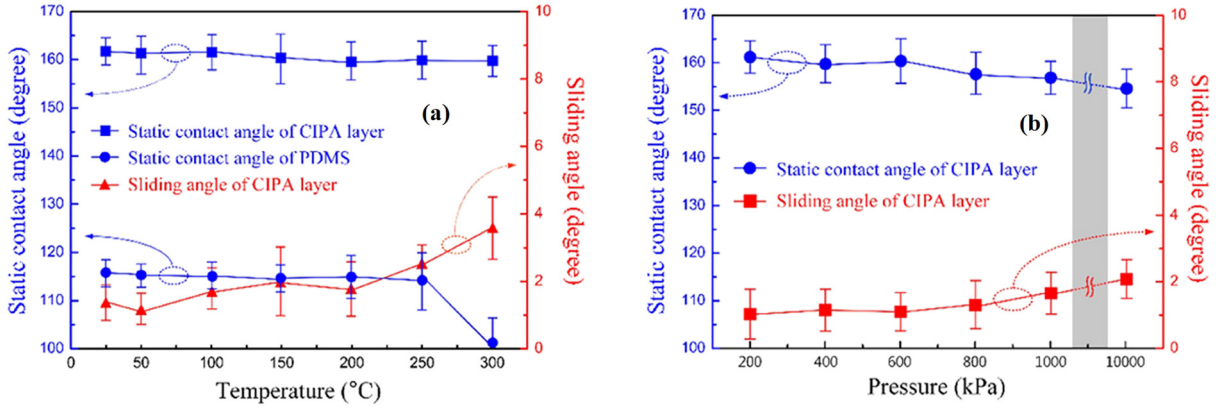

Figure 6: Stability test results of CNT-incorporated PDMS/adhesive (CIPA) layer with (a) heat and (b) pressure [139]. Reproduced with permission from ref. [139] (https://pubs.acs.org/doi/10.1021/acsomega.7b01872); © 2018 American Chemical Society. For further permissions related to the material excerpted should be directed to the ACS.

Highly conductive nanocomposite coatings of fluoropolymer dispersion with CB, CNTs, or GR nanofillers were studied. At 50 wt% of CNTs or CB, the SHPC surface resisted water-drop impalement at 3.7 m/s. GR-based surface displayed the most inferior dynamic impact resistance; however, the best conductive one [138]. Bayer *et al.* fabricated electrically conducting SHPC polymer–CNT coating *via* an emulsion-based spray process. The emulsion was composed of fluoro-acrylic latex solution (capstone ST-100), toluene-MWCNTs, and MtOH. The spray-coated film was cured at a temperature above the melting point of the fluoro-acrylic latex (>160°C) to yield the SHPY (CA >165°, SA < 5°). However, increasing the CNT loading beyond 17 wt% caused coating flaking and poor substrate adhesion [132]. Zhang *et al.* described highly transparent SAPC coating by CVD of PFTS onto SNTs. MWCNTs were employed as the template, and the SNTs were made *via* hydrolytic condensation of silanes followed by calcination. The fabrication steps include preparation of polysiloxane-modified MWCNT suspension, spray coating, and preparation of SNTs and SNTs/PFTS. The SAPY and the film transparency were highly dependent on the solvents used; *n*-octane was optimal [136]. Wu *et al.* fabricated MWCNT–PVDF hybrids through a facile phase-separation method. PVDF crystallization was almost unaffected with the extent of MWCNT loading, and the β-phase crystals dominated the process. The neat PVDF exhibited a CA of ~144°, whereas the hybrids with 8 and 16 wt% of MWCNTs displayed CAs of 163° and 166°, respectively [130]. An SHPC GR/POSS/MWCNT hybrid coating prepared by a two-step casting process on a glass substrate displayed a CA of 155° without compromising the conductivity. MWCNT/POSS was coated on the GO/THF layer, and thermally treated at 200°C [125]. Core–shell-structured polyaniline (PANI)/CNT composite, SiO_2 NPs, and 1*H*,1*H*,2*H*,2*H*-perfluorooctyltriethoxysilane (PFOS) were integrated synergistically into the ethylene tetrafluoroethylene (ETFE) matrix. Here, ETFE powder (1 g in 30 mL ethyl acetate), SiO_2 (0.05 g), and PFOS (0.2 g) were ultrasonicated with a selected amount of PANI/CNTs and the well-dispersed solution was used for the spray coating, followed by curing at 300°C. A composite layer made from 6 wt% of PANI/CNTs revealed superior SAPC property, with CAs of 159°, 163°, and 167° for ethylene glycol, glycerol, and water, respectively (with SAs < 5°). However, at concentrations >6 wt%, surface cracks were evident. The optimum coating demonstrated durable SHPY with droplets of a wider pH range (1–14) and thermal stability at temperatures <400°C. SAPY was preserved even after 30 times bending test or 45,000 times of abrasion. Direct immersion studies in aggressive HCl (1 mol/L, 60 days) and NaCl (3.5 wt%, 90 days) revealed excellent chemical durability [128].

A CNT–organic silicone resin (SiR) composite displayed outstanding mechanical robustness and hot water repellency. The wettability variation was closely dependent on the CNT concentration. Coating with 15 wt% or more CNTs repelled hot water effectively (Figure 7a). The coating displayed excellent mechanical durability during the abrasion test (Figure 7b) and waterfall/jet testing (Figure 7c and d) [140]. Cold-curable silicone sealant was used along with MWCNTs. Here, the required amount of silicone matrix was added into a dispersion of CNTs in hexane and that was used for spray coating. The CA monotonically increased with the increase of CNT content in the polymer matrix, reaching 158.4° for 50 wt% loading [141]. Lv *et al.* prepared robust and F-free SHPC coating from polyphenylene sulphide (PPS)–SiR composite. The SiR also acted as the low SE component, whereas the

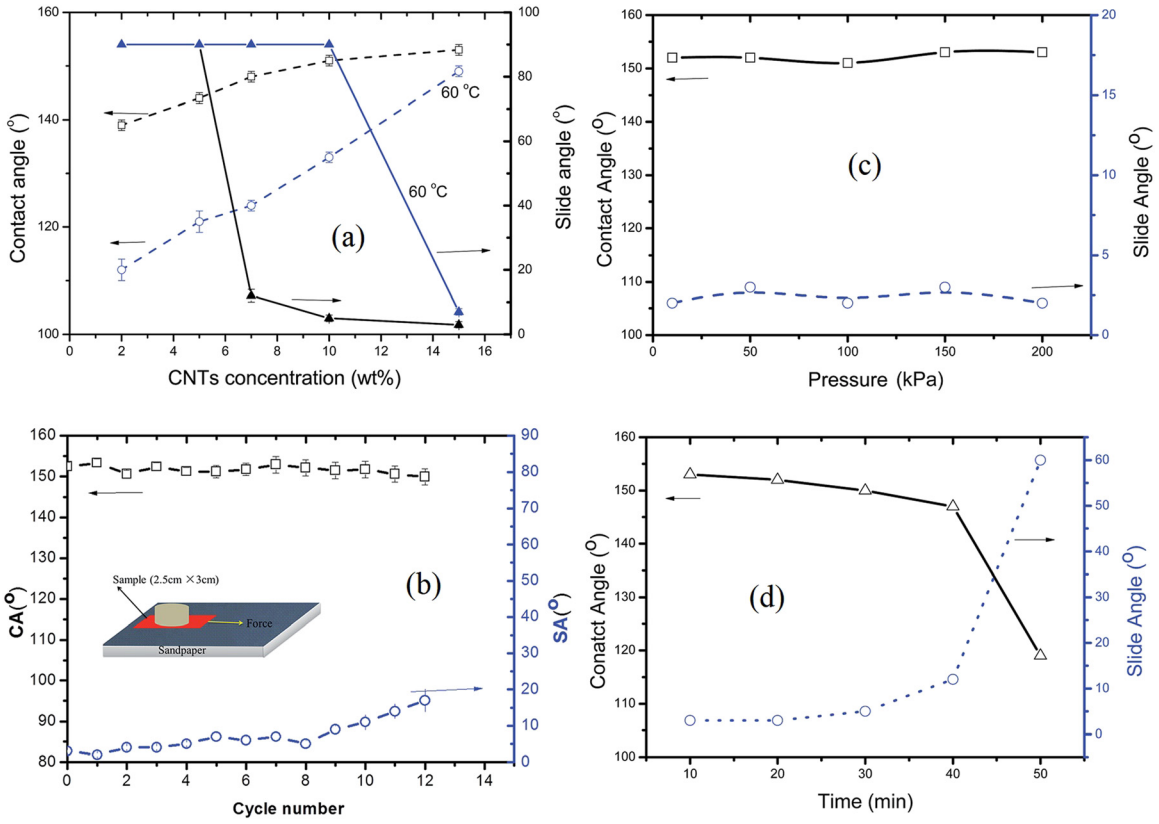

Figure 7: Variation of CAs and SAs of resin-coated samples with (a) concentration of CNTs, (b) abrasion cycles, (c) water pressure, and (d) duration of water-jet test under 200 kPa [140]. Reproduced with permission from ref. [140]; © 2015 The Royal Society of Chemistry.

reinforced fillers (CNTs or GR) provided the required hierarchical surface structure; a silane-coupling agent was also employed. The sprayed and heat-treated (320°C) coating exhibited a CA of ~161° and an SA of 2°. The wettability varied both as a function of SiR and CNT content, and the optimized coating was composed of 10 wt% of SiR and 1 wt% of CNTs. The evenly distributed CNTs with self-lubricating properties were helpful to reduce the abrasion loss significantly. After 2,500 times of friction (1,000 sandpaper, 500 g, 37.5 circles/min), the sample continued to be SHPC with a CA of 150 ± 2°. After 5,000 cycles, the CA becomes ~139°. Compared with the PPS coating (0.2106 g), the SHPC coating's weight loss (0.063 g) considerably decreased [142].

Song *et al.* reported nano-hybrid membrane based on chitosan (as the matrix), cationic chitosan (chitosan-modified by a triazine derivative), MWCNTs, and a silicon coupling agent, which was further modified by low SE perfluorooctanesulphonyl fluoride. The membrane with 3 wt% MWCNTs showed excellent SHPY [144]. Wang *et al.* fabricated nanofibre composite membrane of CNTs and PVDF-*co*-hexafluoropropylene (PVDF-HFP) using electrospinning and pressure-driven filtration processes. After a low SE fluorosilane modification (by CVD), the CNT/PVDF–HFP membrane displayed SHPC and superoleophilic (SOPL) properties [145]. SHPC and SOPL porous CNTs/PVDF composite was prepared *via* gel formation and freeze drying. The study proved that even a small amount of CNTs could considerably enhance the porosity and surface roughness of PVDF [146]. Kousalya *et al.* made a mixed wetting surface with interchanging parallel SHPC/SHPL bands through graphitic petal-decorated CNT coatings *via* PTFE deposition, shadow mask, and oxygen plasma treatment [147].

Wettability transitions in a spray-coated coating of polyfluo 150 wax and fluorocarbon-modified MWCNTs (1:4 wt ratio, acetone–ethyl acetate solvent) were studied as a function of temperature. SHPY was attained at 150, 200, and 360°C, whereas SHLY resulted at 300°C. The variation was associated with the melting/decomposition of the wax and the related phase separation [122]. Rungraeng *et al.* revealed a slippery liquid infused porous surface consisting of SHPC MWCNT–PTFE layer filled with a low surface tension liquid. Water, honey, ketchup, oil, and bacterial biofilms freely slipped off the surface without leaving any apparent wreckage [148].

Peng *et al.*, in earlier work, reported a way for transforming common polymers into SHPC conductive surface by simple pressing of a layer of MWCNTs on a polymer melt (Figure 8). Under appropriate conditions, the CNTs were partly inserted inside and partly exposed outside the coatings' surface, creating a carpet-like structure, providing both SHPY and conductivity [126].

2.1.3.2 With polyurethane/epoxy/PS

Several studies explored CNTs as filler/hydrophobicity promoter with polyurethane (PU), epoxy (EP), and PS resins. Hejazi *et al.* described a single-step pressing method to fabricate SHPC, self-cleaning, and mechanically durable *PU/CNT* composite. After placing the PU sheet into a pre-designed mould, 15 mg of CNT powder (~2 vol%) was distributed, and the surface was pressed under 4 MPa for 10 min and heated to 180°C. The pressing time had a significant effect on the type of SHPC surface. A longer processing time (60 min) resulted in sticky SHPY [149]. A report on spray-coated SAPC coating used fluorinated MWCNTs as a nanoroughness promoter and fluorinated PU as a low SE binder and acetone/toluene cosolvents [150]. Reports on PU-CNT-based aerogels/sponges are described in Section 2.1.5.

Besides SHPY, the CNT fillers in the *EP matrix* could help to overcome their inherent brittleness and poor wear resistance. The high mechanical strength and abrasion resistance of a spray-coated CNT–EP composite were attributed to the even dissemination and strong bonding of CNTs on the EP resin. The suspension for the spray coating was prepared by adding EP resin (200 mg) to a dispersion of CNTs (200 mg) in acetone (100 mL). A subsequent curing step at 120°C facilitated melting and ingression of EP resin to CNT/substrate interface and ensured coating with exposed CNTs (CA ~ 166° and CAH ~ 4°) [151]. Hsu *et al.* reported amphiphilic polyamine-modified CNT/EP SHPC film by using a dispersion of as-purchased CNTs (0.05 g), polyisobutylene-amine copolymer (PB-amine, 0.1 g), THF, and EP resin (0.071 mmol, 0.025 g). The SHPY (CA > 152° and CAH ~ 7°) of the drop coated and cured (80–150°C) surface was primarily attributed to the well-ordered orientation of CNTs. The CA augmented to ~158° at an optimized PB-amine/CNT wt ratio of 1/2; however, it declined with a further increase of PB-amine content (Figure 9a). The corresponding variation of sheet resistance is also shown (Figure 9a). Their time-dependent CA variation studies displayed excellent durability for PB-amine/CNT and PB-amine/CNT/EP coatings. On the other hand, the pristine CNT film failed within 1 h (Figure 9b) [152]. A robust SAPC EP/PVDF/FEP spray coating with incorporated CNTs and SiO_2 (2.5 wt% each) was reported. The synergistic combination of SiO_2 and CNTs was utilized to create the required multilayer structure. Fluorinated ethylene propylene (FEP, 17.8–18.8 mJ/m^2) was employed to reduce the SE [153]. The authors also reported an SAPC and electroactive bilayer

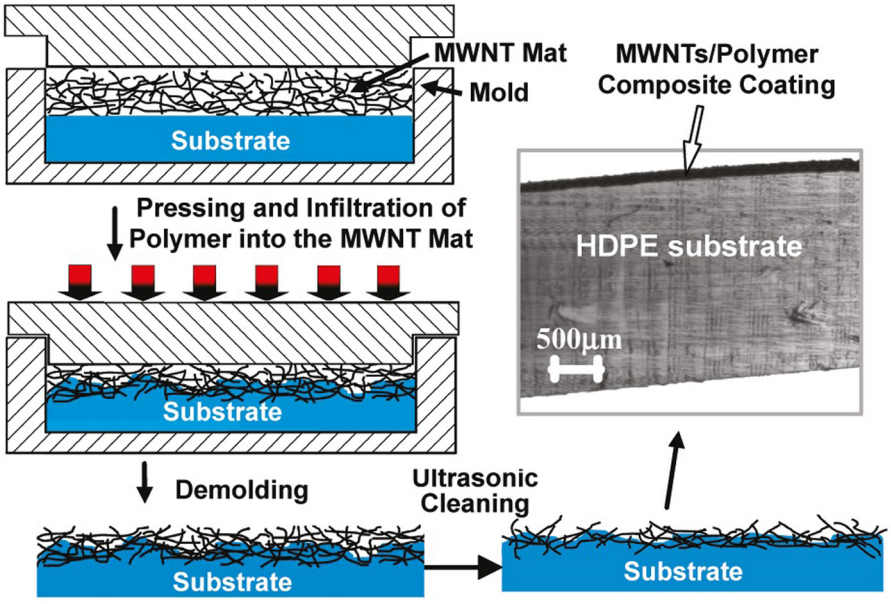

Figure 8: Scheme showing fabrication of SHPC and conductive MWCNTs/polymer composite coating. An optical image of the coated sample is also shown [126]. Reproduced with permission from ref. [126]; © 2010 American Chemical Society.

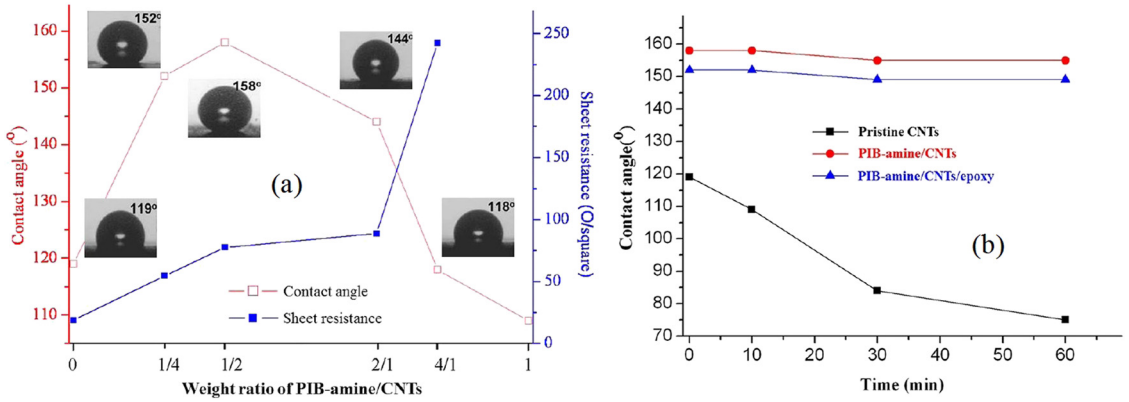

Figure 9: (a) Variation of sheet resistance and CA as a function of PB-amine/CNT weight ratio. (b) Time-dependent CA variation in water [152]. Reproduced with permission from ref. [152]; © 2013 American Chemical Society.

composite coating by integrating EP, PANI, FEP, SiO_2, and CNTs by air and electrostatic spray methods. The brilliant cross-linking effect of EP resin and the nanofillers' reinforcement enhanced the mechanical properties considerably and provided a durable SHPC surface with excellent adhesion and wear resistance [154].

Zhang *et al.* have studied spray-coated SHPC MWCNT/EP nanocomposite coating on carbon steel (CS), where the agglomerated CNTs mainly constituted the hierarchical microstructure. Different amounts of CNTs (0.125, 0.25, 0.5, and 0.75 g) were first dispersed in the EP resin (1.875 g in 40 mL of acetone), to which jeffamine D230 (0.625 g) was added and stirred to prepare the dispersion. The coated/cured (at 60°C, 2 days) sample with 30 wt% CNT loading displayed slippery SHPY. However, a lower (10 wt%) or a higher (40 wt%) loading does not yield SHPY and that was, respectively, attributed to the insufficient CNT content and the wider spacing between the neighbouring agglomerates [155]. An SAPC coating was fabricated by spraying a suspension of fluorinated MWCNTs (hydroxylated MWCNTs dispersed in dry THF with added 1*H*,1*H*,2*H*,2*H*-perfluorodecyltriethoxysilane [PFDTS]) and EP adhesive. The F content was as high as 47.4%. The natural crowding of the CNTs and the solvent evaporation created the required surface roughness and the microstructure. The surface maintained the SAPY even after 40 abrasion cycles. Excellent durability was observed during finger wiping, sand dropping, and sandpaper abrasion tests (Figure 10) [156]. Li *et al.* employed nanoscale (MWCNTs) and microscale (graphite and

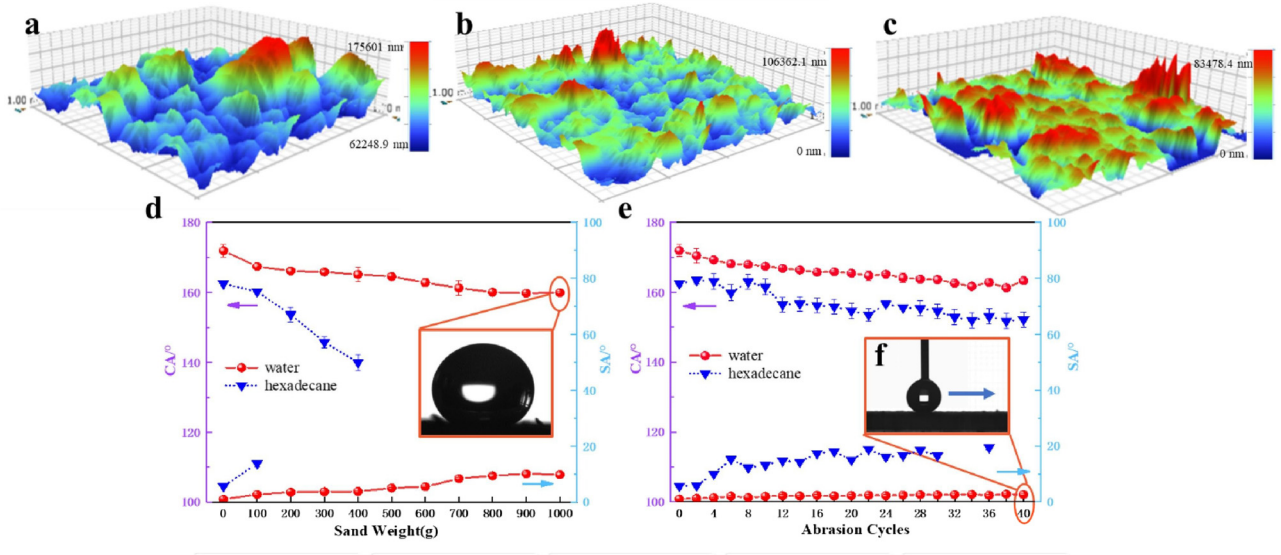

Figure 10: Surface 3D map images after different abrasion cycles: (a) 0, (b) 20, and (c) 40. CA and SA variation with (d) sand impinging weight and (e) abrasion cycles [156]. Reproduced with permission from ref. [156]; © 2020 Elsevier.

expanded graphite) fillers, uniformly dispersed in EP resin. First, E51 EP resin (2 g) and THF (3 g) were stirred and added to a solution comprising MWCNTs (0.16 g), graphite powder (0.5 g), EG (0.04 g), PFOS (0.1 g), and THF (5 g); subsequently, 0.2 g of diethylenediamine was also added. The SHPY was not destroyed during the abrasion testing (200 sandpaper, 500 g, 20 cm, 50 cycles), even if several powders have been worn out and the coating thickness reduced [157].

Several studies explored *PS/CNT* coatings [158–164]. Yang *et al.* reported one-step spray-casted SHPC and transparent (78%, visible) CNT/PS coating. PS capped with 4-hydroxy-2,2,6,6-tetramethyl-piperidinooxy was used [158]. The authors, in a later work, described a versatile strategy for fabricating SHPC PAA-block-PS-functionalized MWCNT (by nitroxide-mediated living free-radical polymerization) film by spray coating (CA ~ 166°, SA ~ 5°) [159]. Song *et al.* also reported a spray-coated PS/MWCNT film. SHPY was achieved after incorporating 1 wt% of γ-aminopropyl trimethoxysilane-modified MWCNTs. The surface displayed excellent durability during 1 week of water immersion, and 1 month of high-humidity air-exposure studies [160]. An SHPC conductive surface with a maximum CA of 165° (SA < 3°) was fabricated *via* drop coating by utilizing α-methylstyrene-butylmethacrylate copolymer-grafted MWCNTs. The CA displayed only a marginal decrease during 210 days of indoor air-exposure study [161]. Kim and Cho employed MWCNTs with PS and THF, and the coating was made on a cover-glass by spraying. The highest SHPY with a CA of 163.8 ± 2.5° and an SA of 5 ± 0.9° was recorded for a film coated from a mixture of 1 wt% of PS and 0.08 wt% of CNTs [162]. An SHPC anti-static coating was fabricated from a blend of poly(styrene-alt-maleic anhydride), SiO_2, and MWCNTs. γ-Aminopropyl-triethoxysilane was utilized to bond the inorganic and organic components. A sharp transition from hydrophobic to SHPC was noted at ~4.6 wt% of CNT's loading. High-temperature curing (220°C) was found to be essential to enhance the coating's durability. The hybrid coating exhibited CA as high as 180°. The surface remained SHPC even after 20 days of immersion in deionized water [164]. Gu *et al.* presented an SHPC PS/CNT hybrid membrane through covalent attachment of PS to CNT network [163].

2.1.3.3 Others

Earlier works by Han *et al.* [165], Li *et al.* [166], and Men *et al.* [167] have used CNTs along with polycarbonate (PC), poly(4-azidophenylmethacrylate-*co*-methyl acrylate), and poly(furfuryl alcohol), respectively. Men *et al.* used poly(furfuryl alcohol) as adhesion and low SE agents, along with fluorocarbon-modified MWCNTs and PTFE. The spray-coated and cured (70–180°C) coating displayed superior SHPY when the three components' mass ratios were 1:1:1 [167]. Han *et al.* employed CNTs and reduced-GO (RGO) sheets to nucleate PC crystallization through phase separation. A 10 s of dipping of the polymer sheet in the MWCNT solution was enough to shape the SHPC surface with a CAH of <5°. An optimized solvent mixture of methyl ethyl ketone and isopropyl alcohol (poor solvent) was used. The study also showed that MWCNT was a better nucleation agent than SWCNT or RGO [165].

A few works explored polybenzoxazine (PBZ)-based SHPC coatings [168–170]. PBZ is also known for its low SE (21 mJ/m^2) [169]. Zhang *et al.* presented an immersion coating comprising pristine MWCNTs and PBZ for ramie fabric [168]. Wang *et al.* sonicated MWCNTs (10 mg) with a BZ solution (10 mg in 10 mL THF) and then poured onto a glass slide, dried, and oven- (at 240°C) or MW cured. Although the as-fabricated surface was SHPC, the curing step, as expected, was essential to improve the thermal and mechanical durability [169]. The authors later developed different CNTs/PBZ coatings and showed that a fluorinated surface with a micro/nanoscale structure possessed the most robust SHPY [170].

The non-solvent-assisted phase separation was utilized to create self-cleaning SHPC porous film based on polyvinyl chloride (PVC) loaded with CNTs. On the other hand, the coatings fabricated in the absence of the non-solvent (EtOH) exhibited sticky behaviour [171]. Su *et al.* reported a robust 3D porous SHPC composite with good cyclic shape memory performance with poly(ethylene-*co*-vinyl acetate)/MWCNT as the skeleton and NaCl as a sacrificial template [172]. Mokarian *et al.* reported a highly durable SHPC nanocomposite comprising silicone rubber and MWCNTs. Outstanding durability was observed during soaking tests in boiling water, 5 wt% NaCl, and condensed HCl [174]. An SHPC conductive paper was conceived by successive dip coatings in CB/CNT/methylcellulose and fumed-SiO_2 suspensions [175].

All these reports unanimously proved that CNT's incorporation is highly beneficial to enhance mechanical durability, surface hydrophobicity, electrical conductivity, and self-cleaning properties of polymer-based nanocomposites. The concentration and aspect ratio of the CNTs are decisive. None of the studies revealed inferior durability during chemical, mechanical, or thermal stability studies. However, a few works showed compromised CAs after more prolonged water immersion or higher abrasion cycles.

2.1.4 CNT/metal/ceramic hybrids

In addition to a few works discussed above, several reports are available on SHPC hybrids of different ceramic oxides and metals with CNTs (with or without polymers) [176–195]. Wang *et al.* combined MWCNTs, Ni NPs, and diamond-like carbon (DLC) film to fabricate a robust SHPC MWCNT-Ni/amorphous-carbon coating by one-step ED. The as-prepared film displayed a CA of 158.89° and an SA of 1.99°. The integration of CNTs and Ni NPs increased the surface roughness and enhanced the abrasion resistance. Even after 20 abrasion cycles (sandpaper, 100 g, 10 cm), the CA maintained at ~152° [176]. The authors also reported a corresponding MWCNT/Co film by ED [177].

Several works employed SiO_2. Hsieh *et al.* decorated polyacrylonitrile-based carbon fibre (CF) fabric with sol–gel-made SiO_2 microparticles and CNTs. A wet chemical impregnation approach was used to disperse SiO_2 onto the fabric, and then CVD (900°C) was employed to grow CNTs. A CA > 170° was observed in the CF/SiO_2/CNT three-tier structure [178]. Peng *et al.* fabricated SHPC conductive coating by air spraying using a mixture of functionalized MWCNTs and aqueous SiO_2 sol, followed by fluorosilane modification. The study explored two types of CNTs: hydroxylated (h-MWCNTs) and copolymer/silane-wrapped (w-MWCNTs). The threshold concentration for achieving the SHPY varied with the type of the CNTs, *i.e.*, 2.7 vol% for w-MWCNTs and 4.8 vol% for h-MWCNTs. The nanocomposite coatings retained SHPY for more than 1 year in outdoor weathering. The study also showed that the w-MWCNTs/SiO_2 coatings' durability increased with coating drying temperature. During continuous water immersion studies, the coatings dried at 160°C and 240°C retained SHPY for 20 and 27 days, respectively. However, for a coating without high-temperature curing, the SHPY was lost within 3 days [179]. Li *et al.* reported spray-coated SAPC CNT–SiO_2 hybrid coating. Here, h-MWCNTs were first ultrasonically dispersed in EtOH and then 5 mL of 25 wt% aq. NH_3 and TEOS-EtOH solution were added. The well-dispersed solution was used for spraying, and the coated glass was vacuum dried and subjected to CVD of PFOTS [180]. Wang *et al.* demonstrated SHPC spray-coated h-CNT–SiO_2 NP composite coating with a post-fluorination step [181]. SHPC SS mesh was fabricated *via* coating of oxidized MWCNT inks with post-modification in perfluorosilane/SiO_2 NP solution and curing at 150°C [183].

Yu *et al.* presented a method to fabricate SHPC nanocomposite film consisting of CNTs and SiC NWs. The Si substrate was coated by Ni and amorphous-carbon films by high vacuum magnetron sputtering, and subsequently heated with Al powder at 1,000°C in a tube furnace. SEM images displayed two different wire-like nanostructures: curl and straight NWs. The composite surface showed CA of 157 ± 2°, compared to 120 ± 2° of pure CNTs, and 86 ± 2° of pure Si wafer. The film retained a CA of 141° even after continuous water immersion for 2 weeks [184]. Jiang *et al.* prepared SHPC coating (CA of 161° and SA < 2°) by spraying a suspension of SiC particles and CNTs on EVA plastic [185].

Liu *et al.* fabricated a durable SHPC Al_2O_3/CNT/PDA/PTFE coating. The synergistic effect of the Al_2O_3 hydration and the addition of CNTs/PTFE promoted mechanical and chemical durability (see Section 3.1.1) [186]. Highly active SHPC Co_3O_4/CNT catalyst was synthesized by *in situ* growth of Co_3O_4 NPs on MWCNTs in the presence of a polymer surfactant, followed by PFDTS modification [187]. Shen *et al.* fabricated antibacterial SHPC Ni/WO_3/CNT metal matrix coating by ED and PFDTS modification, followed by curing at 120°C. The optimized ED parameters for the SHPY (CA ~ 168.5°, SA ~ 3°) were a bath having 0.5 g/L CNTs and a deposition current density of 4 A/dm^2. The coating remained SHPC when abraded for 180 cm (600 sandpaper); however, after 200 cm of abrasion, the CA changed to 148.9°. SHPY was maintained even after 50 cycles of the tape-peeling test; nevertheless, the CA reduced to 145.1° after 55 cycles [188].

A transparent SAPC coating was fabricated using a template approach where CNTs were sol–gel-coated with SiO_2 and the CNTs–SiO_2 suspension was spray coated onto glass slides and cured at 600°C and further subjected to a fluorination step. The coated surface displayed many protrusions composed of SiO_2 NPs and SNTs. The transparent coating sustained SAPY even at 400°C [189]. Li *et al.* fabricated semitransparent SOPC SNT coatings on glass with a post-PFTS modification. The SNT layer was spray coated using a dispersion of PDMS-modified MWCNTs and subsequently calcined to remove the CNT template. The SNT layer's microstructure and hence the SAPY could be controlled by optimizing the diameter and concentration of MWCNTs. The surface displayed excellent superwettability for water, *n*-decane, *n*-hexadecane, toluene, and several hot liquids [190].

Zhu *et al.* fabricated an SHPC film by spray coating a dispersion of ZnO NPs and MWCNTs in PDMS solution [191]. Barthwal *et al.* reported ZnO/MWCNT coating (by sol–gel and dip coating) for Cu mesh, with a subsequent PDMS modification. The SHPY was maintained during direct immersion in 3.5 wt% NaCl for 15 h and ambient air exposure for 2 months. A composite coating with 2.5 wt% MWCNTs presented a CA of 156° and an SA of 4°. The CAs recorded for coatings with 1 and 5 wt% MWCNTs were 151° and 145°, respectively [192].

SWCNT/GR composite was fabricated *via* covalent crosslinking through two different coupling strategies: carbodiimide and Sonogashira. The results showed that the composite assemblies obtained by Sonogashira coupling exhibited higher surface areas and greater CAs (159–163°) when compared to the carbodiimide coupling [193].

2.1.5 Sponges, foams, aerogels, fabrics, and meshes

Several works investigated CNT-based sponge/foam/aerogel/fabric/mesh for different applications including oil separation and sensors. Polymer/CNT composite sponges are mainly studied [196–232].

A few works reported SHPC *CNT-only* sponges/bundles [198–200], whereas a few others studied *CNTs + GR* sponges/monoliths [201–203]. CNT/polymer composite sponges are attractive for practical applications due to their improved mechanical durability. Several works employed composite structures of CNTs with *commercial PU foams*. Ge *et al.* presented a dip-coating method for building SHPC and SOPL CNT/SiO_2-coated PU sponge where the as-purchased PU sponge was consecutively dipped in EtOH suspensions of PVDF-HFP and CNTs/SiO_2, and cured at 140°C, blew off the loose particles and subjected for further fluorination in EtOH solution of perfluorotetradecanoic acid, and dried at 80°C [204]. Sultanov *et al.* also employed a dip-coating method where commercial PU sponges' walls were coated with RGO and MWCNTs [205]. PU/MWCNT composite with a nano/microscale hierarchical porous structure with copious air holes was fabricated *via* non-solvent-assisted thermal phase separation. Morphology analysis revealed uniform dispersion of the carboxylated-CNTs in the porous structure, facilitated by strong hydrogen bonding interaction. The composite monolith displayed excellent mechanical elasticity and chemical durability [206]. Hong *et al.* reported a flexible, conductive SHPC PU/CNT/silane aerogel composite microfibre. CNTs (2.5 wt%) were mixed with PU first and then with PFTS, and further, SiO_2 aerogel particles were embedded in the matrix [207].

A few studies employed *melamine* (*ML*) *sponges* [205, 208,209]. Mechanically robust 3D SHPC composite sponges were prepared using ML as a scaffold, MWCNTs, GR, or activated carbon as SHPC and robust coating material, and a polyphenol–Fe^{3+} complex as a low-cost adhesive. The optimized loading of MWCNTs for the SHPY was 3% [208].

Cellulose-based materials are attractive in terms of abundance and eco-friendliness. Lu *et al.* made SHPC/SOPL sponge by cross-linking epichlorohydrin with ethyl *cellulose* (*CL*) sponge and further complexing with silanized CNTs and modifying with SiO_2/HDTMS. The SHPC/SOPL material (water CA ~ 158.2°, oil CA ~ 0°) displayed superb mechanical strength (withstand 28.6 kPa pressure) due to the facilitated chemical cross-linking and the incorporated nanofillers. The sponge also revealed excellent thermal (up to 330°C) and chemical durability (acid/alkali/salt solutions) [197].

Several works explored SHPC CNT coating on *cotton fabrics*. Makowski *et al.* fabricated SHPC cotton woven fabrics covered with silane-modified MWCNT layer [210]. Zheng *et al.* manufactured a conductive SHPC cotton fabric (CA of 162°) by LbL assembling carboxylated and aminated MWCNTs and further modifying with PDMS. The assembly was repeated for different cycles and subsequently dipped in 5 wt% hexane solution of PDMS and vacuum dried at 135°C [211]. SHPC, flame-retardant, and conductive cotton fabric was fabricated by LbL assembly of poly(ethylenimine), ammonium polyphosphate, and CNTs, followed by PDMS treatment [212].

A few studies explored CNT coating on *SS mesh*. Lee *et al.* described a technique to directly synthesize VACNTs on commercial SS mesh by CVD for oil separation [91]. Lu *et al.* used a spray-coating method for CNT layer deposition onto steel wire mesh. Poly(methylmethacrylate) (PMMA) was used to deliver robust bonding between CNTs and the mesh surface [213].

Several studies on *SHPL and underwater SOPC composite membranes* for oil separation applications are available that include SWCNT/PDA/PEI [216], CNT/FeOOH NR [217], SWCNT/TiO_2 [219], CNT/PS/Au NP [220], Ag/PAA/CNT [221], MWCNT/MnO_2 NW [222], polyzwitterion/TiO_2/CNT [223], magnetic CNT–PVA [224], and CNT/PAA brush [225] membranes. Quite a few works reported CNT-based desalination/water treatment membranes including ACNT membrane [226], MWCNT/PVDF/PDMS [227], CNT/PFDTS [228], CNT/polyvinylidene fluoride-*co*-hexafluoropropylene [229], bauxite/NiO-CNT [230], CNT/PVDF/PP [231], and SS-CNT [232] membranes.

2.2 Carbon nanofibres

2.2.1 CNFs only

This section discusses CNF-based SHPC surfaces [233–270]. A few works on microscale CFs are also included.

Several earlier (before 2010) reports addressed SHPC *vertically aligned CNFs* [233–235,244]. Hsieh *et al.*

demonstrated the influence of the F/C ratio on the SHPY of CNFs prepared by a template-assisted method and showed that the CA increases with the increase of F/C ratio [234]. Wang *et al.* employed an alumina template to fabricate aligned SHPC CNFs (CA of 153.1 ± 2.2°) *via* dipping in hydrophilic PVA polymer followed by a carbonization process (at 600°C) and subsequent partial template removal. No low SE modification was used. The CA of the corresponding disordered CNFs was only 126.3 ± 3.7° [235]. Hima *et al.* studied three different types of CNSs (caterpillar-like fibres, tubes, and interwoven spheres) by CVD (700°C, morphology varied with the growth duration) and showed that the caterpillar-like CFs and interwoven carbon spheres exhibited high CAs of 163 ± 2° and 168 ± 2°, respectively, and that was attributed to their unique surface structures. The corresponding tube structure displayed CA ~ 140° only [244].

Tsai *et al.* provided a detailed account of drop-impact dynamics on SHPC surfaces made up of CNF forest and microscale-patterned polymers. The study showed that the multiscale nanoroughness had only a negligible effect on the impact dynamics when W_n was ≤120; however, it was significant at $W_n \geq 120$ [236]. Ogihara *et al.* demonstrated EPD-made SHPC coloured films using different hydrophobic pigment particles, including vapour-grown CNFs and CB [237].

An SHPC CF coating with boosted corrosion protection capability was developed on Zn *via* CVD at 350°C. The CAs measured on Zn-CF and bare Zn surfaces were 153.3 ± 1° and 68.2 ± 1°, respectively [238]. Durable CNF coatings were developed on mild steel (MS) and AZ31 Mg alloy by subsequent plasma sputtering and CVD. The CA of the bare MS (~69°) increased to ~150° (SA ~ 7°) after the CNF coating. The corresponding transition for the Mg alloy was ~66.7° to ~145° [239].

Several works employed SHPC fabrics made of CFs [241–245]. Meng *et al.* explored the role of CNFs in preparing SHPC and electroconductive surface on glass fabrics. Homogeneous CNFs were grown by CVD, and the surface modified with a fluoropolymer [243]. Ko *et al.* utilized preferential oxygen plasma etching to fabricate high-aspect-ratio CF-network-structures with morphology ranging from nanopillar to hairy. A subsequent siloxane modification increased CA from 147° (pristine CFs) to 163° (30 s of siloxane vapour treatment) with a reduction of CAH from 71° to <5°. Under super-saturated vapour conditions, the pristine CFs were wet with condensation between fibres. They led to flooding, whereas dropwise condensation was dominant on the SHPC surface, allowing the interstitial spaces to remain dry [245].

Siddiqui *et al.* employed a two-step plasma-sputter/CVD (300°C) process to fabricate SHPC CNFs on activated CF (CA ~ 146°) and glass (CA ~ 156°) substrates without the use of fluorosilanes. The CAs of the corresponding bare CF and glass surfaces were ~0° and 36° (Figure 11a–d). SEM images displaying the surface morphology of the SHPC surfaces are also shown (Figure 11e–h). The SHPY was well-maintained during the abrasion test with different sandpapers and applied loads. An already abraded surface (using P1500 for nine cycles) retained excellent durability even after subjecting a second round of abrasion studies (P800, 100 g) (Figure 11i). The surface presented outstanding chemical durability over a wider pH and hot water (95°C). The SHPY was well-maintained during an ultrasonication test for 300 min (Figure 11j) [248]. Xu *et al.* employed an SHPC CF sponge without any chemical modification for oil separation [247].

2.2.2 With polymers

Several works explored CNFs *with silanes/fluorosilanes* [250–258]. In 2011, Das *et al.* reported a spray-coated SHPC self-cleaning CNF/PTFE/composite-polymer coating. CNFs were employed mainly to adjust the conductivity without compromising the SHPY, whereas PTFE particles were used as hydrophobic fillers. A solution blend of PVDF and acrylic PMMA was used as the composite–polymer matrix. The optimized CNF loading amount was 1.1 wt% [250,252]. The authors also reported a water-based spray coating of commercial fluoroacrylic copolymer and hollow CNFs. The study showed that replacing lengthy CNFs with short solid nanowhiskers would help produce more stable fluoropolymer–nanocarbon dispersion. At a CNF concentration of >30 wt%, self-cleaning SHPY was observed, whereas oil-droplet mobility was experienced at 60 wt% loadings only [251].

CNF–PDMS systems were explored. Seo *et al.* prepared CNFs by CVD and surface modified by PDMS (CA ~ 170°). A corresponding STA-modified film showed a CA of ~150° only [253]. Abdulhussein *et al.* employed one-step vacuum filtering to fabricate SHPC (CA > 163° and SA < 5°) and SOPL (oil CA ~ 0°) CNF/PDMS composite block with high mechanical and chemical stability [254]. A robust SHPC (CA ~ 163°) and SOPL CNF/PDMS-modified SS mesh was fabricated by vacuum filtration, followed by PDMS coating. Well-dispersed CNFs with lengths at the range of 20–200 μm and diameters of 100 nm were used, and SS/CNF mesh with a pore diameter of <1 μm was assembled by random cross-linking (Figure 12). Most of

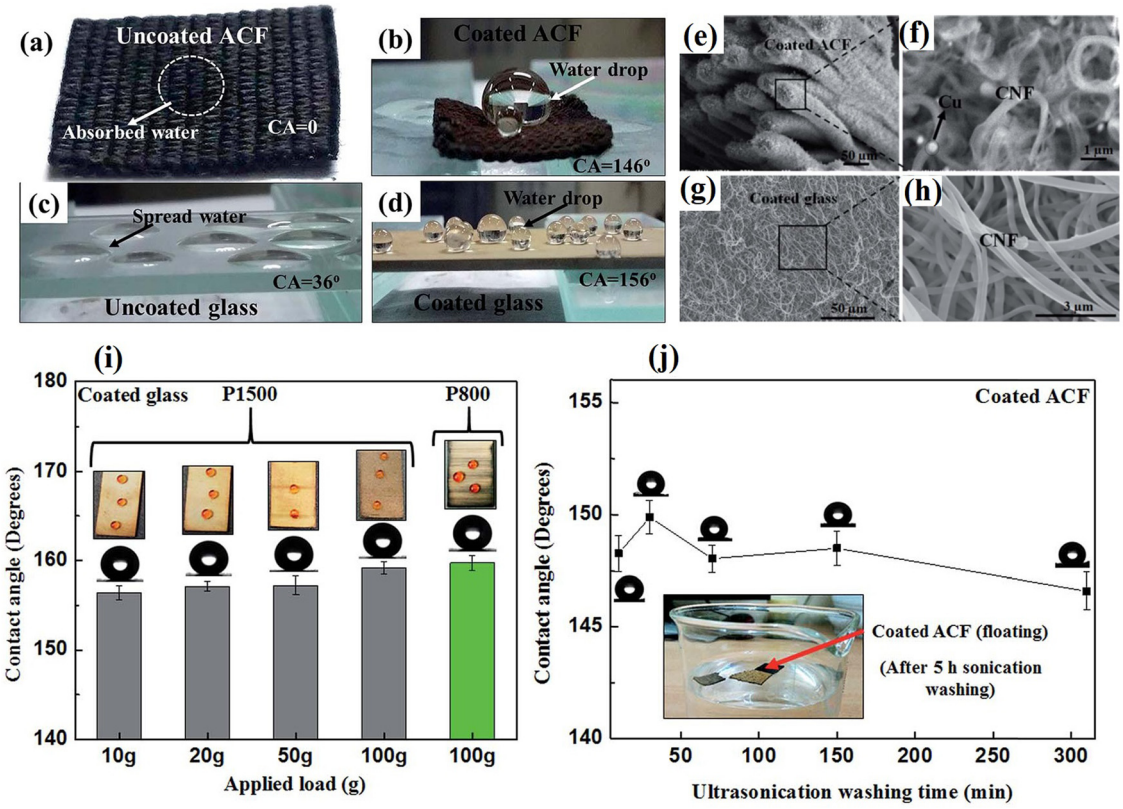

Figure 11: Digital images of (a) uncoated CFs, (b) coated CFs, (c) uncoated glass, and (d) coated glass surfaces. SEM images of (e and f) coated CFs and (g and h) coated glass surfaces. CAs of the coated glass after (i) abrasion and (j) ultrasonication tests [248]. Reproduced with permission from ref. [248]; © 2017 The Royal Society of Chemistry.

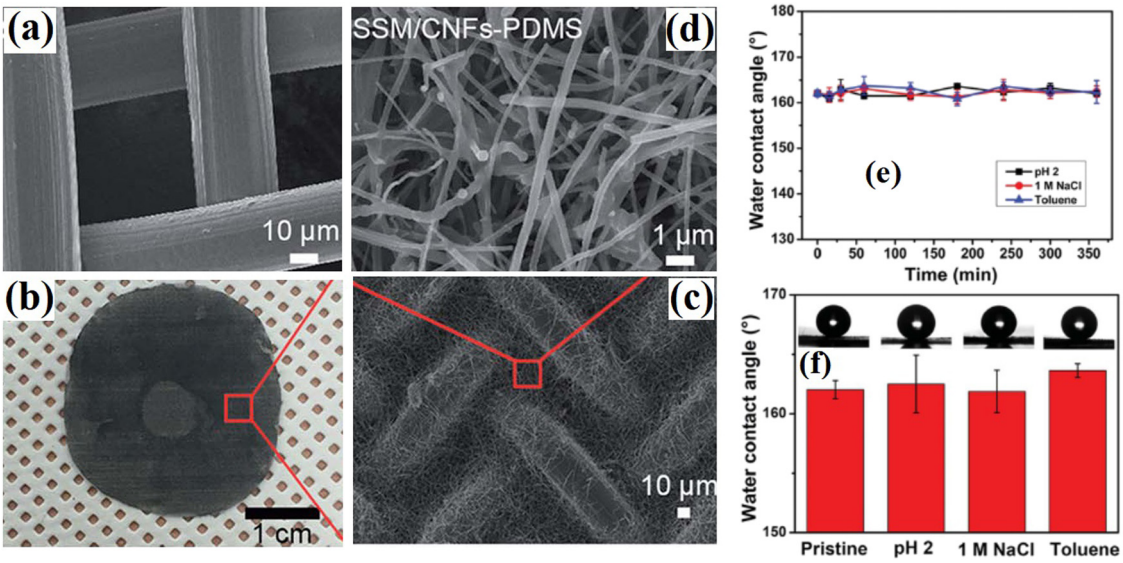

Figure 12: SEM images of (a) SS mesh and (c, d) SS mesh/CNF/PDMS composite membrane. (b) Photograph of the composite membrane. CA variation with (e) time and (f) after 15 days of corrosion test [255]. Reproduced with permission from ref. [255]; © 2016 The Royal Society of Chemistry.

the CNFs were well-placed inside the SS mesh, whereas a few stayed exterior. The SHPC surface displayed extreme chemical durability to 1 M NaCl, pH 2 solution, and toluene solvent. The durability was preserved even after continuous immersion of the membrane for a longer duration (Figure 12) [255].

Yang *et al.* in a recent work presented SHPC and SOPL CNF-reinforced PDMS–metal rubber (MR) composite. CNFs were embedded into MR *via* vacuum filtration, and subsequently, PDMS coated. PDMS acted as an effective binder between CNF fillers and MR. The composite remained SHPC even after 100 cycles of compression at 200 N. Excellent chemical durability against pH 2, pH 10, and 3.5 wt% NaCl solutions was observed [256]. Guo *et al.* reported an SHPC/SOPL foam composite in which CNFs were uniformly distributed on PDMS foam under ultrasonication, followed by an extra PDMS modification to improve the interfacial adhesion [257]. An approach for designing hemostatic wound-dressing material favouring rapid blood clotting and easy clot removal utilized SHPC CNF/PTFE or CNF/PDMS networks [258].

A few works explored *CNFs with PUs* [259–261]. Zhang *et al.* prepared SHPC/SOPL and electrically conducting PU/CNF network. Hollow CNFs were ultrasonically integrated onto the PU nanofibre surface and subsequently subjected to PDMS modification. PDMS served as an interfacial adhesion agent and waterproof protective layer. The composite displayed excellent strain independent superwettability; original CA (153°) was retained even at 100% applied strain. The superb durability was attributed to the robust interfacial (CNFs/PU-nanofibres) adhesion [260]. Baig *et al.* synthesized CNF-grafted PU sponge by dip coating. Besides enhancing the hydrophobicity, the CNF's grafting helped increase the surface area and decrease the average pore size of the PU matrix (improved capillary action) [261].

2.2.3 With metals/ceramics

Li *et al.* employed CVD grown herringbone CNFs along with commercial carbon felt and SiO_2. Here, fumed SiO_2 NPs were distributed onto the carbon felt and then exposed to CNF growth condition. The CNF/SiC/carbon-felt hybrid composite formation happened at high temperatures (1,650°C, Ar) *via* carbothermal reduction at SiO_2/carbon interfaces. The composite was superbly mechanically robust [240]. Aljumaily *et al.* synthesized two types of hierarchical SHPC CNMs on Ni-doped activated carbon surface, namely, carbon sphere-free CNFs (CA ~ 167°) and carbon sphere-mixed CNFs (CA ~ 177°), *via* CVD at 650 and 750°C, respectively. The study suggested that such mixed structures could be an attractive way to enhance hydrophobicity. The spheres on the CNF network divulged a rougher surface and minimized the cavities [246].

Earlier reports explored SHPC SiO_2 NP-coated CFs [263] and hydrothermal (HT)-synthesized ZnO/CNF hybrid [264]. Wu *et al.* in a recent work presented nanocomposite of CFs, PVDF, CB, and CeO_2 NPs with excellent SHPY (CA ~ 156° and SA ~ 5°), mechanical properties (tensile strength and tensile modulus were ~109 MPa and 10 GPa, respectively), and electrical conductivity (~6.8 S/cm). The SHPY remained stable even after 60 min of strong acid and 24 h of strong base immersion, and 200 cycles of sandpaper abrasion [265]. SHPC fluoroalkylsilane-modified Ni-electrodeposited CFs displayed a water CA of ~159.1° and an oil CA of ~0°. The surface remained SHPC with a CA of ~158° even after 24 months of air exposure [266]. A few works on SHPL and underwater SOPC membranes/monoliths are also available [267,268].

2.3 Carbon nanosphere/nanothorn/others

Micro/nanoscale carbon spheres can be synthesized by various methods, including CVD, pyrolysis, HT/solvothermal, and chemical routes. Qu *et al.* fabricated SHPC carbon nanosphere film by depositing the soot of burning rapeseed oil without any surface modification [271]. The authors also reported an SAPC film *via* an additional fluorosilane modification where the fluorosilane acted as a glue to the loose carbon nanospheres [272]. Joula *et al.* reported a method for preparing SHPC surface by spin coating EtOH colloidal solution of HT-synthesized carbon nanospheres on glass substrate [273]. EPD at 30 V, followed by heat treatment at 250–350°C, was utilized to obtain SHPC carbon micro/nanosphere thin film on FTO glass. HT (glucose solution, 160°C) prepared carbon spheres with different diameters were used [274].

A multifunctional composite coating based on mesoporous carbon nanocapsules and PVDF displayed a CA of ~160° and an SA of ~5°. Excellent chemical durability was achieved over wider pH (1.29–13.54), and humidity (35–83%) ranges. The film displayed thermal durability up to 350°C. The surface maintained the SHPY after 30 s of abrasion with a CA of ~155° and an SA of ~15° (150 rotations, 200 g, dragged while rotating at 300 rpm). After 60 s, even though the SHPY maintained, the SA increased to ~43°. The surface lost SHPY after 90 s of abrasion [275,276]. A few other studies also described

different carbon nanosphere-based SHPC coatings [41,80, 277,278].

In recent work, Li *et al.* designed an SHPC carbon nanothorn array by a single-step reaction in a liquid-phase environment containing 1,3,5-triethynyl-2,4,6-trimethylbenzene, pyridine, acetone, and *N,N,N′,N′*-tetramethylethylenediamine. The fabricated SHPC surface on a commercial Cu form displayed excellent long-term durability during 800 days of water immersion study. When the experiment was conducted at pH 5 or 9 solutions, the SHPY marginally compromised (CA of ~145° after 800 days) [279].

SHPC powder sample composed of hierarchical carbon microflowers (CMFs) and dispersed-MoO_3-NPs was fabricated by utilizing the wet chemistry of $(NH_4)_6Mo_7O_{24}4H_2O$ and dopamine, followed by annealing (700°C) and PFDTS modification (0.5 g of CMF/MoO_3 was added to 40 mL of 0.5% PFDTS–hexane solution). An SHPC coating was fabricated by using the powder, EP resin, and a curing agent *via* sieve-deposition technique. The surface displayed excellent mechanical durability until 50 abrasion cycles (400 Cw sandpaper, 200 g, moved back and forth for 10 cm). A corresponding coating without EP resin performed poorly in the abrasion testing. Good acid/alkali resistance (pH 1 and 14) was also noted. The addition of MoO_3 was found to be helpful to enhance the chemical durability [280]. Ghosh *et al.* deposited SHPC vertically aligned tree-like carbon nanospheres by CVD. The robust sticky SHPY was attributed to the highly roughened porous surface [281].

Onion-like carbon microspheres comprised of nanoflakes were made from waste polyethylene terephthalate *via* pyrolyzing (650°C, supercritical CO_2) and vacuum annealing (1,500°C). The authors fabricated an F-free SHPC coating on polyester fabric by using the prepared carbon microspheres with PDMS [282].

2.4 Nanodiamond

In earlier work, Zhou *et al.* achieved self-cleaning SHPY on the two topmost hardest materials, diamond and cubic BN, *via* reactive ion etching (H/Ar plasma) and surface fluorination [283]. Coffinier *et al.* reported SHPC (CA ~ 160°, CAH < 2°) B-doped diamond nanograss by reactive ion etching with oxygen plasma, followed by octadecyltrichlorosilane or PFTS modification [284]. The authors also fabricated heterogenous SHPC/SHPL patterns where the SHPL regions were generated by selective UV light exposure [285]. Yang *et al.* reported an SHPC/SOPL robust diamond mesh [286]. SHPC diamond microspheres were deposited on Si by MW CVD. The microspheres were then collected by blade scratching and employed in fabricating an EP-based SHPC film with excellent mechanical and chemical durability [287]. Deshmukh *et al.* studied the electrowetting transition of diamond nanostructures [288].

2.5 Fullerene

A few works addressed SHPC fullerene assemblies [194,195, 289–296]. In earlier work, Nakanishi *et al.* prepared SHPC surfaces with two-tier nano/microroughness by the molecular assembly of a fullerene derivative bearing a long aliphatic chain, without using fluorinated compounds [290]. The authors also reported the formation of a self-assembled hierarchical fullerene derivative with long hydrocarbon chains and perfluoroalkyl tails [292]. An SHPC thin film was prepared *via* self-assembly of Au NPs and fullerene pyridyl derivatives [291]. Mansurov presented the formation of SHPC fullerenes and CNTs on Ni and Si supports in benzene–oxygen and propane–oxygen diffusion flames [194]. A supramolecular method was used to fabricate C60/tetracene flower-like microstructure comprised of nanoplates. FCC C60 microstructures were further derived *via* sublimation of tetracene component at 330°C. Thin films prepared with FCC C60 and C60/tetracene displayed SHPY with CAs of 156.3° and 150.2°, respectively [293].

A two-step self-assembly strategy was reported for the preparation of SHPC fullerene hierarchical architectures. The process was composed of a precipitation method to synthesize the initial fullerene microstructure and a subsequent drop-drying process to facilitate the self-assembled hierarchical structure [294]. Pérez-Ojeda *et al.* also reported hierarchical self-assembly of fullerene derivative with SHPY [296]. Partheeban and Sathish demonstrated the formation of SHPC flower and octahedron-like fullerene microcrystals using a liquid–liquid interfacial precipitation method [295]. Ayyappan *et al.* presented an SHPC surface by covalent functionalization of methacrylate polymers with CNTs and fullerenes [195].

2.6 Nanostructured carbon soot/graphitic carbon/others

This section briefs works reported with nanoscale-activated carbon, CB, carbon soot, carbon sponges *etc.* that

are not mentioned in other sections. Carbon soot is one of the earliest known hydrophobic materials. Despite the advantages of easy availability and robustness [297–301], the amorphous nature and loose structural binding between the carbon NPs restrict their applications [298]. The mechanical robustness and hydrophobicity of carbon soot can be further attuned through composite formation or proper chemical treatment. Several works employed *carbon soot-only* SHPC surfaces [298–316] that include carbon film prepared by pyrolysis of nanostructured polyacrylonitrile film [299], soot particles *via* camphor combustion [302], layered soot formed in candle flame [303], carbon soot from ignited paper-based wick *via* cone-shaped Al chimney [304], soot synthesized in flames of various hydrocarbons using metallic catalysts [305], soot coating by combustion of rapeseed oil [307], and amorphous carbon NPs synthesized by EtOH-flame method [308]. The SHPY of such surfaces typically ascribed to the nanostructured graphite-like structures and the soot particle's hydrophobicity [299,302,303]. A few works employed *composites of carbon soots with polymers* that include SHPC candle-soot/PVDF porous composite [310], fluorocarbon-treated soot [312], PDMS/camphor-soot coating [313], and nanoscale-sawdust/polychloroprene/carbon soot/silicon polymer coating [314]. A few works are reported on *composites of carbon soot with inorganic oxides* such as candle soot-derived TiO_2 fractal network film [298], candle soot/SiO_2 NPs dip-coated PU sponge [315], and Ag-doped carbon soot spray coating [316].

Several works investigated *SHPC graphite carbon and their composites* [317–333] that include ODA-functionalized SHPC graphite oxide film [318], graphite-reinforced metal-matrix composites [320], graphite nanoplatelet/ethylene–acrylic acid copolymer emulsion coating [322], PVDF/graphite composite coating [323], ultra-thin graphite sponge [324], nano-graphite-PDMS/ML sponge modified with HDTMS [325], SHPC/SOPL cotton fabric composed of Cu–graphite/styrene–butadiene–styrene nanocomposite [327], TiO_2–graphite blended with fluorinated methyltris(methylethylketoxime)silane and polysiloxane [329], Ge–graphite core–shell NWs produced by CVD [330], and MoO_2/graphitic carbon [331].

A number of works reported with a mention on nanostructured *CB/activated carbon* such as perfluorocarbon/perfluoropolyether-anchored CB [334], spray-casted composite coating of nanostructured CB and submicrometre-sized PTFE particles dispersed in nitrile rubber [335], gas diffusion electrode based on CB-PTFE-modified graphite felt cathode [336], highly porous GR/CB-fluorinated acrylic copolymer nanocomposite for solid-state ion-selective electrode [337], and CB-based SHPC gauze for solar evaporation [338]. Several other reports are also available [339–351].

Many works investigated SHPC *carbon aerogels* [352–358] such as biomass aerogel from corn bracts [352], magnetic porous aerogel from biorenewable popcorn *via* carbonization/magnetization and successive surface treatment [353], aerogel designed *via* carbonization of *Typha orientalis* fibres [354], aerogel from *Platanus orientalis* fibres by carbonization [356], magnetic SHPC carbon sponge [357], hybrid aerogel prepared *via* HT growth of TiO_2 NRs on biomass carbon aerogel [358], and carbon/graphitic C_3N_4 aerogel by *in situ* urea pyrolysis on cotton [355].

A few studies on SHPC carbon Qdots, DLC films, CNTs, and others, not included in previous sections, could be found in refs. [359–370].

2.7 Graphene

SHPC surfaces and coatings based on GR and its derivatives are briefly provided here [377–621]. A detailed discussion is out of the scope of this review.

Several works endorsed the SHPY primarily to the surface roughness and the reduction (removal of hydrophilic oxygen groups) processes. Different reduction methods were explored for achieving SHPY with GR/GO, including thermal [371], chemical [372], and photoreduction [39]. A significant extent of research has been performed on laser-assisted approaches since 2009 [373–376]. The wettability of hydrophobic GR is similar to that of graphite; however, dynamic wettability could significantly depend on the layered structure [36,377].

Liu *et al.* fabricated SHPC anti-corrosion GR film on Al alloy by spin coating EtOH-dispersed graphene sheets [382]. Zhong *et al.* reported a multifunctional paper where dopamine was concurrently used as a reductant for GO and a crosslinking adhesive for the adjacent GR [398]. Highly complex wrinkled/crumpled textures were created through extreme compression of GR coating [383]. Choi *et al.* reported a thermally controlled transfer printing technique for multiple patterned GR layers [384]. A shrinking method was used to generate strain-sensitive hierarchical RGO buckling patterns [408]. Multifunctional, rose-petal-like SHPC GR film was fabricated *via* self-assembly of GO. Here, vacuum filtration was used to make a hollow GO film on a PTFE membrane and subsequently reduced by HI vapour at 100°C [399]. Spark plasma sintering was shown to be a superior GO reduction method to achieve SHPC RGO in a single step. The

SHPY was attributed to the sintering-assisted removal/reduction of oxygenated functional groups in GO where the surface roughness was ~10 times larger, with a higher C:O atomic ratio of ~83 [401,402]. Lin *et al*. deposited vertical aligned GR nanosheet-embedded carbon film using an ultrasonic extrusion method to fabricate SHPC, photo-sterilize, and reusable mask [403]. Most of these studies, however, resulted in sticky SHPY.

Recent studies extensively employed *laser processing* [385–397,404,405]. Rough micropatterns and nanoscale layers shaped from laser reduction could readily lead to SHPY [385]. Shi *et al*. fabricated microflower structures comprised of GR nanoflakes *via* a single femtosecond laser pulse. The GR film was composed of LbL GR nanosheets with ~10–50 nm gaps; GR monolayers with ~0.37 nm interlayer spacing constituted each GR nanosheet [386]. Two-beam laser treatment of GO film was used to create microscale grating-like assemblies with fine nanoscale roughness. The hierarchical micro/nanostructuring and the elimination of oxygen-containing groups endowed the resultant GR film with unique SHPY [404,405]. Das *et al*. demonstrated a direct-pulsed laser approach to adjust the electrical conductivity and hydrophobicity of the inkjet-printed GR. The study showed that the laser writing converted hydrophilic (CA ~ 47.6°) and resistive (sheet resistance ~21 MΩ/sq) GR surface to SHPC (CA ~157.1°) and conductive (~1.1 kΩ/sq). Molecular dynamic simulations revealed that the laser-induced nanoscale GR flake alignment and the hydrophobic surface chemistry contributed to SHPY [389]. Hall *et al*. presented a method to make open microfluidic podiums by controlling the hydrophobicity of spin-coated GR on a flexible plastic substrate *via* laser-assisted patterning [392]. Jiang *et al*. first fabricated micro-grooved structures on a GO film *via* photolithography, and then two-beam laser treatment was performed on the corrugated surface to remove the hydrophilic groups and upsurge the nanoscale surface roughness [390]. Luong *et al*. investigated an infiltration process that enabled the devolution of laser-induced GR onto different commercial materials and produced SHPC composites with Portland cement, PDMS, EP, and wax for multipurpose applications [396].

2.7.1 With polymers

Several earlier works employed silanes/fluorosilane modification intended for different applications. Fluoropolymers [410–414] and silane/fluorosilane polymers [378,381,406,415–417,427,429,431–433,444] are the most used low SE modifiers. A few works used ODA or phenylenediamines [379,380,400,428,409,472]. Some works employed long-chain fatty acids, such as MA [456,457]. Zhou *et al*. prepared SHPC GR film with a CA of ~160.5° *via* heptadecafluoro-1,1,2,2-tetradecyl-trimethoxysilane's functionalization followed by vacuum drying at 60°C [378]. Gao *et al*. employed a triethoxyoctylsilane surface modification on CVD-made graphenic carbon nanowalls. The sample without the surface modification displayed SHPY only when the deposition pressure was 50 Pa [381].

As discussed in Section 2.1, GR was widely used as a filler to improve the mechanical performance and the hydrophobicity of polymers. Several works are available on *GR–PDMS* systems, where GR could act as a filler, and PDMS could serve as a binder or a porous network. Reports include fluorinated GO/PDMS spray coating [418], RGO-modified PDMS fabric coating [419], GR/PDMS anti-corrosion coating on Al alloy [420], PDMS/GR coating on Cu mesh [421], arc-like PDMS macromolecular bridge-grafted GR sheet hybrid membrane [422], PDMS/GR-based coating on glass [423], RGO/PDMS composite film-based acoustic sensor [424], GR/PDMS-based bilayer actuator [425], PDMS/open-cell GR network *via* simple inverse drying [426], RGO and diatomaceous earth modified with PDMS [440], PDMS/GO decorated with ZnO NRs [445], and spin-coated Fe_3O_4/GR/PDMS film on Ti [454]. Many works explored *GR–PVDF*, such as GR/PVDF gel by phase separation [465], GR/Nafion film [467], GR/PTFE by phase separation [469], RGO/PVDF composite [468], GR/PVDF electrospun film [470], and PVDF/RGO/SiO_2/PFOS coating [471].

Several works employed *GR together with PU coatings*. The reports include transparent, flexible, SHPC film of siloxane-functionalized GO/micropillar-patterned poly (urethane acrylate) [475], PU film loaded with TiO_2 NPs and GR [451], perfluorosilane-coated GR/PU [476], flexible conductive film of PU/cellulose-modified RGO [477], SiO_2-GR shell/PU nanofibre core conductive composite [439], electrospun PU nanofibres wreathed by GR and modified by PDA/PFDT [478], and spray-coated hexamethyldisilazane-functionalized fumed SiO_2 NPs thermally welded PU coating [479]. Several works explored *GR/EP composite coatings* such as GO-diatomaceous earth/EP [441], POSS-functionalized-GO/EP [481], EP-PTFE/PDA-modified-GR/SiO_2/PFOS [483], POSS-modified GO/EP [484], and thiol-coupled GR/2-(perfluorooctyl)-Et-acrylate/EP [485]. A few studies used *GR with polyethylene and polypropylene* [486,488–491].

Other reported works in this category deal with electrospinning PS and PVC fibres incorporated with TiO_2 NPs and GR nanoflakes [492], fluorosilane-modified GR added siloxane–acrylic resin coating [494], amine-grafted-GO/amine-reactive-polymeric nanocomplex [495], GO-grafted ODA-incorporated polylactide [496], PEDOT:PSS/RGO/

wool-nylon composite textile [497], fumed SiO_2-modified cellulose nanocrystal/GR coating on non-woven fabric [498], GR/poly(3-hexyl thiophene) [503], GR-decorated with poly[2-methoxy-5-(2′-ethyl-hexyloxy)-1,4-phenylene-vinylene] [504], and poly(vinylbenzyl-chloride-*co*-divinylbenzene)-grafted GR [505].

2.7.2 With metals/ceramics

Several works explored SHPC *composites of GR with other CNSs*, including GR/POSS/CNT coating [125], GR/SWCNT composite by coupling reaction [193], carbon NP-decorated GR [434], LbL deposited MWNT/RGO film onto SiO_2 colloids followed by fluorination [202], nanocomposite coating of CB, CNTs, GR nanoplatelets, and their combinations in fluoropolymer dispersion [138], and APTES/MWCNT-GR/PDMS/Ag/fluorosilane multilayer coating [430]. A number of works are available where *ceramic oxides* such as SiO_2 [435–440,442,443,471,479,483], ZnO [445], Al_2O_3 [446], SnO_2 [452], SnS_2 [453], Fe_3O_4 [454], Er_2O_3 [455], and TiO_2 [447–451] were used in GR-based SHPC coatings (with/without polymers).

A few works reported SHPC hybrid film of GO with metals, such as Ni/GR film on MS by ED followed by MA modification [456], Ni/RGO/MA coating on CS by ED [457], RGO/Ni coating on SS by ED [458], GR/amorphous carbon/Ni-based film by high-voltage ED [459], GR/amorphous carbon/Co by ED [460], Co/Ni/GR composite coating on Cu by ED [461], and GO/Ag NW/fluoride polyvinyl butyral spray coating [462]. Most of these works employed ED as a means to incorporate metallic NPs in the composite.

2.7.3 Sponges, foams, aerogels, fabrics, and meshes

A significant extent of works were reported in this category, especially for oil separation application. Analogous to CNTs, the superwettability, mechanical properties, and absorption capacity of 3D foams could be precisely manipulated by covalent grafting of GO [506]. Significant information is available on SHPC/SOPL or SHPL/underwater SOPC GR-based sponges/aerogels/monoliths. They are shown to be effective absorbents for wide-ranging organic solvents/oils with high absorption capacities and good recyclability [507]. Several works are available on *pristine/doped/fluorosilane-modified GR aerogels/sponges* [499,512,516,517,519,521,524–528,532,534,544,570]. A number of works explored *hybrid/composite structures* of GR aerogel with PDMS [508,522,529,541], PTFE [509,538–540], PVDF [520,523,533], polyborosiloxane (PBS) [515], PAA [530], lignin [536], agarose [537], Cu NWs [543], Au NPs and PFDT [556], and diatomite/carbon-nanobelts [608]. A few works explored hybrid sponges of *GR with other CNSs*. The reports include MWCNT/GR hybrid aerogel [203], PFOS-modified RGO/CNT/chitosan aerogel [542], and 3D monolith of GR/CNT [201].

A few works reported *GR/MOF* systems, including RGO/MOFs [500,518], GO and oleic acid-modified ZIF-8/cotton fabric [557], highly fluorinated GO/ZIF-8 [463], UIO-66-F4/RGO hybrid [464], PDA-coated porous GR/MOF [609], and ZIF-8/thiolated-GR-based polyimide nanofibrous membrane [613].

Several studies employed *GR with commercial PU sponge*. A simple dipping–drying process was typically used to functionalize GR onto PU sponge [510,513,555]. Reports include GR-coated PU sponge [567], RGO-coated PU sponge [568], GR-grafted PU foam [563], γ-methacryloxypropyltrimethoxy silane-modified GR-coated PU sponge [566], fluorosilane-modified ammonium polyphosphate/GO-decorated PU foam [480], fluorothiol-modified-PDA-coated-GO/PU sponge [572], RGO and orthoaminophenol-functionalized PU [574], fluorosilane-modified-RGO/PU sponge [573], RGO and MoS_2 NP-incorporated PU foam [576], Fe_3O_4 NP-incorporated magnetic GR/PU foam [565], oleic acid–Fe_3O_4 NP/GO/PU sponge [575], lignin-based PU foam grafted with PDA-RGO and ODA [571], tetradecylamine-amidated-GO-modified/TiO_2–PU composite foam [578], and GR aerosol/PU sponge [569].

Similar works were reported on *GR-incorporated ML sponges* [209,501,511,514,577,579,581–593,595,615,618], *GR–CL sponges* [531,545,547,580,664,665], and others [594,596,597]. Several reports employed GR-coated cotton fabrics with/without silane/fluorosilane modification [549–555,610,611]. Reports also explored GR with polypropylene [555,558], polyester [559], PS [493,561], and polycarbonate [562].

Several works used GR with steel [598–604] and Cu/wire [605–607] meshes. A few reports focused on water treatment/desalination membranes [614,616,619,620].

3 Application areas

3.1 CNT/nanofibre/others

3.1.1 Anti-corrosion

Corrosion continues to be a major industrial threat necessitating costly preventive measures [622–634]. In general, reported works with SHPC surfaces showed superior

corrosion resistance than the corresponding bare surfaces attributed to the robust interface air layer that could effectively withstand the ingression of water/aggressive ions. The long-term durability of such surfaces in aggressive chloride and acidic solutions remains an area to be further advanced. As far as CNSs are considered, the superior mechanical/chemical durability is advantageous; however, graphite's more noble position in the galvanic series could intensify the corrosion once local damages initiated. On the other hand, CNMs are economical and effective fillers to polymeric resins to enhance mechanical/chemical durability, hydrophobicity, barrier protection, and substrate adhesion.

Only a few works explored *CNT-only SHPC anti-corrosion coatings*. A recent work showed that a sprayed SAPC coating (on glass) of fluorinated MWCNTs and a spray adhesive greatly promoted the chemical robustness [156]. Electrochemical corrosion studies by Belsanti *et al.* on spray-coated SHPC CNT film on Al alloy in 0.1 M NaCl presented a positive shift of corrosion potential (E_{corr}) and significantly reduced corrosion current density (i_{corr}). The pitting corrosion resistance was much improved [118]. Most of the reports in this area explored CNT-incorporated polymer coatings.

Several studies investigated *CNT/EP coatings* [153–155, 157]. Zhang *et al.* explored an one-step spray-coated SHPC nanocomposite coating of EP resin and MWCNTs on CS and showed that suitable optimization of the filler could improve the corrosion resistance considerably. The highest CA (~154°) and corrosion resistance was noted for a 30 wt% CNT-incorporated coating. The property enhancement was correlated with the surface roughness (Figure 13). Their EIS results with different CNT contents showed that the low-frequency modulus in the Bode plot first decreased with the increase of CNT content (due to the conductivity enhancement); however, after reaching SHPY at 30 wt%, the impedance raised to noble values. A similar trend was observed in Nyquist plots where the capacitive arcs' diameter reduced first and then augmented (Figure 13). The trend confirmed that the trapped air layer considerably

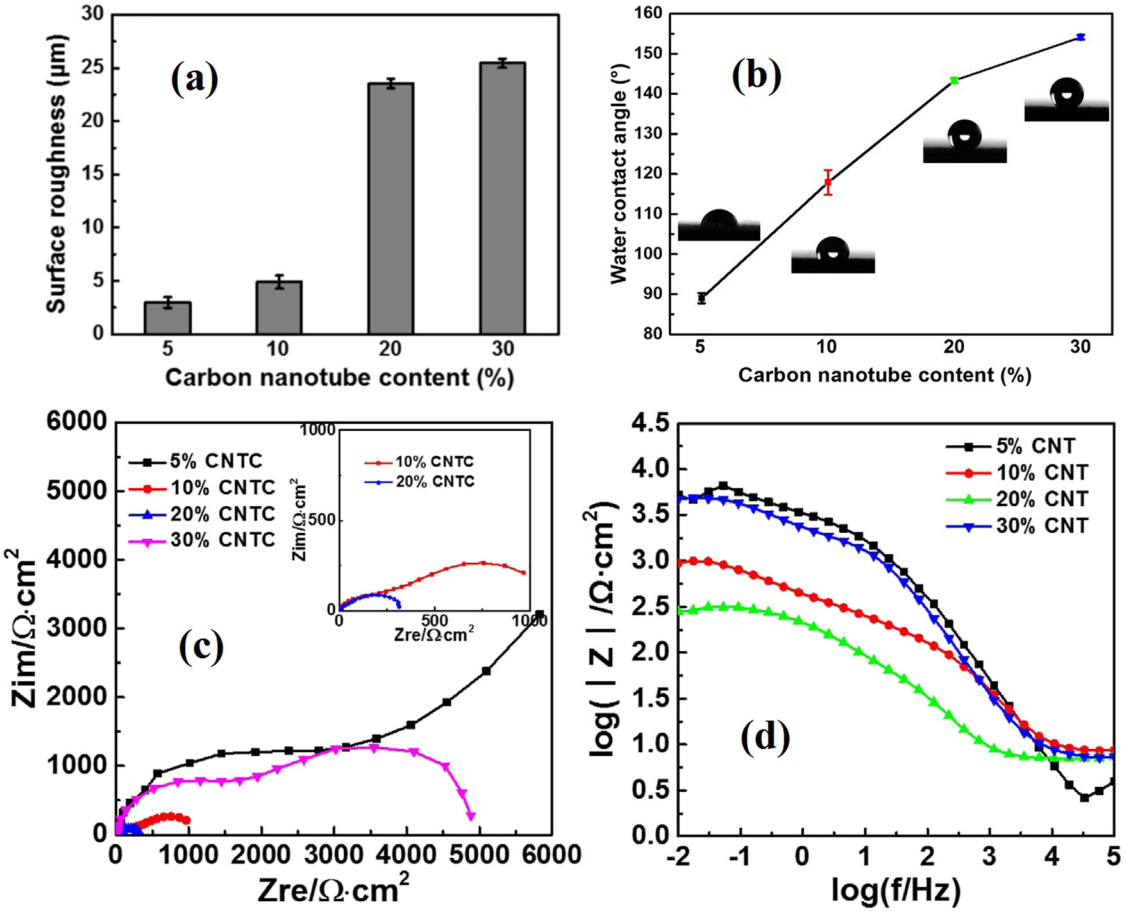

Figure 13: Evolution of (a) surface roughness and (b) CA of MWCNTs/EP coatings. (c) Nyquist and (d) Bode plots recorded in 3.5 wt% NaCl [155]. Reproduced with permission from ref. [155]; © 2018 Elsevier B.V.

resisted the interface electron transfer. The surface displayed extraordinary mechanical durability and retained SHPY even after 100 cycles of tape-peeling [155]. Potentiodynamic polarization (PDP) studies of spray-coated SAPC EP/PVDF/FEP/SiO_2/CNT-coated Al in 3.5 wt% NaCl revealed highly competent barrier protection to aggressive ions. The brittleness and meagre abrasion resistance of EP resin were considerably enhanced [153]. The authors also reported spray-coated SAPC EP/PANI/FEP/SiO_2/CNT coating for Al. Electrochemical studies demonstrated significantly enhanced anti-corrosion performance ascribed to the better barrier effect and entrenched PANI's redox catalytic ability. The CA of the coating retained high values even after 10,000 times of abrasion and ~3 months of immersion studies in pH 14 or pH 1 solutions [154]. Li *et al.* also showed much-enhanced corrosion resistance for an SHPC composite EP coating for Q235 steel. The E_{corr} of the bare, EP-coated, and SHPC samples were −0.462, −0.714, and −0.876 V (*vs* SCE), respectively. The corresponding i_{corr} were 6.46×10^{-4}, 3.47×10^{-5}, and 3.43×10^{-6} A/cm^2 [157].

PDP studies on spray-coated and cured (300°C) SAPC PANI/CNTs/SiO_2/ETFE/PFOS coating displayed exceptional corrosion resistance for Al. The E_{corr} of bare Al was −0.797 V (*vs* SCE), whereas the SHPC sample exhibited a positive E_{corr} of 0.129 V and a low i_{corr} of 6.1×10^{-11} A/cm^2 after 1 day of immersion in 3.5% NaCl. After 90 days, the E_{corr} decreased to 0.051 V. The corresponding value for a composite coating without PANI/CNT was −0.792 V. The i_{corr} of the SHPC sample after 90 days was 3.5×10^{-10} A/cm^2, which was ~3 and 5 orders lesser than the composite-coated (without PANI/CNTs) and the bare samples, respectively. The SAPY remained unchanged during continuous immersion in 3.5 wt% NaCl and 1 mol/L HCl for 90 and 60 days, respectively [128].

PDP and EIS studies of PPS/SiR/CNT/RGO spray-coated and heat-treated (320°C) Al in 3.5 wt% NaCl disclosed that the E_{corr} was shifted from −0.889 V of bare Al to −0.810 V for PPS/SiR/CNT-coated sample and further to −0.726 V for PPS/SiR/RGO/CNT-coated sample. The i_{corr} of the SHPC sample was three orders of higher magnitude (1.47×10^{-8} A/cm^2) than the bare (3.5×10^{-5} A/cm^2). The high protection efficiency (>99%) was retained even after 28 days of continuous immersion in 3.5 wt% NaCl [142]. Composite spray coating of Al_2O_3/CNT/PDA/PTFE (calcined at 500°C) on steel plate demonstrated a significant shift of i_{corr} from $10^{-2.2}$ to $10^{-3.8}$ μA/cm^2 and E_{corr} from −0.672 to −0.388 V (Figure 14a). The CA of the coating demonstrated only a slight decrease even after 15 days of immersion in pH 14 and pH 1 solutions (Figure 14b). The CNT's addition significantly enhanced the wear resistance. The coating also displayed excellent hot water repellency (99°C) and withstood water jet (20 m/s) test. A few other reports also have the potential for anti-corrosion application [132,134].

A few works explored metal NP-incorporated coatings [176,177]. Zhou *et al.* reported Ni NPs and MWCNTs doped DLC film by one-step ED. As the CNT concentration in the coating increased, the i_{corr} regularly decreased and reached the best protection ($i_{corr} \sim 3.124 \times 10^{-10}$ A/cm^2) at an optimum concentration of 0.07 mg/mL. Higher concentrations of CNTs, however, increased the i_{corr} further [176]. The authors also reported a similar study with Co NPs [177].

Only a few works are available on *CNFs in anti-corrosion* application. Qiu *et al.* have shown that the CVD-grown SHPC CF layer on Zn presented significant corrosion inhibition. Although CF's inherent SHPY did not endure long-term immersion in NaCl solution, the SHPC

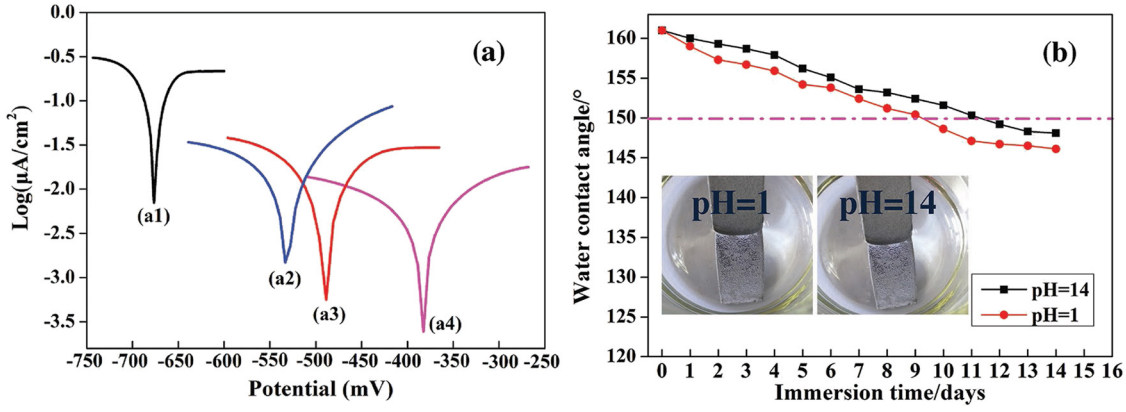

Figure 14: (a) PDP plots: (a1) bare steel, (a2) pure Al_2O_3, (a3) Al_2O_3/CNTs, and (a4) SHPC Al_2O_3/CNT/PTFE-coated samples in 3.5 wt% NaCl. (b) CA variation of the SHPC coating in pH 14 and pH 1 solutions as a function of immersion time [186]. Reproduced with permission from ref. [186]; © 2017 WILEY-VCH.

surface remained steady during 13 months of air exposure [238]. A two-step plasma sputter-coated SHPC CNF coating fabricated on MS and AZ31 alloy displayed excellent corrosion protection in 3.5 wt% NaCl with respective i_{corr} values of 0.16 and 14.90 μA/cm^2. The corresponding i_{corr} of the bare MS and AZ31 samples were 5.56 and 691.8 μA/cm^2. The coated surface remained SHPC even after a severe abrasion test (P800 sandpaper, 100 g, 9 cycles). High chemical stability over a broader pH (1–14) and robust air-exposure durability (6 months) were noted [239]. A few works on different SHPC CNS-based coatings not discussed above also revealed enhanced corrosion resistance [345–347,349,350,364].

3.1.2 Oil separation

Compared to traditional separation methods with low efficiency and selectivity, the unique wettability materials (filtration materials such as meshes/membranes and absorption materials such as sponges/aerogels) are deemed promising for oil/water separation. Significant research efforts are dedicated to fabricating CNM-based SHPC–SOPL or SHPL–SOPC materials in this line [198,277].

CNT-based materials are attractive due to their unique high porosity and interconnected nanopores. Several reports investigated *CNT-only* cases. Fard *et al.* employed high-quality CVD-made CNT packs for oil removal. The sample could hold oil up to 17 times its weight. Higher removal efficiency of ~97% was recorded compared to a commercial counterpart (87%) [198]. Hang *et al.* employed CVD CNT-coated anodized Al template. High oil flux (~300 L/m^2/h/bar) with >99% purity was sustained even after 20 cycles of separation [94]. A 3D porous SiC cellular skeleton with long and aligned CVD-grown MWCNTs was used [69]. A MnO_2 NW/MWCNT hybrid membrane made up by vacuum filtration displayed excellent separation performance (4,900 L/m^2/h/bar with >99.7% efficiency) for surfactant-free and surfactant-stabilized oil/water emulsions. The high separation capacity was maintained even after ten cycles. The filtrate's oil contents were <33 ppm. A simple EtOH cleaning was enough to clean a fouled membrane [222].

Several works employed SHPC/SOPL *composites of CNTs with different organic compounds* such as CNT/PVDF composite porous membrane [146], PFDTS/CNT hybrid membrane [228], and MWCNT/PDMS cotton fabric [211]. Wu *et al.* have studied MWCNT/PDMS membrane fabricated using vacuum filtration through which chloroform quickly permeated, while the surfactant-stabilized water droplets were blocked. The filtrate's oil purity was >99.9 wt% [218]. Makowski *et al.* employed MWCNT-coated and methyltrichlorosilane-modified cotton fabric with a separation efficiency of ~95%. After 30 separation cycles, the efficiency still maintained >90% [210].

SHPC polymer/CNT membrane fabricated *via* covalent linking of PS onto CNT network (Figure 15) displayed a sorption capacity of ~270 times of its weight and that was retained even after ten repetitions. Excellent separation efficiency (~99.9%) and high flux (5,000 L/m^2/h/bar) were recorded for surfactant-stabilized emulsions also. After the sorption process, alcohol rinsing removed the absorbed oil, and the dried membrane at 40°C displayed excellent SHPY [163].

Li *et al.* employed SHPC/SOPL PC/MWCNT monolith with 90.1% porosity, fabricated *via* non-solvent-induced phase separation (Figure 16a–c). The monolith had excellent mechanical properties and can withstand 400 times its weight without any deformation. The saturated adsorption capacity and equilibrium adsorption time recorded with soybean oil were 12.62 g/g and 20 s, respectively (Figure 16d and e). The adsorption capacity maintained at 4.57–6.24 g/g even after ten cycles [214].

Wang *et al.* employed SOPL and under-oil SHPC CNT/poly(vinylidene-fluoride-*co*-hexafluoropropylene) nanofibre membrane and achieved high flux (632.5 L/m^2/h/bar) and separation efficiencies >99.90% for various emulsions [145]. Several works employed SHPL and underwater SOPC composites that include SWCNT/TiO_2 [219], SWCNT/PDA/PEI [216], tannic acid-MWCNTs [365], CNT/CS/TA-FeOOH [217], CNT–core–shell PS/Au [220], CNT/PAA [225], Ag/PAA/CNTs [221], magnetic CNT/PVA [224], and polyzwitterion/TiO_2/PDA/CNT [223].

SHPC and SOPL *CNT-based sponges/aerogels* were employed [203,215]. Several works used commercial *PU sponges* incorporated with CNTs. The monolith's superior mechanical elasticity facilitated easy reuse after multiple absorbing/squeezing cycles [206,208]. Ge *et al.* showed that CNT/SiO_2-coated PU sponge displayed excellent mechanical stability and separation efficiency. No apparent change in saturated adsorption capacity was observed even after five cycles [204]. A PU/MWCNT monolith exhibited an efficiency of 98.4% even after ten cycles of separation. High absorption capacities at the range of 6.9–42.3 g/g were recorded for different oils and solvents [206]. A few studies employed *ML sponges* [208,209]. MWCNT-coated ML sponge using polyphenol–Fe^{3+} adhesive exhibited absorption capacities at the range of 38–127 times of its weight and a separation efficiency of ~97% [208]. LbL covalent grafted CNT/GO on ML foam presented absorption capacity ~113 times its weight and a notable flux of 32.6 L/m^2/s. Instead, PDA grafting resulted in SHPL/

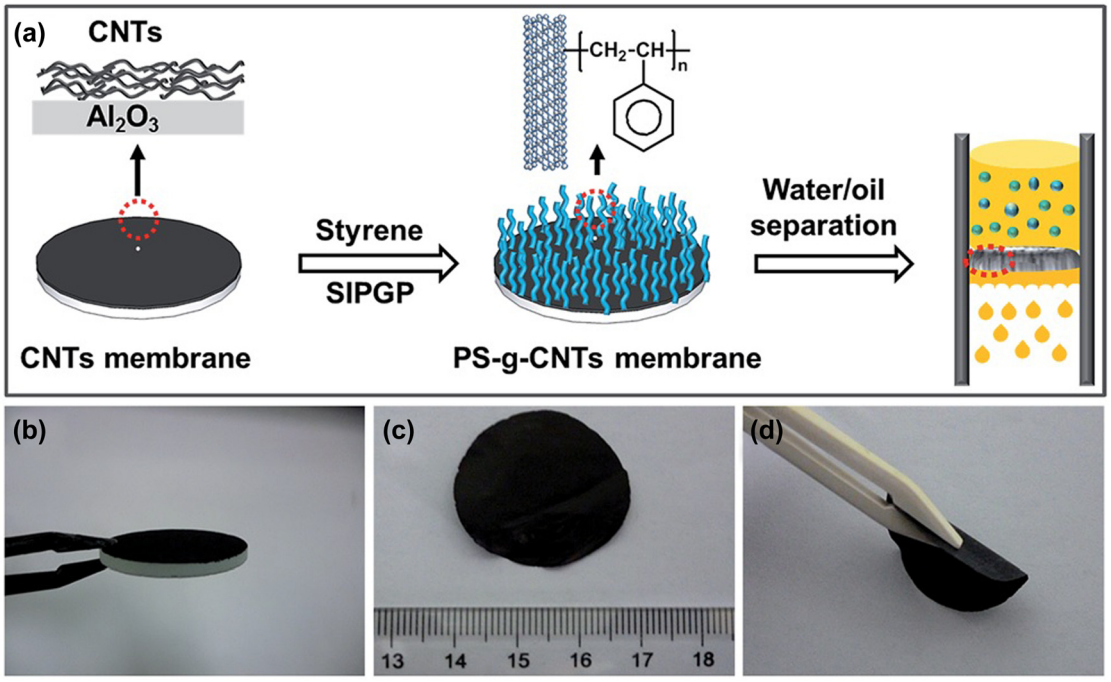

Figure 15: (a) Fabrication scheme of PS/CNT membrane. Photographs of (b) composite on Al_2O_3 membrane substrate, and (c and d) free-standing durable PS/CNT composite membrane after etching Al_2O_3 [163]. Reproduced with permission from ref. [163]; © 2014 The Royal Society of Chemistry.

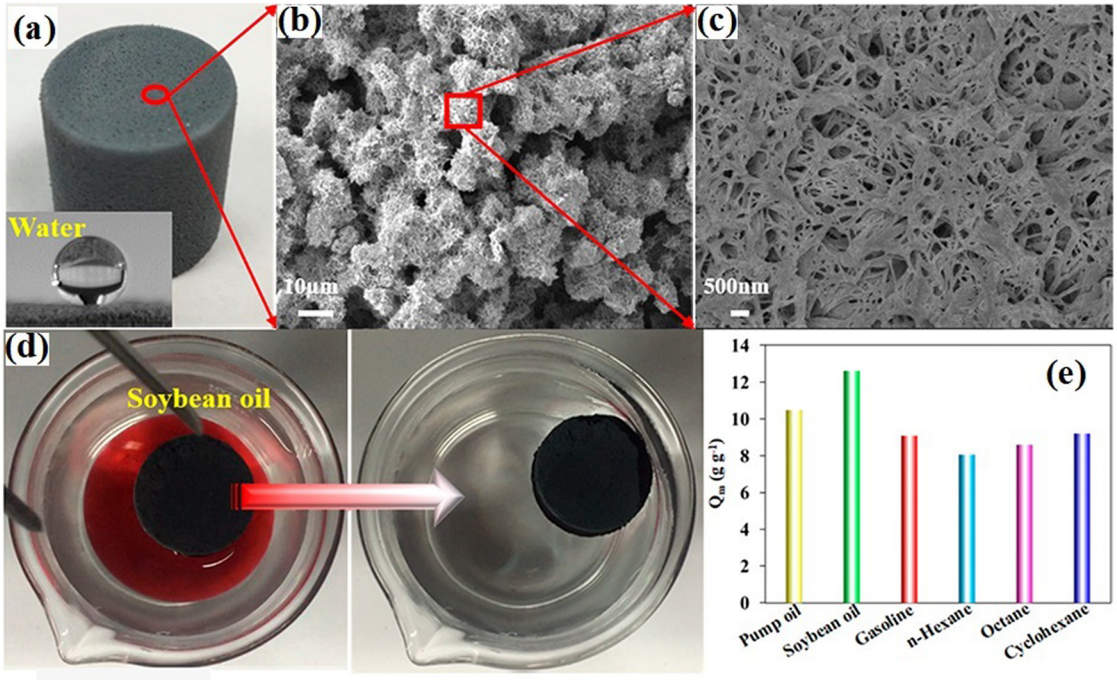

Figure 16: (a) Photograph and (b and c) SEM images of PC/MWCNT monolith. (d) Photographs showing the separation process of oil from water surface. (e) Saturation adsorption capacities for various oils/solvents [214]. Reproduced with permission from ref. [214]; © 2018 American Chemical Society.

underwater SOPC foam with a flux of 19.3 L/m^2/s [506]. *CL sponges* with incorporated CNMs were also used [197,262]. Lu *et al.* employed SHPC/SOPL-reinforced-Et–cellulose sponge prepared by cross-linking Et–cellulose with epichlorohydrin and complexing with silanized CNTs (Si-CNTs) (freeze-drying), followed by SiO_2 NP coating and HDTMS modification (Figure 17). The sponge displayed high porosity (>98%), low density (<20 mg/cm^3), excellent chemical durability (over wider pH), good mechanical strength (withstand 28.6 kPa), and absorption capacity of ~64 times its weight. Even after 50 separation cycles, the absorption capacity was 86.4% [197].

A few reports employed *steel* [90,91,213] *or Cu meshes* [192]. CVD grown VACNTs on SS mesh demonstrated efficiencies >80% [91]. A 2.5 wt% CNT-added PDMS/MWCNT/ZnO-coated Cu mesh presented separation efficiencies >95% with high reusability [192].

SHPC and SOPL CNF-based systems are also widely investigated that include CNF-coated activated CF [248], fluoroacrylic co-polymer-hollow-core CNF conductive film [251], CNF/PDMS nanocomposite prepared by vacuum filtration [254], CNF–PDMS foam [257], and CNF-reinforced PDMS deposited into MR pores *via* vacuum filtration [256]. A few works addressed SHPL and underwater SOPC membranes [260,261,268], and mesh [255]. Several works on different CNS-based systems not discussed above are also available [277,286,311,314,315,325,327,353,356,357,635–641].

3.1.3 Anti-icing

Ice accumulation could significantly decrease the performance of ships, wind turbines, and various other systems. SHPC surfaces are known for their anti-icing properties that can prevent surface ice nucleation. The conductivity and photothermal effect of CNTs are added advantages.

Reports are available on SHPC CNT-only [99,115,199] and CNT-based composite [135,155,174,185,191,218] coatings in anti-icing applications. Rajiv *et al.* showed excellent anti-icing properties for MWCNT/CNF-coated FRP sheet. Ice formation was absent when supercooled water (–20°C) was poured onto the coated surface, whereas rapid ice formation observed on the uncoated plate [115]. Su *et al.* investigated electrothermal and photothermal performances of SHPC ODA/(carboxylated-MWCNTs/aminated-MWCNTs)*n* film (Figure 18a). Under 30 V, the SHPC film quickly (within 60 s) gets heated to 60°C and the ice slides of within 34 s. The ice on the unheated SHPC film was not removed even after 2 min (Figure 18f and g). The film's temperature variation was dependent on the number of bilayers of MWCNTs (Figure 18b). The film maintained SHPY and thermal effect even after several heating/cooling cycles (Figure 18c). [99]. SHPC anti-icing coating was fabricated from peeled MWCNT agglomerates from a milled xerogel [199].

Wu *et al.* employed flexible SHPC PDMS/MWCNT membrane fabricated by vacuum filtration. An ice layer (4 mm) dyed by methylene blue was then prepared on the membrane at –15°C, and a potential of 15 V was applied (vertically fixed, 70% RH, –5°C). Due to the SHPY and the electrothermal conversion effect, the covered ice layer was totally detached from the membrane in 120 s itself [218]. Studies with a composite coating of MWCNTs and silicone rubber showed that the sample retained SHPY under 0°C and the droplet freezes with a CA of ~158°. On shifting the plate to room temperature, the ice melted, and water rolls off rapidly. The SHPY was retained even after 12 times freezing/melting steps. Their ice-accumulation studies showed that the gathered ice on the SHPC

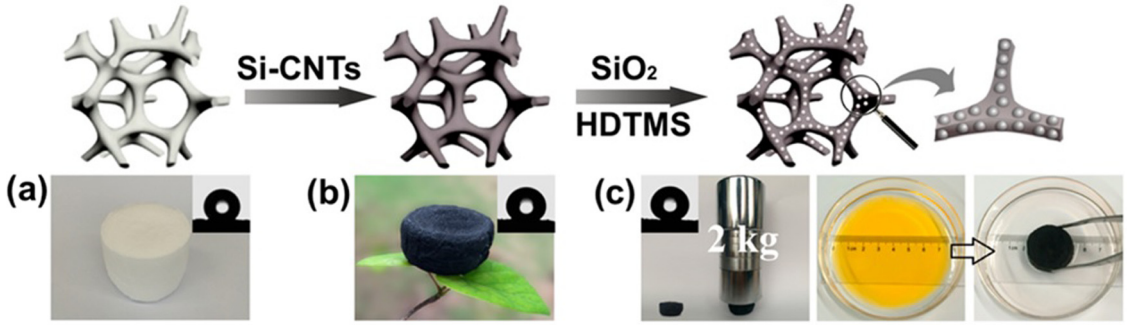

Figure 17: (Top) Schematic of the sponge preparation. (Bottom) Photographs/CAs corresponding to (a) cross-linked Et-cellulose sponge, (b) CNT-reinforced sponge, (c) load-bearing, and oil-absorption tests [197]. Reproduced with permission from ref. [197]; © 2017 American Chemical Society.

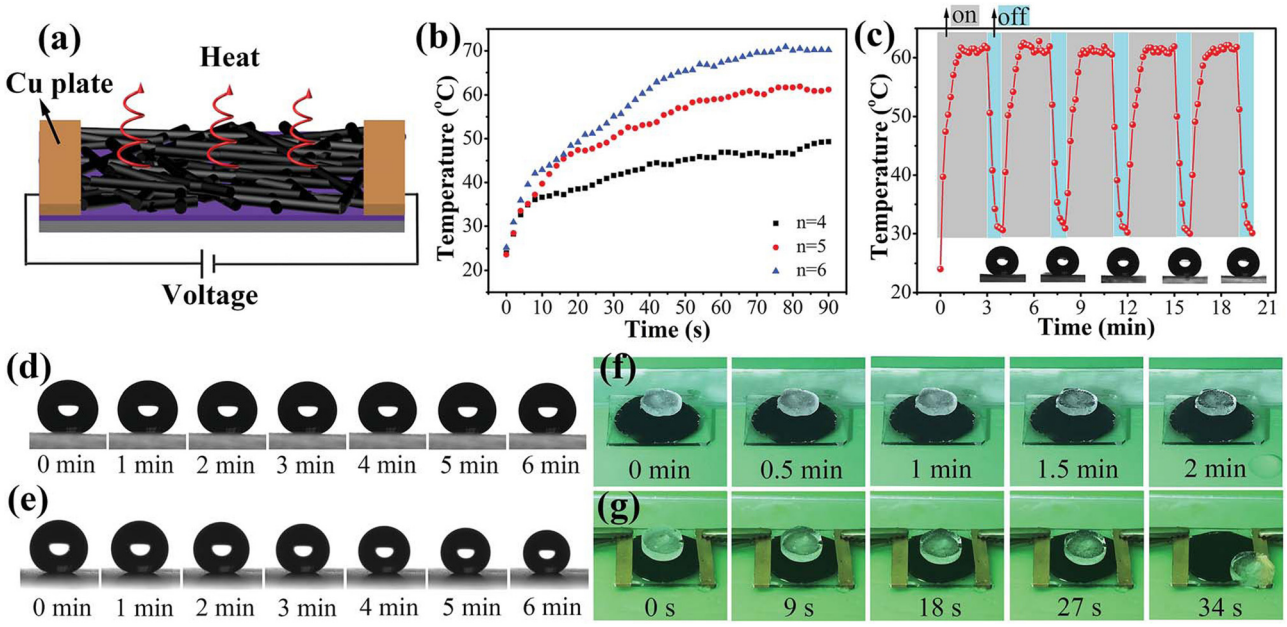

Figure 18: (a) Schematic of heat production of the composite film under applied voltage. (b and c) Temperature variation of the ODA/(carboxylated-MWCNTs/aminated-MWCNTs)*n* film (*n* = 4, 5, 6) with (b) time and (c) repeated heating/cooling cycles. The evolution of droplets (d and f) on unheated SHPC film and (e and g) heated SHPC film at 30 V [99]. Reproduced with permission from ref. [99]; © 2018 The Royal Society of Chemistry.

surface (~0.213 g) was significantly lesser when compared to the ordinary plate (~0.478 g) [174]. Anti-icing studies on spray-coated SiC/CNT coating showed that the water droplet was spherical even after freezing. The ice adhesion strength of the uncoated EVA was 25.65 kPa, while that of the SHPC surface was only 2.65 kPa. With the SHPC surface, the droplet's freezing time increased ~340% to that of the bare (from 15 to 66 s) [185]. Zhu *et al.* studied icing time of a spray-coated ZnO/MWCNT/PDMS film on various substrates at −6°C. The freezing time of the droplet on uncoated and coated SiR substrates were 150 and 300 s, respectively. The superior effect was explained because of the reduced droplet/surface contact area and the hindered heat transfer due to the air layer [191]. Remarkable anti-icing properties were also reported with EP/MWCNTs [155], flame-synthesized amorphous carbon NP-based [308], and CNT/adhesive polymer/SiO_2 [135] coatings.

3.1.4 Anti-biofouling/biomedical

SHPC surfaces are highly desirable for anti-bacterial/anti-biofouling applications for marine equipment, biomedical implants *etc.* [275]. Both SHPC and SHPL surfaces are shown to be effective in minimizing microbial adhesion. Yoon *et al.* compared the extent of bacteria adherence on SHPC and SHPL coatings (fabricated *via* annealing SS plates coated with CNT–PTFE and TiO_2, respectively) under different fluid flow conditions. Fluorescence intensities of adhered *E. coli* on SHPC and SHPL surfaces were ~80% and 65% lower than that of the bare sample. For the SHPL surface, the readily spread out water could form a tightly bound layer. It could act as a lubricating film or water shield, lessening the foulant/surface electrostatic attraction. On the other hand, SHPY and self-cleaning attributes were decisive in determining the property enhancement of the SHPC surface. The results were further confirmed by aerobic plate count data (Figure 19). The bacterial attachment was considerably affected by the wall shear rate as well (Figure 19). The upsurge of flow rates resulted in reduced bacteria adherence [124].

Mittal *et al.* have shown that SHPC mesoporous carbon-nanocapsule/PVDF coating rarely contained *E. coli* bacterial colonies. More than 90% decline of bacterial attachment was observed [275]. Song *et al.* revealed excellent anti-microbial property for a fluorosilane-modified nanohybrid membrane based on chitosan matrix, cationic chitosan, MWCNTs, and silane coupling additive [144]. A nanocomposite film made up using CNT/Ag/PTFE composite target also showed similar results where the surface SHPY and the Ag NPs's anti-microbial effect provided positive effect and suppressed the bacterial

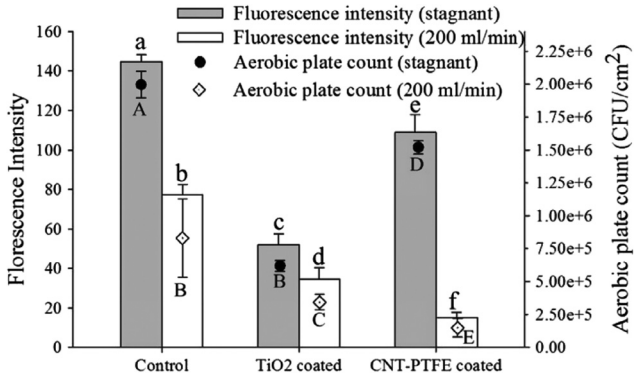

Figure 19: Fluorescence intensities and aerobic plate counts. The significant differences corresponding to fluorescence intensity and aerobic plate count measurements are indicated by lower and uppercase letters [124]. Reproduced with permission from ref. [124]; © 2013 Elsevier Ltd.

growth/proliferation [642]. Ionic liquid-functionalized MWCNT coatings were studied as antibacterial coatings by Bains *et al.* [173].

SHPC surfaces with immobilized CNFs are shown to be excellent hemostatic materials. The CNFs encouraged rapid fibrin growth and clotting. The SHPC surface severely limited blood wetting and radically diminished bacteria adhesion. The clot detachment was also easy [258]. Marcon *et al.* achieved selective cell patterning on SHPC–SHPL patterns on diamond NW surfaces [285]. A few reports addressed SHPC CNS-based coatings for microfluidics applications [643]. Several works explored CNS-based anti-biofouling desalination membranes [231,232,341,644,645].

3.1.5 Others

A few works focused on various *sensor applications* such as CNT/PDMS-modified cotton woven fabrics for pressure/strain sensor [109,210–212], LbL spray-coated APTES/MWCNT-GR/PDMS and further decorated with Ag NPs and PFOS for strain sensor [430], paper-based strain sensor *via* successive dip coating in CNT/CB/methylcellulose and fumed-SiO_2 suspensions [175], MWCNT/poly(ethylene-*co*-vinyl acetate) for underwater vibration detection [172], SHPL and SOPC CNT/PU-based humidity/vapour sensor [646], sandwich-like film consisting of thermoplastic elastomer, MWCNT and PDMS as wearable sensor [137], and conductive PDMS/CNF/PU nanofibre composite for chemical vapour sensor [260].

SHPC CNS materials are also studied for various other applications such as electrocatalysts [187,647], supercapacitors [331], EMI shielding [250,252], gas diffusion electrodes [336], and others [116,294,648].

3.2 Graphene

3.2.1 Anti-corrosion

GR-only and GR-based composite SHPC anti-corrosion coatings are widely investigated. As discussed in Section 2.1, GR-based composite coatings could provide a more effective barrier effect and reduced coating cracking. However, the graphite's more noble position in the electrochemical series can harm the base metal at localized defects. More details of anti-corrosion GR coatings are described elsewhere [649–653]. As discussed earlier, SHPC surfaces always presented better corrosion resistance than the bare surface. This section briefs reported works on SHPC GR-based anti-corrosion coatings based on the coating deposition method used.

3.2.1.1 Electrodeposited coatings

ED is a simple approach in fabricating protective coatings [622,654]. GR-based SHPC and self-cleaning anti-corrosion coatings fabricated by ED displayed superior corrosion resistance that includes reduced GR coating on Cu [407], carbon-based film doped with GO and Co on Si [460], MA-modified Ni/GR hybrid film on MS [456], Ni-RGO-MA coating on CS [457], and RGO/Ni coating on SS [458]. Yan *et al.* showed that GO and Co were well embedded in the amorphous carbon matrix and the SHPC film displayed better protection at a GO doping concentration of 0.007 mg/mL [460]. Jena *et al.* achieved good adhesion and mechanical stability of the fabricated SHPC coating by a phosphate pre-treatment. The SHPC sample presented ~2 orders reduced i_{corr} and ~3 orders higher EIS impedance when compared to the bare [457]. Bai *et al.* showed that ED RGO/Ni composite coating on SS showed more than 99.9% protection in 3.5 wt% NaCl [458]. A novel SHPC GR/amorphous carbon/Ni film fabricated by high-voltage non-aqueous ED also displayed superior corrosion resistance [459].

3.2.1.2 Solution/spin coatings

A facile design of ternary nanocomposite of PDMS/GO nanosheets with ZnO NRs was studied for steel. GO–ZnO hybrid nanofiller was synthesized using one-step chemical bath deposition, and the nanocomposite coating was fabricated by solution casting. The dried and cured coating with 1 wt% of GO–ZnO addition provided the best protection [445]. Liu *et al.* reported a spin-coated SHPC GR

film with excellent corrosion protection for Al alloys [382]. Abbas *et al.* described a drop-coated fluorinated GR coating on Cu with an insignificant decrease of CA in 3.5 wt% NaCl [411]. A homogeneous SHPC coating was made on Zn using EtOH–xylene solution of HDPE containing 1–5 wt% of GO *via* drop coating. A 5 wt% GR-incorporated SHPC film provided adequate corrosion protection during continuous immersion in 3 wt% NaCl for up to 29 days [486]. Liquid-phase exfoliated fluoro-GR nanosheets were spatially trapped on the surface of EP resin coating. The fabrication process consisted of two steps, dip coating in EP resin/curing agent and then surface fixing the fluoro-GR nanosheets (fluoro-GR powder dispersed on the EP coating' surface and pressurized using ~10 g/cm^2 weight). The coating displayed superior protection for Cu [655]. PFDTS-modified GO/Cu silicate coating also showed excellent anti-corrosion property [444].

3.2.1.3 Spraying/painting

POSS-modified GO's proper blending could significantly enhance the anti-corrosion capability of EP-based coatings [484]. A 0.5 wt% POSS-GO-incorporated EP coating presented ~2 orders of greater impedance than pure EP coating after 150 days of immersion in 3.5 wt% NaCl, and that was ascribed to the combined effect of barrier protection, self-lubrication effect, and improved mechanical properties [481]. Zhang *et al.* studied electrostatic-sprayed EP-PTFE/GP-SiO_2-PFOS coating on steel. The GR-PDA (GP)/SiO_2 interfacial strength was enhanced by *in situ* growth of SiO_2 on the GP surface by utilizing dopamine self-polymerization and sol–gel methods. The surface was further modified by PFOS. The resultant SHPC coating survived more than 105 abrasion cycles with significantly less weight loss (54.4 mg). The SHPY was maintained even after 60 days of immersion in 3.5 wt% NaCl [483]. A simple painted SHPC surface with a mixture of electrochemically exfoliated GR and PDMS showed 8,868-fold reduced i_{corr} than the bare Al sample [420]. Nine *et al.* presented a method to make GR-based SHPC composite anti-corrosion coating with a formulation of RGO, PDMS-modified diatomaceous earth, and TiO_2 NPs [440]. A fluorosilane-modified-GR incorporated siloxane-acrylic coating also displayed excellent corrosion resistance [494].

3.2.2 Oil separation

3D GR sponges and aerogels are known for their distinctive properties of SHPY, low density, high porosity, high specific surface area, excellent irradiation robustness, and thermal/chemical durability [507,521]. As discussed in the previous sections, composite formation is the preferred strategy to enhance such aerogels' hydrophobicity and mechanical property. Several works showed that neat/doped/fluorosilane-modified GR sponges/aerogels displayed first-rate absorption capacity for various solvents/oils [512,516,517,524–528,534,546,569,579,621,656,657]. Excellent performances were also revealed by various SHPC and SOPL composite sponges/aerogels/monoliths/membranes such as MWCNT–GR [203], GO/PAA [530], N-doped CF/RGO [535], fluorosilane/GO/agarose [537], PFDT-modified and chitosan-reinforced-RGO/PDA [658], GR/PVDF [520,523,533], GR/PDMS [508,529,541], GR/PTFE [509,538,539], GR/PBS [515], GO/lignin [536], Au NP-loaded GR modified with PFDT [556], EP-functionalized POSS/GO [564], RGO–PDA functionalized with PFDT [612], RGO/PS monolith [561], RGO/PC monolith [562], GR/MOF-based composites [463,500,518,557,609,613,661–663], and others [499,608,659,660].

Several studies employed neat or fluorosilane-modified *PU/GR* systems [510,555,563,566–570,572,573] as well as their multi-component composites as discussed in Section 2.7.3. *ML/GR* [511,209,581–586,592,595] and their various nanocomposites, including soot-RGO/ML [514], ODA/RGO/ML [588], PDMS/GR/ML [587], HDTMS/RGO/ML [589], kaolinite-modified GO/ML [591], magnetic Fe_3O_4 NP-decorated-RGO/ML [590]. RGO-TiO_2/ML [593], and MOF/RGO/ML [464] were investigated. A study on SHPC GR-based carrageenan sponge [594] and a few works on SHPL/oleophobic sponge [577] are also available. A few works explored *CL/GR* [664,665] and their composites, namely, PBZ/RGO-wrapped-CL [580], GO/cellulose-nanofibril/SiO_2 [531], cellulose nanofibre/PVA/GO [545], nanofibrillated cellulose/PEI/RGO [547], cellulose nanofibre-GO/glucose–kaolin [666], GO/microcrystalline-cellulose complex [667], konjac glucomannan/RGO [597], and silane-modified-GO/kapok fibre [596].

GR-coated cotton/fabric is shown to be a good oil absorbent material [549]. Several reports in this line are available, including RGO-coated cotton prepared by dip coating/thermal reduction/silane modification [551,553,610], one-step-HT-made RGO/cotton [554], dip-coated/HT-reduced RGO/cotton [552], hot-iron-treated-GO sprayed fabric [611], trimethoxysilane-modified-GO/PDMS/polyester [559], and SiO_2-GO/PP [558]. A few works employed steel *mesh* [598–604], Cu mesh, janus wire mesh, or Ni foam [511,605–607].

3.2.3 Others

A significant number of reports are available on SHPC GR in *biomedical* applications such as anti-bacterial/antibiofouling coating [402,438,451], anti-thrombogenic coating

[668], bioactive coating [669], microfluidics [381,392], and photo-sterilizable/reusable mask [393,403]. Several works addressed *anti-icing* coatings [410,417,441–443, 670,671].

A number of reports addressed different types of *sensors* such as temperature/strain/pressure [384,408,424, 439,476,478,493,497,498,532,542–544,674], underwater [426], UV [452], and gas [401,453]. A few works aimed for various applications such as supercapacitors [395,519, 656,672], flame-retardant coatings [462,480], protective layer for solar module [475], photothermal energy conversion [502], electrocatalysts [540], and anti-scaling coating [673].

4 Conclusions and perspectives

Here, we have provided a comprehensive review of CNS-based SHPC surfaces and coatings. SHPC composites/hybrids of CNSs with metals, ceramics, and polymers are detailed. SOPC and SAPC surfaces are also included. Works reported in specific applications areas are presented separately. All the information available in this area is systematically classified and presented.

Among the different SHPC CNSs, the most investigated is GR, and the second most is CNTs. The present review mainly focuses on CNT- and CNF-based SHPC surfaces. Both aligned and non-aligned CNT arrays/coatings and their various composites/hybrids are presented. Works reported on sponge, foam, aerogel, fabric, mesh, and membrane-based systems are discussed separately. Due to the availability of a few reviews, the section on GR is presented concisely. The idea was to provide an overall outlook on the research trends in the entire domain of CNS-based SHPC surfaces.

The higher surface roughness with nano and micro (aggregates) scale hierarchical surface structuring is highly beneficial for SHPY. Surface reduction processes (removal of hydrophilic surface groups) and low SE component/treatment enhance it. CNM-based polymer composite coatings are well known for their multi-functionalities such as conductivity, photothermal effect, superior mechanical/thermal/chemical durability, barrier protection, and several others. A durable SHPC surface could enhance the device performance in several applications, as discussed in this review.

Earlier studies, before 2005, were focused on fabricating SHPC VACNT arrays. Although the high-temperature reduction associated with the CVD process and the enhanced surface roughness of the CNT arrays could make an SHPC surface, the durability gets compromised with time as the droplets can eventually seep into the inter-spaces. Later studies categorically proved that durable SHPC VACNTs could be realized *via* an additional low SE polymer modification to alleviate the water ingression. VACNTs fabricated by Si or SiC template-assisted methods also displayed excellent durability against water ingression, which were closely dependent on the template structural parameters. Later studies proved that a simple vacuum annealing treatment could be enough to regain the SHPY of ACNT arrays. Several studies, however, showed that the as-grown ACNTs had high SA/CAH values leading to water pinning. An optimized high-temperature treatment or a low SE modification could reduce the SA to the desired limit of self-cleaning surfaces. Several attempts were made *via* nanocomposite/hybrid formation with other CNMs, ceramic oxides, and polymers to enhance the durability further. All these studies support that such an additional modification is mandatory to achieve long-term durable SHPC VACNT arrays. The most used method for the CNT's fabrication is indeed CVD. A few works attempted EPD.

Since 2006, researchers started exploring non-aligned SHPC CNT coatings with superior durability. Other than CVD, several fabrication methods, including vacuum filtering, spray coating, drop/dip coating, laser-assisted approaches, sintering approaches, and pressing, were employed in making CNT-based SHPC surfaces. Quite a few studies demonstrated SHPY without added low SE component or high-temperature annealing. However, most works employed a low SE component in the formulation or a post-low SE treatment. Some studies used a combined vacuum filtration-LbL assembly to fabricate SHPC membranes/papers. Many works were dedicated to nanocomposite polymer coatings where CNTs were used as fillers to the polymeric matrix. The aspect ratio and the concentration of the CNTs were decisive for the property enhancement. One of the widely studied systems is CNT–PDMS. A significant number of reports are available on PU, EP, and PS-based nanocomposite coatings. Spray coating is perhaps the best method in making highly robust CNT/polymer-based coatings. Several studies showed that superior durability was achieved only after a high-temperature curing. A few studies used CNTs as templates. There exist further scopes for the fabrication of nanocomposites of CNTs with several other polymers and ceramic oxides. More studies can be focused on flexible SHPC surfaces. For practical applications of SHPC CNT-based coatings, it is desirable to further enhance the durability against severe mechanical abrasion and longer-term water immersion.

A number of reports are available on SHPC hybrids and composites of CNTs with different ceramic oxides and metals such as SiO_2, SiC, Al_2O_3, Co_3O_4, WO_3, ZnO, Ni, and Co. The most used is SiO_2. A significant extent of works are available on SHPC and SOPL or SHPL and SOPC CNT-based foams, sponges, aerogels, meshes, and membranes. Several studies focused on developing CNT-incorporated commercial sponges with improved mechanical properties and durability. More works can be focused on composites of eco-friendly and abundant materials such as CL sponges. MOF-based systems can be further explored.

SHPC CNF-based systems displayed exceptional chemical and mechanical durability. The research trend is similar to CNTs; however, the quantum of reported works is significantly less. A few earlier reports, before 2010, addressed SHPC vertically aligned CNFs. Most of the works explored CNFs as fillers in organic coatings. Several studies presented CNF-added foams and aerogels. A preferred combination is CNF/PDMS/PU. The superb durability of such systems was attributed to the robust interfacial adhesion, where the PDMS could act as an effective interfacial adhesion agent and waterproof protective layer. Different hybrids of CNFs with ceramic oxides and metals were also explored. A few studies addressed SHPC surfaces based on carbon nanospheres. HT-synthesized or soot-based carbon nanospheres were mainly employed. Like CNTs, an optimized mixed structure of CNFs with carbon spheres could yield enhanced hydrophobicity. A few works are available on SHPC carbon nanothorn array, tree-like carbon nanospheres, CMFs, and onion-like carbon microspheres. Excellent durability during long-term water immersion up to 800 days was noted. All these areas, however, demand more works to arrive at precise decisions and products.

A few works are available on nanodiamond. The typically used method of fabrication is reactive ion etching followed by fluorination. Several works addressed SHPC fullerenes. The most employed fabrication strategy utilized with fullerenes is molecular self-assembly. The review also provided a concise description of SPHC surfaces of nanostructured carbon soots, graphitic carbons, CB, carbon aerogels, and their various composites.

A detailed discussion of SHPC graphene is out of the scope of this review. However, all the information available in this area have been comprehensively collected, systematically classified, and briefly presented. A significantly higher number of reports are available on SHPC GR and their various composite coatings with silanes/fluorosilanes, PU, and EP. More works can be focused on PS, polyethylene, and polypropylene systems. Among the silanes/fluorosilanes, the trend was similar to that of CNTs; the most investigated was GR–PDMS, followed by GR–PVDF. Several works explored SHPC composites of GR with other CNSs, ceramic oxides and metals. Many reports are available on GR-based composite sponges, aerogels, and monoliths. Eco-friendly and naturally abundant materials can be explored with GR in this line. GR Qdots could be explored.

CNSs, in particular GR-based coatings, were widely investigated for anti-corrosion applications. Due to the potential galvanic effect, more studies are desirable in this direction to arrive at precise conclusions. The long-term durability of such surfaces in aggressive chloride and acidic solutions needs to be further improved. Significant data are available on CNS-based materials for oil separation applications. This is an area explored to a great extent. A few reports are dedicated to biomedical, anti-icing, sensors, and several other applications. There exists high scope for further research in these areas.

Despite the extensive information available, as discussed in this review, further in-depth studies and pilot plant experiments are required to widespread practical usage of SHPC CNMs in different applications. Areas to be further improved are the mechanical and chemical durability of such SHPC surfaces in extreme exposure conditions for longer durations. Systematic studies are demanding the development of protocols and standards for commercial products.

Funding information: The author would like to acknowledge the support and fund provided by King Fahd University of Petroleum & Minerals (KFUPM), Saudi Arabia.

Author contribution: The author has accepted responsibility for the entire content of this manuscript and approved its submission.

Conflict of interest: The author states no conflict of interest.

Abbreviations

ACNT	aligned CNT
CA	contact angle
CAH	contact angle hysteresis
CB	carbon black
CF	carbon fibre
CL	cellulose
CMF	carbon microflower
CNF	carbon nanofibre

CNM	carbon nanomaterial
CNS	carbon nanostructure
CNT	carbon nanotube
CS	carbon steel
CVD	chemical vapour deposition
DLC	diamond-like carbon
ED	electrodeposition
EIS	electrochemical impedance spectroscopy
EMI	electromagnetic interference
EP	epoxy
EPD	electrophoretic deposition
FEP	fluorinated ethylene propylene
GO	graphene oxide
GR	graphene
HDTMS	hexadecyltrimethoxysilane
HT	hydrothermal
LbL	layer-by-layer
MA	myristic acid
ML	melamine
MOF	metal-organic framework
MR	metal rubber
MS	mild steel
MWCNT	multi-walled CNT
NP	nanoparticle
NR	nanorod
NT	nanotube
NW	nanowire
ODA	octadecylamine
PAA	polyacrylic acid
PANI	polyaniline
PBZ	polybenzoxazine
PC	polycarbonate
PDA	polydopamine
PDMS	polydimethylsiloxane
PDP	potentiodynamic polarization
PEI	polyethylenimine
PFDT	1*H*,1*H*,2*H*,2*H*-perfluorodecanethiol
PFDTS	1*H*,1*H*,2*H*,2*H*-perfluorodecyltriethoxysilane
PFOS	1*H*,1*H*,2*H*,2*H*-perfluorooctyltriethoxysilane
PFTS	1*H*,1*H*,2*H*,2*H*-perfluorodecyltrichlorosilane
POSS	polyhedral oligomeric silsesquioxane
PPS	polyphenylene sulphide
PS	polystyrene
PTFE	polytetrafluoroethylene
PU	polyurethane
PVA	polyvinyl alcohol
PVDF	polyvinylidene fluoride
RGO	reduced graphene oxide
SA	sliding angle
SAPC	superamphiphobic
SAPY	superamphiphobicity
SE	surface energy
SHLY	superhydrophilicity
SHPC	superhydrophobic
SHPL	superhydrophilic
SHPY	superhydrophobicity
SiR	silicone resin
SNT	SiO_2 nanotubes
SOLY	superoleophilicity
SOPC	superoleophobic
SOPL	superoleophilic
SOPY	superoleophobicity
SS	stainless steel
STA	stearic acid
SWCNT	single-walled CNT
TEOS	tetraethoxysilane
THF	tetrahydrofuran
TMSS	trimethylsiloxysilicate
VACNT	vertically aligned CNT
Wn	weber number

References

[1] Schur DV, Zaginaichenko SY. Carbon Nanostructured Materials – I, Nanoscience and Nanotechnologies, Encyclopedia of Life Support Systems. UNESCO-EOLSS. Paris, France: Eolss Publishers.

[2] Tasis D, Tagmatarchis N, Bianco A, Prato M. Chemistry of carbon nanotubes. Chem Rev. 2006;106:1105–36.

[3] Allen MJ, Tung VC, Kaner RB. Honeycomb carbon: a review of graphene. Chem Rev. 2010;110:132–45.

[4] American Chemical Society National Historic Chemical Landmarks. Discovery of fullerenes. http://www.acs.org/content/acs/en/education/whatischemistry/landmarks/fullerenes.html (accessed 15 June 2021).

[5] Iijima S. Helical microtubules of graphitic carbon. Nature. 1991;354:56–8.

[6] Iijima S, Ichihashi T. Single-shell carbon nanotubes of 1-nm diameter. Nature. 1993;363:603–5.

[7] Geim AK, Novoselov KS. The rise of graphene. Nature Mater. 2007;6:183–91.

[8] Novoselov KS, Geim AK, Morozov SV, Jiang D, Zhang Y, Dubonos SA, et al. Electric field effect in atomically thin carbon films. Science. 2004;306:666–9.

[9] Yang Z, Tian J, Yin Z, Cui C, Qian W, Wei F. Carbon nanotubes-and graphene-based nanomaterials and applications in high-voltage supercapacitor: a review. Carbon. 2019;141:467–80.

[10] Baldelli A, Ou J, Li W, Amirfazli A. Spray-on nanocomposite coatings: wettability and conductivity. Langmuir. 2020;36:11393–410.

[11] Taherian F, Marcon V, van der Vegt NFA, Leroy F. What is the contact angle of water on graphene? Langmuir. 2013;29:1457–65.

[12] Roh SC, Choi EY, Choi YS, Kim CK. Characterization of the surface energies of functionalized multi-walled carbon nanotubes and their interfacial adhesion energies with various polymers. Polymer. 2014;55:1527–36.
[13] Wang S, Zhang Y, Abidi N, Cabrales L. Wettability and surface free energy of graphene films. Langmuir. 2009;25:11078–81.
[14] Barthlott W, Neinhuis C. Purity of the sacred lotus, or escape from contamination in biological surfaces. Planta. 1997;202:1–8.
[15] Neinhuis C, Barthlott W. Characterization and distribution of water-repellent, self-cleaning plant surfaces. Ann Bot. 1997;79:667–77.
[16] Koch K, Barthlott W. Superhydrophobic and superhydrophilic plant surfaces: an inspiration for biomimetic materials. Phil Trans R Soc A. 2009;367:1487–509.
[17] Darmanin T, Guittard F. Superhydrophobic and superoleophobic properties in nature. Mater Today. 2015;18:273–85.
[18] Barthlott W, Mail M, Bhushan B, Koch K. Plant surfaces: structures and functions for biomimetic innovations. Nano-Micro Lett. 2017;9:23.
[19] Webb HK, Crawford RJ, Ivanova EP. Wettability of natural superhydrophobic surfaces. Adv Colloid Interface Sci. 2014;210:58–64.
[20] Wang S, Liu K, Yao X, Jiang L. Bioinspired surfaces with superwettability: new insight on theory, design, and applications. Chem Rev. 2015;115:8230–93.
[21] Jiaqiang E, Jin Y, Deng Y, Zuo W, Zhao X, Han D, et al. Wetting models and working mechanisms of typical surfaces existing in nature and their application on superhydrophobic surfaces: a review. Adv Mater Interfaces. 2018;5:1701052.
[22] Cassie ABD, Baxter S. Wettability of porous surfaces. Trans Faraday Soc. 1944;40:546–51.
[23] Timmons CO, Zisman WA. Effect of liquid structure on contact angle hysteresis. J Colloid Interface Sci. 1966;22:165–71.
[24] Feng L, Li S, Li Y, Li H, Zhang I, Zhai J, et al. Super-hydrophobic surfaces: from natural to artificial. Adv Mater. 2002;14:1857–60.
[25] Su B, Tian Y, Jiang L. Bioinspired interfaces with superwettability: from materials to chemistry. J Am Chem Soc. 2016;138:1727–48.
[26] Shirtcliffe NJ, McHale G, Atherton S, Newton MI. An introduction to superhydrophobicity. Adv Colloid Interface Sci. 2010;161:124–38.
[27] Valipour N, Birjandi FC, Sargolzaei J. Super-non-wettable surfaces: a review. Colloids Surf A. 2014;448:93–106.
[28] Scarratt LRJ, Steiner U, Neto C. A review on the mechanical and thermodynamic robustness of superhydrophobic surfaces. Adv Colloid Interface Sci. 2017;246:133–52.
[29] Saji VS. Wax-based artificial superhydrophobic surfaces and coatings. Colloid Surf A. 2020;602:125132.
[30] Saji VS. Superhydrophobic surfaces and coatings by electrochemical anodic oxidation and plasma electrolytic oxidation. Adv Colloid Interface Sci. 2020;283:102245.
[31] Saji VS. Recent progress in superhydrophobic and superamphiphobic coatings for magnesium and its alloys. J Magnes Alloy. 2021. doi: 10.1016/j.jma.2021.01.005.
[32] Saji VS. Electrophoretic-deposited superhydrophobic coatings. Chem Asian J. 2021;16:474–91.
[33] Young T. An essay on the cohesion of fluid. Philos Trans R Soc. 1805;95:65–87.
[34] Wenzel RN. Resistance of solid surfaces to wetting by water. Ind Eng Chem. 1936;28:988–94.
[35] Whyman G, Bormashenko E, Stein T. The rigorous derivation of Young, Cassie–Baxter and Wenzel equations and the analysis of the contact angle hysteresis phenomenon. Chem Phys Lett. 2008;450:355–9.
[36] Chen Z, Dong L, Yang D, Lu H. Superhydrophobic graphene-based materials: surface construction and functional applications. Adv Mater. 2013;25:5352–9.
[37] Wang JN, Zhang YL, Liu Y, Zheng W, Lee LP, Sun HB. Recent developments in superhydrophobic graphene and graphene -related materials: from preparation to potential applications. Nanoscale. 2015;7:7101–14.
[38] Gupta S, Tai NH. Carbon materials as oil sorbents: a review on the synthesis and performance. J Mater Chem A. 2016;4:1550–65.
[39] Liu YQ, Zhang YL, Liu Y, Jiang HB, Han DD, Han B, et al. Surface and interface engineering of graphene oxide films by controllable photoreduction. Chemical Record. 2016;16:1244–55.
[40] Khan A, Habib MR, Kumar RR, Islam SM, Arivazhagan V, Salman M, et al. Wetting behaviors and applications of metal-catalyzed CVD grown graphene. J Mater Chem A. 2018;6:22437–64.
[41] Li MT, Liu M, Yu YH, Li AW, Sun HB. Laser-structured graphene/reduced graphene oxide films towards bio-inspired superhydrophobic surfaces. Bull Chem Soc Jp. 2019;92:283–9.
[42] Jishnu A, Jayan JS, Saritha A, Sethulekshmi AS, Venu G. Superhydrophobic graphene-based materials with self-cleaning and anticorrosion performance: an appraisal of neoteric advancement and future perspectives. Colloids Surf A. 2020;606:125395.
[43] Sharma V, Sharma V, Goyat MS, Hooda A, Pandey JK, Kumar A, et al. Recent progress in nano-oxides and carbon nanotubes based corrosion resistant superhydrophobic coatings: a critical review. Prog Org Coat. 2020;140:105512.
[44] Ma ZC, Li CH, Hu XY, Han B, Zhang YL, Chen QD, et al. Laser fabrication of bioinspired graphene surfaces with superwettability. Front Chem. 2020;8:525.
[45] Kausar A. Polydimethylsiloxane-based nanocomposite: present research scenario and emergent future trends. Polym Plast Technol Mater. 2020;59:1148–66.
[46] Seth M, Jana S. Nanomaterials based superhydrophobic and antimicrobial coatings. NanoWorld J. 2020;6:26–9.
[47] Han JT, Kim SY, Woo JS, Lee GW. Transparent, conductive, and superhydrophobic films from stabilized carbon nanotube/silane sol mixture solution. Adv Mater. 2008;20:3724–7.
[48] Jung YC, Bhushan B. Mechanically durable carbon nanotube-composite hierarchical structures with superhydrophobicity, self-cleaning, and low-drag. ACS Nano. 2009;3:4155–63.
[49] Li BC, Zhang JP. Polysiloxane/multiwalled carbon nanotubes nanocomposites and their applications as ultrastable, healable and superhydrophobic coatings. Carbon. 2015;93:648–58.
[50] Dai HJ. Carbon nanotubes: synthesis, integration, and properties. Acc Chem Res. 2002;35:1035–44.

[51] Gooding JJ, Wibowo R, Liu J, Yang W, Losic D, Orbons S, et al. Protein electrochemistry using aligned carbon nanotube arrays. J Am Chem Soc. 2003;125:9006–7.
[52] Lau KKS, Bico J, Teo KBK, Chhowalla M, Amaratunga GAJ, Milne WI, et al. superhydrophobic carbon nanotube forests. Nano Lett. 2003;3:1701–5.
[53] Sun T, Feng L, Gao X, Jiang L. Bioinspired surfaces with special wettability. Acc Chem Res. 2005;38:644–52.
[54] Liu H, Zhai J, Jiang L. Wetting and anti-wetting on aligned carbon nanotube films. Soft Matter. 2006;2:811–21.
[55] Wang Z, Koratkar N, Ci L, Ajayan PM. Combined micro-/nanoscale surface roughness for enhanced hydrophobic stability in carbon nanotube arrays. Appl Phys Lett. 2007;90:143117.
[56] Wang Z, Lopez C, Hirsa A, Koratkar N. Impact dynamics and rebound of water droplets on superhydrophobic carbon nanotube arrays. Appl Phys Lett. 2007;91:023105/1–3.
[57] Aria AI, Gharib M. Physicochemical characteristics and droplet impact dynamics of superhydrophobic carbon nanotube arrays. Langmuir. 2014;30:6780–90.
[58] Li H, Wang X, Song Y, Liu Y, Li Q, Jiang L, et al. Super-"amphiphobic" aligned carbon nanotube films. Angew Chem. 2001;113:1793–6.
[59] Aria AI, Beizai M, Gharib M. Simple method for producing superhydrophobic carbon nanotube array. WO2011127207A2; 2011.
[60] Li S, Li H, Wang X, Song Y, Liu Y, Jiang L, et al. Superhydrophobicity of large-area honeycomb-like aligned carbon nanotubes. J Phys Chem. 2002;106:9274–6.
[61] Sun T, Liu H, Song W, Wang X, Jiang L, Li L, et al. Responsive aligned carbon nanotubes. Angew Chem Int Ed. 2004;43:4663–6.
[62] Xu D, Liu H, Yang L, Wang Z. Fabrication of superhydrophobic surfaces with non-aligned alkyl-modified multi-wall carbon nanotubes. Carbon. 2006;44:3226–31.
[63] Sun T, Wang G, Liu H, Feng L, Jiang L, Zhu D. Control over the wettability of an aligned carbon nanotube film. J Am Chem Soc. 2003;125:14996–7.
[64] Qu J, Zhao Z, Qiu J, Gogotsi Y. Self-assembly of carbon nanotube polyhedrons inside microchannels. Chem Commun. 2008;24:2747–9.
[65] Lu SH, Tun MHN, Mei ZJ, Chia GH, Lim X, Sow CH. Improved hydrophobicity of carbon nanotube arrays with micropatterning. Langmuir. 2009;25:12806–11.
[66] Ramos SC, Vasconcelos G, Antunes EF, Lobo AO, Trava-Airoldi VJ, Corata EJ. Total re-establishment of superhydrophobicity of vertically-aligned carbon nanotubes by CO_2 laser treatment. Surf Coat Technol. 2010;204:3073–7.
[67] Lepore E, Giorcelli M, Saggese C, Tagliaferro A, Pugno N. Mimicking water striders' legs superhydrophobicity and buoyancy with cabbage leaves and nanotube carpets. J Mater Res. 2013;28:976–83.
[68] He S, Wei J, Wang H, Sun D, Yao Z, Fu C, et al. Stable superhydrophobic surface of hierarchical carbon nanotubes on Si micropillar arrays. Nanoscale Res Lett. 2013;8:412.
[69] Román-Mansoa B, Vega-Díaz SM, Morelos-Gómez A, Terrones M, Miranzo P, Belmontea M. Aligned carbon nanotube/silicon carbide hybrid materials with high electrical conductivity, superhydrophobicity and superoleophilicity. Carbon. 2014;80:120–6.
[70] Journet C, Moulinet S, Ybert C, Purcell ST, Bocquet L. Contact angle measurements on superhydrophobic carbon nanotube forests: Effect of fluid pressure. Europhys Lett. 2005;71:104–9.
[71] Joseph P, Cottin-Bizonne C, Benoit JM, Ybert C, Journet C, Tabeling P, et al. Slippage of water past superhydrophobic carbon nanotube forests in microchannels. Phys Rev Lett. 2006;97:156104/1–4.
[72] Santhanagopalan S, Teng F, Meng DD. High-voltage electrophoretic deposition for vertically aligned forests of 1D nanoparticles. Langmuir. 2011;27:561–9.
[73] Jeong DW, Shin UH, Kim JH, Kim SH, Lee HW, Kim JM. Stable hierarchical superhydrophobic surfaces based on vertically aligned carbon nanotube forests modified with conformal silicone coating. Carbon. 2014;79:442–9.
[74] Sojoudi H, Kim S, Zhao H, Annavarapu RK, Mariappan D, Hart AJ, et al. Stable wettability control of nanoporous microstructures by iCVD coating of carbon nanotubes. ACS Appl Mater Interfaces. 2017;9:43287–99.
[75] Yung CS, Tomlin NA, Heuerman K, Keller MW, White MG, Stephens M, et al. Plasma modification of vertically aligned carbon nanotubes: superhydrophobic surfaces with ultra-low reflectance. Carbon. 2018;127:195–201.
[76] Aria AI, Gharib M. Reversible tuning of the wettability of carbon nanotube arrays: the effect of ultraviolet/ozone and vacuum pyrolysis treatments. Langmuir. 2011;27:9005–11.
[77] Babu DJ, Varanakkottu SN, Eifert A, de Koning D, Cherkashinin G, Hardt S, et al. Inscribing wettability gradients onto superhydrophobic carbon nanotube surfaces. Adv Mater Interface. 2014;1:1300049/1–6.
[78] Babu DJ, Mail M, Barthlott W, Schneider JJ. Superhydrophobic vertically aligned carbon nanotubes for biomimetic air retention under water (*Salvinia* effect). Adv Mater Interface. 2017;4:1700273.
[79] Hsiao CH, Lin JH. Growth of a superhydrophobic multi-walled carbon nanotube forest on quartz using flow-vapor-deposited copper catalysts. Carbon. 2017;124:637–41.
[80] Shakerzadeh M, Teo HTE, Tan CW, Tay BK. Superhydrophobic carbon nanotube/amorphous carbon nanosphere hybrid film. Diam Relat Mater. 2009;18:1235–8.
[81] Han ZJ, Tay BK, Shakerzadeh M, Ostrikov K. Superhydrophobic amorphous carbon/carbon nanotube nanocomposites. Appl Phys Lett. 2009;94:223106/1–3.
[82] Han ZJ, Tay BK, Tan C, Shakerzadeh M, Ostrikov K. Electrowetting control of Cassie-to-Wenzel transitions in superhydrophobic carbon nanotube-based nanocomposites. ACS Nano. 2009;3:3031–6.
[83] Huang L, Lau SP, Yang HY, Leong ESP, Yu SF, Prawer S. Stable superhydrophobic surface via carbon nanotubes coated with a ZnO thin film. J Phys Chem B. 2005;109:7746–8.
[84] Balram A, Santhanagopalan S, Hao B, Yap YK, Meng DD. Electrophoretically-deposited metal-decorated carbon nanotube nanoforests with high thermal/electric conductivity and wettability tunable from hydrophilic to superhydrophobic. Adv Funct Mater. 2016;26:2571–9.
[85] Hong YC, Shin DH, Cho SC, Uhm HS. Surface transformation of carbon nanotube powder into superhydrophobic and measurement of wettability. Chem Phys Lett. 2006;427:390–3.

[86] Hong YC, Uhm SH. Superhydrophobicity of a material made from multiwalled carbon nanotubes. Appl Phys Lett. 2006;88:244101/1–3.
[87] Kakade B, Mehta R, Durge A, Kulkarni S, Pillai V. Electric field induced, superhydrophobic to superhydrophilic switching in multiwalled carbon nanotubes papers. Nano Lett. 2008;8:2693–6.
[88] Zhang L, Resasco DE. Single-walled carbon nanotube pillars: a superhydrophobic surface. Langmuir. 2009;25:4792–8.
[89] Li SS, Hou PX, Liu C. Growth of a cup-stacked carbon nanotube carpet with a superhydrophobic surface. New Carbon Mater. 2013;28:295–9.
[90] Lee CS, Baik SH. Vertically-aligned carbon nanotube membrane filters with superhydrophobicity and superoleophobicity. Carbon. 2010;48:2192–7.
[91] Lee CH, Johnson N, Drelich J, Yap YK. The performance of superhydrophobic and superoleophobic carbon nanotube meshes in water-oil filtration. Carbon. 2011;49:669–76.
[92] De Nicola F, Castrucci P, Scarselli M, Nanni F, Cacciotti I, De Crescenzi M. Superhydrophobic multiwalled carbon nanotubes coatings for stainless steel. Nanotechnology. 2015;26:1–6.
[93] Wang P, Zhao T, Bian R, Wang G, Liu H. Robust superhydrophobic carbon nanotubes film with lotus leaf mimetic multiscale hierarchical structures. ACS Nano. 2017;11:12385–91.
[94] Yin H, Wang X, Sheng G, Chen W, Lai Z. Facile single-step fabrication of robust superhydrophobic carbon nanotubes films on different porous supports. Ind Eng Chem Res. 2019;58:2976–82.
[95] Wu T, Pan Y, Li L. Study on superhydrophobic hybrids fabricated from multiwalled carbon nanotubes and stearic acid. J Colloid Interface Sci. 2010;348:265–70.
[96] Yao H, Chu CC, Sue HJ, Nishimura R. Electrically conductive superhydrophobic ODA-functionalized multiwall carbon nanotubes films. Carbon. 2013;53:366–73.
[97] Chen F, Jia Y, Wang Q, Cao X, Li Y, Lin Y, et al. Strong and superhydrophobic hybrid carbon nanotubes films with superior loading capacity. Carbon. 2018;137:88–92.
[98] Liao KS, Wan A, Batteas JD, Bergbreiter DE. Superhydrophobic surfaces formed using LBL self-assembly with aminated multiwall carbon nanotubes. Langmuir. 2008;24:4245–53.
[99] Su XJ, Li HQ, Lai XJ, Yang ZP, Chen ZH, Wu WJ, et al. Vacuum-assisted layer-by-layer superhydrophobic carbon nanotubes films with electrothermal and photothermal effects for deicing and controllable manipulation. J Mater Chem A. 2018;6:16910–9.
[100] Yang J, Zhang ZZ, Men XH, Xu XH, Zhu XT. Xiaotao, Reversible superhydrophobicity to superhydrophilicity switching of a carbon nanotube film via alternation of UV irradiation and dark storage. Langmuir. 2010;26:10198–202.
[101] Yang J, Zhang ZZ, Men XH, Xu XG, Zhu XT. Thermo-responsive surface wettability on a pristine carbon nanotubes film. Carbon. 2011;49:19–23.
[102] Li J, Ling J, Yan L, Wang Q, Zha F, Lei Z. UV/mask irradiation and heat induced switching on-off water transportation on superhydrophobic carbon nanotube surfaces. Surf Coat Technol. 2014;258:142–5.
[103] Wang CF, Chen WY, Cheng HZ, Fu SL. Pressure-proof superhydrophobic films from flexible carbon nanotube/polymer coatings. J Phys Chem C. 2010;114:15607–11.
[104] Zhu XT, Zhang ZZ, Ge B, Men XH, Zhou XY. Fabrication of a superhydrophobic carbon nanotube coating with good reusability and easy repairability. Colloid Surf A. 2014;444:252–6.
[105] Ogihara H, Xie J, Saji T. Spraying carbon nanotube dispersions to prepare superhydrophobic films. J Mater Sci. 2014;49:3183–8.
[106] Zhai N, Fan L, Li LX, Zhang J. Durable superamphiphobic coatings repelling both cool and hot liquids based on carbon nanotubes. J Colloid Interface Sci. 2017;505:622–30.
[107] Zhang JP, Yu B, Gao ZQ, Li BC, Zhao X. Durable, transparent, and hot liquid repelling superamphiphobic coatings from polysiloxane-modified multiwalled carbon nanotubes. Langmuir. 2017;33:510–8.
[108] De Nicola F, Castrucci P, Scarselli M, Nanni F, Cacciotti I, De Crescenzi M. Super-hydrophobic multi-walled carbon nanotube coatings for stainless steel. Nanotechnology. 2015;26:145701.
[109] Sahoo BN, Woo JH, Algadi H, Lee JH, Lee TY. Superhydrophobic, transparent, and stretchable 3D hierarchical wrinkled film-based sensors for wearable applications. Adv Mater Technol. 2019;4:1900230.
[110] Li Y, Huang XJ, Heo SH, Li CC, Choi YK, Cai WP, et al. Superhydrophobic bionic surfaces with hierarchical microsphere/multiwalled carbon nanotubes composite arrays. Langmuir. 2007;23:2169–74.
[111] Kinoshita H, Ogasahara A, Fukuda Y, Ohmae N. Superhydrophobic/superhydrophilic micropatterning on a carbon nanotube film using a laser plasma-type hyperthermal atom beam facility. Carbon. 2010;48:4403–8.
[112] Tang M, Hong MH, Choo YS, Tang Z, Chua DHC. Superhydrophobic transparent surface by femtosecond laser micro-patterned catalyst thin film for carbon nanotube cluster growth. Appl Phys A. 2010;101:503–8.
[113] Li JL, Wang LJ, Jiang W. Super-hydrophobic surface of bulk carbon nanotubes compacted by spark plasma sintering followed by modification with polytetrofluoroethylene. Carbon. 2010;48:2668–71.
[114] Łukawski D, Lekawa-Raus A, Lisiecki F, Koziol K, Dudkowiak A. Towards the development of superhydrophobic carbon nanomaterial coatings on wood. Prog Org Coat. 2018;125:23–31.
[115] Rajiv S, Kumaran S, Sathish M. Long-term-durable anti-icing superhydrophobic composite coatings. J Appl Polym Sci. 2019;136:47059.
[116] Tan SC, Yan F, Crouch LI, Robertson J, Jones MR, Welland ME. Superhydrophobic carbon nanotube electrode produces a near-symmetrical alternating current from photosynthetic protein-based photoelectrochemical cells. Adv Funct Mater. 2013;23:5556–63.
[117] Xu J, Gong X, Yong Z, Ramakrishna S. Construction of various nanostructures on carbon nanotube films. Mater Today Chem. 2020;16:100253.
[118] Belsanti L, Ogihara H, Mahanty S, Luciano G. Electrochemical behaviour of superhydrophobic coating fabricated by spraying a carbon nanotube suspension. Bull Mater Sci. 2015;38:579–82.
[119] Georgakilas V, Bourlinos AB, Zboril R, Trapalis C. Synthesis, characterization and aspects of superhydrophobic

functionalized carbon nanotubes. Chem Mater. 2008;20:2884–6.
[120] Hsieh CT, Chen WY, Wu FL. Fabrication and superhydrophobicity of fluorinated carbon fabrics with micro/nanoscaled two-tier roughness. Carbon. 2008;46:1218–24.
[121] Meng LY, Park SJ. Effect of fluorination of carbon nanotubes on superhydrophobic properties of fluoro-based films. J Colloid Interface Sci. 2010;342:559–63.
[122] Men XH, Zhang ZZ, Yang J, Wang K, Jiang W. Superhydrophobic/superhydrophilic surfaces from a carbon nanotube based composite coating. Appl Phys A. 2010;98:275–80.
[123] Talaeemashhadi S, Sansotera M, Gambarotti C, Famulari A, Bianchi CL, Guarda PA, et al. Functionalization of multiwalled carbon nanotubes with perfluoropolyether peroxide to produce superhydrophobic properties. Carbon. 2013;59:150–9.
[124] Yoon SH, Rungraeng N, Song W, Jun S. Superhydrophobic and superhydrophilic nanocomposite coatings for preventing Escherichia coli K-12 adhesion on food contact surface. J Food Eng. 2014;131:135–41.
[125] Jin J, Wang X, Song M. Graphene-based nanostructured hybrid materials for conductive and superhydrophobic functional coatings. J Nanosci Nanotech. 2011;11:7715–22.
[126] Peng M, Liao Z, Qi J, Zhou Z. Nonaligned carbon nanotubes partially embedded in polymer matrixes: a novel route to superhydrophobic conductive surfaces. Langmuir. 2010;26:13572–8.
[127] Sethi S, Dhinojwala A. Superhydrophobic conductive carbon nanotube coatings for steel. Langmuir. 2009;25:4311–3.
[128] Yuan R, Wu S, Yu P, Wang B, Mu L, Zhang X, et al. Superamphiphobic and electroactive nanocomposite toward self-cleaning, antiwear, and anticorrosion coatings. ACS Appl Mater Interfaces. 2016;8:12481–93.
[129] Caffrey PO, Gupta MC. Electrically conducting superhydrophobic microtextured carbon nanotube nanocomposite. Appl Surf Sci. 2014;314:40–5.
[130] Wu TF, Pan YZ, Li L. Fabrication of superhydrophobic hybrids from multiwalled carbon nanotubes and poly(vinylidene fluoride). Colloid Surf A. 2011;384:47–52.
[131] Wang K, Hu NX, Xu G, Qi Y. Stable superhydrophobic composite coatings made from an aqueous dispersion of carbon nanotubes and a fluoropolymer. Carbon. 2011;49:1769–74.
[132] Bayer IS, Steele A, Loth E. Superhydrophobic and electroconductive carbon nanotube-fluorinated acrylic copolymer nanocomposites from emulsions. Chem Eng J. 2013;221:522–30.
[133] Zhang HF, Teo MK, Yang C. Superhydrophobic carbon nanotube/polydimethylsiloxane composite coatings. Mater Sci Technol. 2015;31:1745–8.
[134] Wang K, Xiong P, Xu X, Wang K, Li YL, Zheng Y. Chemically robust carbon nanotube-PTFE superhydrophobic thin films with enhanced ability of wear resistance. Prog Nat Sci: Mater Int. 2017;27:396–9.
[135] Park MH, Ha JH, La M, Ko YB, Kim D, Park SH. Conducting super-hydrophobic thin film for electric heating applications. J Nanosci Nanotechnol. 2019;19:1506–10.
[136] Zhang J, Yu B, Wei Q, Li B, Li L, Yang Y. Highly transparent superamphiphobic surfaces by elaborate microstructure regulation. J Colloid Interface Sci. 2019;554:250–9.
[137] Ding YR, Xue CH, Fan QQ, Zhao LL, Tian QQ, Guo XJ, et al. Fabrication of superhydrophobic conductive film at air/water interface for flexible and wearable sensors. Chem Eng J. 2021;404:126489.
[138] Asthana A, Maitra T, Buchel R, Tiwari MK, Poulikakos D. Multifunctional superhydrophobic polymer/carbon nanocomposites: graphene, carbon nanotubes, or carbon black? ACS Appl Mater Interfaces. 2014;6:8859–67.
[139] Jung KK, Jung Y, Choi CJ, Ko JS. Highly reliable superhydrophobic surface with carbon nanotubes immobilized on a PDMS/adhesive multilayer. ACS Omega. 2018;3:12956–66.
[140] Wan F, Yang DQ, Sacher E. Repelling hot water from superhydrophobic surfaces based on carbon nanotubes. J Mater Chem A. 2015;3:16953–60.
[141] KA, Shashkeev, VS, Nagornaya, IA, Volkov, et al. Superhydrophobic conducting coatings based on silicone matrix and carbon nanotubes, Russ. J Appl Chem. 2017;90:1107–16.
[142] Lv C, Wang H, Liu Z, Wang C, Zhang W, Li M, et al. Fabrication of durable fluorine-free polyphenylene sulfide/silicone resin composite superhydrophobic coating enhanced by carbon nanotubes/graphene fillers. Prog Org Coat. 2019;134:1–10.
[143] Han JT, Kim BK, Woo JS, Jang JI, Cho JY, Jeong HJ, et al. Bioinspired multifunctional superhydrophobic surfaces with carbon-nanotube-based conducting pastes by facile and scalable printing. ACS Appl Mater Interfaces. 2017;9:7780–6.
[144] Song K, Gao A, Cheng X, Xie K. Preparation of the superhydrophobic nano-hybrid membrane containing carbon nanotube based on chitosan and its antibacterial activity. Carbohyd Polym. 2015;130:381–7.
[145] Wang Y, Yue G, Li D, Hou L, Zhao X, Cui Z, et al. A robust carbon nanotube and PVDF-HFP nanofiber composite superwettability membrane for high-efficiency emulsion separation. Macromol Rapid Commun. 2020;41:2000089.
[146] Yu Y, Chen H, Liu Y, Craig VSJ, Li LH, Chen Y, et al. Porous carbon nanotube/polyvinylidene fluoride composite material: superhydrophobicity/superoleophilicity and tunability of electrical conductivity. Polymer. 2014;55:5616–22.
[147] Kousalya AS, Singh KP, Fisher TS. Heterogeneous wetting surfaces with graphitic petal-decorated carbon nanotubes for enhanced flow boiling. Int J Heat Mass Transfer. 2015;87:380–9.
[148] Rungraeng N, Yoon SH, Li Y, Jun S. Development of a self-slippery liquid-infused porous surface (SLIPS) coating using carbon nanotube composite for repelling food debris and microbial biofilms. Trans ASABE. 2015;58:861–7.
[149] Hejazi I, Sadeghi GMM, Jafari SH, Khonakdar HA, Seyfi J, Holzschuh M, et al. Transforming an intrinsically hydrophilic polymer to a robust self-cleaning superhydrophobic coating via carbon nanotube surface embedding. Mater Des. 2015;86:338–46.
[150] Wang X, Hu H, Ye Q, Gao T, Zhou F, Xue Q. Superamphiphobic coatings with coralline-like structure enabled by one-step spray of polyurethane/carbon nanotube composites. J Mater Chem. 2012;22:9624–31.
[151] Jung YC, Bhushan B. Mechanically durable carbon nanotube-composite hierarchical structures with superhydrophobicity, self-cleaning, and low-drag. ACS Nano. 2009;3:4155–63.
[152] Hsu CP, Chang LY, Chiu CW, Lee PTC, Lin JJ. Facile fabrication of robust superhydrophobic epoxy film with polyamine

dispersed carbon nanotubes. ACS Appl Mater Interfaces. 2013;5:538–45.
[153] Wang H, Liu Z, Wang E, Zhang X, Yuan R, Wu S, et al. Facile preparation of superamphiphobic epoxy resin/modified poly (vinylidene fluoride)/fluorinated ethylene propylene composite coating with corrosion/wear-resistance. Appl Surf Sci. 2015;357:229–35.
[154] Yuan R, Wu S, Wang B, Liu Z, Mu L, Ji T, et al. Superamphiphobicity and electroactivity enabled dual physical/chemical protections in novel anticorrosive nanocomposite coatings. Polymer. 2016;85:37–46.
[155] Zhang F, Qian H, Wang L, Wang Z, Du C, Li X, et al. Superhydrophobic carbon nanotubes/epoxy nanocomposite coating by facile one-step spraying. Surf Coat Technol. 2018;341:15–23.
[156] Zhang D, Wu G, Li H, Cui Y, Zhang Y. Superamphiphobic surfaces with robust self-cleaning, abrasion resistance and anti-corrosion. Chem Eng J. 2021;406:126753.
[157] Li W, Wang Y, Feng Y, Wang Q, Xu X, Li G, et al. Fabrication of robust conductive and superhydrophobic coating based on carbon nanotubes. Mater Res Exp. 2020;7:055009.
[158] Yang J, Zhang Z, Men X, Xu X. Fabrication of stable, transparent and superhydrophobic nanocomposite films with polystyrene functionalized carbon nanotubes. Appl Surf Sci. 2009;255:9244–7.
[159] Yang J, Zhang Z, Men X, Xu X, Zhu X. Reversible conversion of water-droplet mobility from rollable to pinned on a superhydrophobic functionalized carbon nanotube film. J Colloid Interface Sci. 2010;346:241–7.
[160] Song HJ, Shen XQ, Meng XF. Superhydrophobic surfaces produced by carbon nanotube modified polystyrene composite coating. J Disp Sci Technol. 2010;31:1465–8.
[161] Zhao L, Liu WL, Zhang LD, Yao JS, Xu WH, Wang XQ, et al. Fabrication of superhydrophobic and conductive surface based on carbon nanotubes. Colloid Surf A. 2013;423:69–76.
[162] Kim HY, Cho YS. Fabrication of a superhydrophobic surface via spraying with polystyrene and multi-walled carbon nanotubes. Colloid Surf A. 2015;465:77–86.
[163] Gu J, Xiao P, Chen J, Liu F, Huang Y, Li G, et al. Robust preparation of superhydrophobic polymer/carbon nanotube hybrid membranes for highly effective removal of oils and separation of water-in-oil emulsions. J Mater Chem A. 2014;2:15268–72.
[164] Liu J, Liu R, Yuan Y, Zhang S, Liu X. Preparation of superhydrophobic antistatic coatings from branched alternating copolymers P(St-alt-MAn) and carbon nanotubes based on organic–inorganic hybrid approach. Prog Org Coat. 2013;76:1251–7.
[165] Han JT, Kim JS, Kim SH, Lim HS, Jeong HJ, Jeong SY, et al. Nanocarbon-induced rapid transformation of polymer surfaces into superhydrophobic surfaces. ACS Appl Mater Interfaces. 2010;2:3378–83.
[166] Li G, Wang H, Zheng H, Bai R. A facile approach for the fabrication of highly stable superhydrophobic cotton fabric with multi-walled carbon nanotubes-azide polymer composites. Langmuir. 2010;26:7529–34.
[167] Men XH, Zhang ZZ, Song HJ, Wang K, Jiang W. Fabrication of superhydrophobic surfaces with poly(furfuryl alcohol)/multi-walled carbon nanotubes composites. Appl Surf Sci. 2008;254:2563–8.
[168] Zhang T, Yan H, Fang Z, Yuping E, Wu T, Chen F. Superhydrophobic and conductive properties of carbon nanotubes/polybenzoxazine nanocomposites coated ramie fabric prepared by solution-immersion process. Appl Surf Sci. 2014;309:218–24.
[169] Wang CF, Chen HY, Kuo SW, Lai YS, Yang PF. Rapid, low temperature microwave synthesis of durable, superhydrophobic carbon nanotube-polybenzoxazine nanocomposites. RSC Adv. 2013;3:9764–9.
[170] Wang CF, Hung SW, Kuo SW, Chang CJ. Combining hierarchical surface roughness with fluorinated surface chemistry to preserve superhydrophobicity after organic contamination. Appl Surf Sci. 2014;320:658–63.
[171] Molla-Abbasi P. Effect of nano-size nodular structure induced by CNT-promoted phase separation on the fabrication of superhydrophobic polyvinyl chloride films. Polym Adv Technol. 2021;32:391–401.
[172] Su X, Li H, Lai X, Chen Z, Zeng X. 3D porous superhydrophobic CNT/EVA composites for recoverable shape reconfiguration and underwater vibration detection. Adv Funct Mater. 2019;29:1900554.
[173] Bains D, Singh G, Bhinder J, Agnihotri PK, Singh N. Ionic liquid-functionalized multiwalled carbon nanotube-based hydrophobic coatings for robust antibacterial applications. ACS Appl Bio Mater. 2020;3:2092–103.
[174] Mokarian Z, Rasuli R, Abedini Y. Facile synthesis of stable superhydrophobic nanocomposite based on multi-walled carbon nanotubes. Appl Surf Sci. 2016;369:567–75.
[175] Li Q, Liu H, Zhang S, Zhang D, Liu X, He Y, et al. Superhydrophobic electrically conductive paper for ultrasensitive strain sensor with excellent anticorrosion and self-cleaning property. ACS Appl Mater Interfaces. 2019;11:21904–14.
[176] Zhou S, Zhu X, Ma L, Yan Q, Wang S. Outstanding superhydrophobicity and corrosion resistance on carbon-based film surfaces coupled with multi-walled carbon nanotubes and nickel nano-particles. Surf Sci. 2018;677:193–202.
[177] Zhu X, Zhou S, Yan Q, Wang S. Multi-walled carbon nanotubes enhanced superhydrophobic multiwalled carbon nanotubes-Co/a-C:H carbon-based film for excellent self-cleaning and corrosion resistance. Diam Relat Mater. 2018;86:87–97.
[178] Hsieh CT, Chen WY, Wu FL, Hung WM. Superhydrophobicity of a three-tier roughened texture of microscale carbon fabrics decorated with silica spheres and carbon nanotubes. Diam Relat Mater. 2010;19:26–30.
[179] Peng M, Guo H, Liao Z, Qi J, Zhou Z, Fang Z, et al. Percolation-dominated superhydrophobicity and conductivity for nanocomposite coatings from the mixtures of a commercial aqueous silica sol and functionalized carbon nanotubes. J Colloid Interface Sci. 2012;367:225–33.
[180] Li Y, Zhu X, Zhou X, Ge B, Chen S, Wu W. A facile way to fabricate a superamphiphobic surface. Appl Phys A. 2014;115:765–70.
[181] Wang S, Zhang J, Yu X, Zhang Y. Condensed dewdrops self-ejecting on sprayable superhydrophobic CNT/SiO_2 composite coating. RSC Adv. 2017;7:27574–7.

[182] Peng M, Qi J, Zhou Z, Liao Z, Zhu Z, Guo H. Carbon nanotubes noncovalently functionalized by an organic-inorganic hybrid: new building blocks for constructing superhydrophobic conductive coatings. Langmuir. 2010;26:13062–4.
[183] Yang HJ, Cho JY, Kim JH, Kim HY, Lee JW, Wang JW, et al. Efficient oxidation and rational reduction of long carbon nanotubes for multifunctional superhydrophobic surfaces. Carbon. 2020;157:649–55.
[184] Yu H, Zhu J, Yang L, Dai B, Baraban L, Cuniberti G, et al. Superhydrophobic carbon nanotube/silicon carbide nanowire nanocomposites. Mater Des. 2015;87:198–204.
[185] Jiang G, Chen L, Zhang S, Huang H. Superhydrophobic SiC/carbon nanotubes coatings with photothermal deicing and passive anti-icing properties. ACS Appl Mater Interfaces. 2018;10:36505–11.
[186] Liu Z, Wang H, Zhang X, Lv C, Wang C, Zhu Y. Robust and chemically stable superhydrophobic composite ceramic coating repellent even to hot water. Adv Mater Interface. 2017;4:1601202.
[187] Kuo CH, Li W, Song W, Luo Z, Poyraz AS, Guo Y, et al. Facile synthesis of Co_3O_4@CNT with high catalytic activity for CO oxidation under moisture-rich conditions. ACS Appl Mater Interfaces. 2014;6:11311–7.
[188] Shen J, Ming PM, Zhang XM, Yan L, Zheng XS, Wang W. Broad spectrum anti-fouling, photocatalytic antibacterial and superamphiphobic coating fabricated by composite electrodeposition process. J Electrochem Soc. 2019;166:E564–75.
[189] Zhu X, Zhang Z, Ren G, Men X, Ge B, Zhou X. Designing transparent superamphiphobic coatings directed by carbon nanotubes. J Colloid Interface Sci. 2014;421:141–5.
[190] Li B, Zhang J, Gao Z, Wei Q. Semitransparent superoleophobic coatings with low sliding angles for hot liquids based on silica nanotubes. J Mater Chem A. 2016;4:953–60.
[191] Zhu MX, Song HG, Li JC, Xue JY, Yu QC, Chen JM, et al. Superhydrophobic and high-flashover-strength coating for HVDC insulating system. Chem Eng J. 2021;404:126476.
[192] Barthwal S, Barthwal S, Singh B, Singh NB. Multifunctional and fluorine-free superhydrophobic composite coating based on PDMS modified MWCNTs/ZnO with self-cleaning, oil–water separation, and flame retardant properties. Colloid Surface A. 2020;597:124776.
[193] Pramoda K, Kumar R, Rao CNR. Graphene/single-walled carbon nanotube composites generated by covalent cross-linking. Chem Asian J. 2015;10:2147–52.
[194] Mansurov Z. Synthesis of carbon nanomaterials in flames. ECTJ. 2011;13:5–16.
[195] Ayyappan VG, Prakash D, Jaisankar SN, Sadhukhan N, Alam MS, Samanta D. Nanoconjugates of methacrylic polymers: synthesis, characterization, and immobilization to leather. J Appl Polym Sci. 2020;137:48627.
[196] Kausar A. Overview on nanocarbon sponges in polymeric nanocomposite. Mater Res Innov. 2020;24:309–20.
[197] Lu Y, Yuan W. Superhydrophobic/superoleophilic and reinforced ethyl cellulose sponges for oil/water separation: synergistic strategies of cross-linking, carbon nanotube composite, and nanosilica modification. ACS Appl Mater Interfaces. 2017;9:29167–76.
[198] Fard AK, Mckay G, Manawi Y, Malaibari Z, Hussien MA. Outstanding adsorption performance of high aspect ratio and super-hydrophobic carbon nanotubes for oil removal. Chemosphere. 2016;164:142–55.
[199] Eseev M, Goshev A, Kapustin S, Tsykareva Y. Creation of superhydrophobic coatings based on MWCNTs xerogel. Nanomaterials. 2019;9:1584.
[200] Yao S, Zhou S, Zhang J, Yang Z, Zhang X. Improved wettability and enhanced ionic transport in highly porous CNT sponge. Nanotechnology. 2020;32:105709.
[201] Dong X, Chen J, Ma Y, Wang J, Chan-Park MB, Liu X, et al. Superhydrophobic and superoleophilic hybrid foam of graphene and carbon nanotube for selective removal of oils or organic solvents from the surface of water. Chem Commun. 2012;48:10660–2.
[202] Hong J, Kang SW. Hydrophobic properties of colloidal films coated with multi-wall carbon nanotubes/reduced graphene oxide multilayers. Colloid Surf A. 2011;374:54–7.
[203] Hu H, Zhao Z, Gogotsi Y, Qiu J. Compressible carbon nanotube-graphene hybrid aerogels with superhydrophobicity and superoleophilicity for oil sorption. EnvironSci Technol Lett. 2014;1:214–20.
[204] Ge B, Zhang Z, Zhu X, Men X, Zhou X. A superhydrophobic/superoleophilic sponge for the selective absorption oil pollutants from water. Colloid Surf A. 2014;457:397–401.
[205] Sultanov FR, Bakbolat B, Mansurov ZA, Azizov ZM, Pei SS, Ebrahim R, et al. Spongy structures coated with carbon nanomaterials for efficient oil/water separation. ECTJ. 2017;19:127–32.
[206] Ye S, Wang B, Shi Y, Wang B, Zhang Y, Feng Y, et al. Superhydrophobic and superelastic thermoplastic polyurethane/multiwalled carbon nanotubes porous monolith for durable oil/water separation. Composites Commun. 2020;21:100378.
[207] Hong T, Jeong SM, Choi YK, Lim T, Ju S. Superhydrophobic, elastic, and conducting polyurethane-carbon nanotube-silane-aerogel composite microfiber. Polymers. 2020;12:1772.
[208] Ye X, Cui Y, Ke L, Gao K, Huang X, Shi B. Fabrication of 3D porous superhydrophobic sponges using plant polyphenol-Fe^{3+} complexes as adhesive and their applications in oil/water separation. Colloid Surf A. 2018;551:9–16.
[209] Gupta S, He WD, Tai NH. A comparative study on superhydrophobic sponges and their application as fluid channel for continuous separation of oils and organic solvents from water. Compos B Eng. 2016;101:99–106.
[210] Makowski T, Kowalczyk D, Fortuniak W, Jeziorska D, Brzezinski S, Tracz A. Superhydrophobic properties of cotton woven fabrics with conducting 3D networks of multiwall carbon nanotubes. Cellulose. 2014;21:4659–70.
[211] Zheng L, Su X, Lai X, Chen W, Li H, Zeng X. Conductive superhydrophobic cotton fabrics via layer-by-layer assembly of carbon nanotubes for oil–water separation and human motion detection. Mater Lett. 2019;253:230–3.
[212] Xue CH, Wu Y, Guo XJ, Liu BY, Wang HD, Jia ST. Superhydrophobic, flame-retardant and conductive cotton fabrics via layer-by-layer assembly of carbon nanotubes for flexible sensing electronics. Cellulose. 2020;27:3455–68.
[213] Lu Z, Huang X, Wang L. Superhydrophobic hierarchical structure carbon mesh films for oil/water separation application. Appl Phys A. 2017;123:538.
[214] Li Z, Wang B, Qin X, Wang Y, Liu C, Shao Q, et al. Superhydrophobic/superoleophilic polycarbonate/carbon

nanotubes porous monolith for selective oil adsorption from water. ACS Sust Chem Eng. 2018;6:13747–55.
[215] Fu Y, Xu F, Weng D, Li X, Li Y, Sun J. Superhydrophobic foams with chemical- and mechanical-damage-healing abilities enabled by self-healing polymers. ACS Appl Mater Interface. 2019;11:37285–94.
[216] Gao SJ, Zhu YZ, Zhang F, Jin J. Superwetting polymer-decorated SWCNT composite ultrathin films for ultrafast separation of oil-in-water nanoemulsions. J Mater Chem A. 2015;3:2895–902.
[217] Zhao X, Cheng L, Jia N, Wang R, Liu L, Gao C. Polyphenol-metal manipulated nanohybridization of CNT membranes with FeOOH nanorods for high-flux, antifouling and self-cleaning oil/water separation. J Membr Sci. 2020;600:117857.
[218] Wu J, Li H, Lai X, Chen Z, Zeng X. Superhydrophobic polydimethylsiloxane@multiwalled carbon nanotubes membrane for effective water-in-oil emulsions separation and quick deicing. Ind Eng Chem Res. 2019;58:8791–9.
[219] Gao SJ, Shi Z, Zhang WB, Zhang F, Jin J. Photoinduced superwetting single-walled carbon nanotube/TiO_2 ultrathin network films for ultrafast separation of oil-in-water emulsions. ACS Nano. 2014;8:6344–52.
[220] Zhang L, Gu J, Song L, Chen L, Huang Y, Zhang J, et al. Underwater superoleophobic carbon nanotubes/core-shell polystyrene@Au nanoparticles composite membrane for flow-through catalytic decomposition and oil/water separation. J Mater Chem A. 2016;4:10810–5.
[221] Gu J, Xiao P, Zhang L, Lu W, Zhang G, Huang Y, et al. Construction of superhydrophilic and under-water superoleophobic carbon-based membranes for water purification. RSC Adv. 2016;6:73399–403.
[222] Yue X, Zhang T, Yang D, Qiu F, Li Z. Ultralong MnO_2 nanowire enhanced multiwall carbon nanotube hybrid membrane with underwater superoleophobicity for efficient oil-in-water emulsions separation. Ind Eng Chem Res. 2018;57:10439–47.
[223] Zhao X, Cheng L, Wang R, Jia N, Liu L, Gao C. Bioinspired synthesis of polyzwitterion/titania functionalized carbon nanotube membrane with superwetting property for efficient oil-in-water emulsion separation. J Membr Sci. 2019;589:117257.
[224] Dudchenko AV, Rolf J, Shi L, Olivas L, Duan W, Jassby D. Coupling underwater superoleophobic membranes with magnetic pickering emulsions for fouling-free separation of crude oil/water mixtures: an experimental and theoretical study. ACS Nano. 2015;9:9930–41.
[225] Yan L, Zhang G, Zhang L, Zhang W, Gu J, Huang Y, et al. Robust construction of underwater superoleophobic CNTs/nanoparticles multifunctional hybrid membranes via interception effect for oily wastewater purification. J Membr Sci. 2019;569:32–40.
[226] Yoon D, Lee C, Yun J, Jeon W, Cha BJ, Baik S. Enhanced condensation, agglomeration, and rejection of water vapor by superhydrophobic aligned multiwalled carbon nanotube membranes. ACS Nano. 2012;6:5980–7.
[227] Madaeni SS, Zinadini S, Vatanpour V. Preparation of superhydrophobic nanofiltration membrane by embedding multiwalled carbon nanotube and polydimethylsiloxane in pores of microfiltration membrane. Sep Purif Technol. 2013;111:98–107.
[228] Gu J, Xiao P, Huang Y, Zhang J, Chen T. Controlled functionalization of carbon nanotubes as superhydrophobic material for adjustable oil/water separation. J Mater Chem A. 2015;3:4124–8.
[229] Tijing LD, Woo YC, Shim WG, He T, Choi JS, Kim SH, et al. Superhydrophobic nanofiber membrane containing carbon nanotubes for high-performance direct contact membrane distillation. J Membr Sci. 2016;502:158–70.
[230] Dong Y, Ma L, Tang CY, Yang F, Quan X, Jassby D, et al. Stable superhydrophobic ceramic-based carbon nanotube composite desalination membranes. Nano Lett. 2018;18:5514–21.
[231] Fan X, Liu Y, Quan X, Zhao H, Chen S, Yi G, et al. High desalination permeability, wetting and fouling resistance on superhydrophobic carbon nanotube hollow fiber membrane under self-powered electrochemical assistance. J Membr Sci. 2016;514:501–9.
[232] Si Y, Sun C, Li D, Yang F, Tang CY, Quan X, et al. Flexible superhydrophobic metal-based carbon nanotube membrane for electrochemically enhanced water treatment. Environ Sci Technol. 2020;54:9074–82.
[233] Dhindsa MS, Smith NR, Heikenfeld J, Rack PD, Fowlkes JD, Doktycz MJ, et al. Reversible electrowetting of vertically aligned superhydrophobic carbon nanofibers. Langmuir. 2006;22:9030–4.
[234] Hsieh CT, Chen JM, Huang YH, Kuo RR, Li CT, Shih HC, et al. Influence of fluorine/carbon atomic ratio on superhydrophobic behavior of carbon nanofiber arrays. J Vacuum Sci Technol B. 2006;24:113–7.
[235] Wang N, Xi J, Wang S, Liu H, Feng L, Jiang L. Long-term and thermally stable superhydrophobic surfaces of carbon nanofibers. J Colloid Interface Sci. 2008;320:365–8.
[236] Tsai P, Pacheco S, Pirat C, Lefferts L, Lohse D. Drop impact upon micro- and nanostructured superhydrophobic surfaces. Langmuir. 2009;25:12293–8.
[237] Ogihara H, Okagaki J, Saji T. A facile fabrication of superhydrophobic films by electrophoretic deposition of hydrophobic particles. Chem Lett. 2009;38:132–3.
[238] Qiu R, Zhang D, Wang P. Superhydrophobic-carbon fibre growth on a zinc surface for corrosion inhibition. Corros Sci. 2013;66:350–9.
[239] Siddiqui AR, Maurya R, Katiyar PK, Balani K. Superhydrophobic, self-cleaning carbon nanofiber CVD coating for corrosion protection of AISI 1020 steel and AZ31 magnesium alloys. Surf Coat Technol. 2020;404:126421.
[240] Li J, Sambandam S, Lu W, Lukehart CM. Carbon nanofibers "spot-welded" to carbon felt: a mechanically stable, bulk mimic of lotus leaves. Adv Mater. 2008;20:420–4.
[241] Jiang ZX, Geng L, Huang YD. Fabrication of superhydrophobic 3-D braided carbon fiber fabric boat. Mater Lett. 2010;64:2441–3.
[242] Meng LY, Park SJ. Effect of growth of graphite nanofibers on superhydrophobic and electrochemical properties of carbon fibers. Mater Chem Phys. 2012;132:324–9.
[243] Meng LY, Rhee KY, Park SJ. Enhancement of superhydrophobicity and conductivity of carbon nanofibers-coated glass fabrics. J Ind Eng Chem. 2014;20:1672–6.
[244] Hima HI, Xiang X, Zhang L, Li F. Novel carbon nanostructures of caterpillar-like fibers and interwoven spheres with

excellent surface super-hydrophobicity produced by chemical vapor deposition. J Mater Chem. 2008;18:1245–52.
[245] Ko TJ, Her EK, Shin B, Kim HY, Lee KR, Hong BK, et al. Water condensation behavior on the surface of a network of superhydrophobic carbon fibers with high-aspect-ratio nanostructures. Carbon. 2012;50:5085–92.
[246] Aljumaily MM, Alsaadi MA, Das R, Abd Hamid SB, Hashim NA, Al Omar MK, et al. Optimization of the synthesis of superhydrophobic carbon nanomaterials by chemical vapor deposition. Sci Rep. 2018;8:2778.
[247] Xu C, Shen Y, Li J, Zhang Y, Luo Z, She H. Robust superhydrophobic carbon fiber sponge used for efficient oil/corrosive solution mixtures separation. Vacuum. 2017;141:57–61.
[248] Siddiqui AR, Maurya R, Balani K. Superhydrophobic self-floating carbon nanofiber coating for efficient gravity-directed oil/water separation. J Mater Chem A. 2017;5:2936–46.
[249] Feng S, Luo W, Wang L, Zhang S, Guo N, Xu M, et al. Preparation and property of extremely stable superhydrophobic carbon fibers with core-shell structure. Carbon. 2019;150:284–91.
[250] Das A, Megaridis CM, Liu L, Wang T, Biswas A. Design and synthesis of superhydrophobic carbon nanofiber composite coatings for terahertz frequency shielding and attenuation. Appl Phys Lett. 2011;98:174101.
[251] Das A, Schutzius TM, Bayer IS, Megaridis CM. Superoleophobic and conductive carbon nanofiber/fluoropolymer composite films. Carbon. 2012;50:1346–54.
[252] Das A, Hayvaci HT, Tiwari MK, Bayer IS, Erricolo D, Megaridis CM. Superhydrophobic and conductive carbon nanofiber/PTFE composite coatings for EMI shielding. J Colloid Interface Sci. 2011;353:311–5.
[253] Seo HO, Kim KD, Jeong MG, Kim YD, Choi KH, Hong EM, et al. Superhydrophobic carbon fiber surfaces prepared by growth of carbon nanostructures and polydimethylsiloxane coating. Macromol Res. 2012;20:216–9.
[254] Abdulhussein AT, Kannarpady GK, Ghosh A, Barnes B, Steiner RC, Mulon PY, et al. Facile fabrication of a free-standing superhydrophobic and superoleophilic carbon nanofiber-polymer block that effectively absorbs oils and chemical pollutants from water. Vacuum. 2018;149:39–47.
[255] Lin X, Heo J, Jeong H, Choi M, Chang M, Hong J. Robust superhydrophobic carbon nanofiber network inlay-gated mesh for water-in-oil emulsion separation with high flux. J Mater Chem A. 2016;4:17970–80.
[256] Yang Y, Ren Z, Zhao S, Guo Z. Robust superhydrophobic composite featuring three-dimensional porous metal rubber with an embedded carbon nanofiber network for emulsion separation. Ind Eng Chem Res. 2020;59:6172–82.
[257] Guo Z, Long B, Gao S, Luo J, Wang L, Huang X, et al. Carbon nanofiber based superhydrophobic foam composite for high performance oil/water separation. J Hazardous Mater. 2021;402:123838.
[258] Li Z, Milionis A, Zheng Y, Yee M, Codispoti L, Tan F, et al. Superhydrophobic hemostatic nanofiber composites for fast clotting and minimal adhesion. Nature Commun. 2019;10:5562.
[259] Il'darkhanova FI, Mironova GA, Bogoslovkii KG, Kopteva VN, Bykov ED. Design of superhydrophobic nanomodified anticorrosive antifouling coatings. Lakokrasochnye Materialy i Ikh Primenenie. 2010;8:18–21.
[260] Zhang S, Huang X, Wang D, Xiao W, Huo L, Zhao M, et al. Flexible and superhydrophobic composites with dual polymer nanofiber and carbon nanofiber network for high-performance chemical vapor sensing and oil/water separation. ACS Appl Mater Interfaces. 2020;12:47076–89.
[261] Baig N, Alghunaimi FI, Dossary HS, Saleh TA. Superhydrophobic and superoleophilic carbon nanofiber grafted polyurethane for oil–water separation. Proc Saf Environ Prot. 2019;123:327–34.
[262] Li J, Zhou L, Jiang X, Tan S, Chen P, Zhou H, et al. Directional preparation of superhydrophobic magnetic CNF/PVA/MWCNT carbon aerogel. IET nanobiotech. 2019;13:565–70.
[263] Hsieh CT, Wu FL, Yang SY. Superhydrophobicity from composite nano/microstructures: carbon fabrics coated with silica nanoparticles. Surf Coat Technol. 2008;202:6103–8.
[264] Lee DJ, Kim HM, Song YS, Youn JR. Water droplet bouncing and superhydrophobicity induced by multiscale hierarchical nanostructures. ACS Nano. 2012;6:7656–64.
[265] Wu B, Lyu J, Peng C, Liu J, Xing S, Jiang D, et al. Compression molding processed superhydrophobic CB/CeO_2/PVDF/CF nanocomposites with highly robustness, reusability and multifunction. Colloid Surf A. 2020;590:124533.
[266] Huang L, Zhang L, Song J, Wang X, Liu H. Superhydrophobic nickel-electroplated carbon fibers for versatile oil/water separation with excellent reusability and high environmental stability. ACS Appl Mater Interfaces. 2020;12:24390–402.
[267] Wu X, Luo Z, Lei Y, Wen B, Yang D. Hierarchical TiO_2 nanorod arrays/carbon nanofiber membranes for oil-in-water emulsion separation. Ind Eng Chem Res. 2020;59:21097–105.
[268] Chen Y, Xie A, Cui J, Lang J, Li C, Yan Y, et al. One-step facile fabrication of visible light driven antifouling carbon cloth fibers membrane for efficient oil–water separation. Sep Purif Technol. 2019;228:115769.
[269] Shen L, Qiu W, Wang W, Xiao G, Guo Q. Facile fabrication of superhydrophobic conductive graphite nanoplatelet/vapor-grown carbon fiber/polypropylene composite coatings. Comp Sci Technol. 2015;117:39–45.
[270] Li Y, Zhu X, Ge B, Men X, Li P, Zhang Z. Versatile fabrication of magnetic carbon fiber aerogel applied for bidirectional oil–water separation. Appl Phys A. 2015;120:949–57.
[271] Qu M, He J, Cao B. Facile fabrication of large-scale stable superhydrophobic surfaces with carbon sphere films by burning rapeseed oil. Appl Surf Sci. 2010;257:6–9.
[272] He J, Li H, Liu X, Qu M. Fabricating superamphiphobic surface with fluorosilane glued carbon nanospheres films. J Nanosci Nanotechnol. 2013;13:1974–9.
[273] Joula MH, Farbod M. Synthesis of uniform and size-controllable carbon nanospheres by a simple hydrothermal method and fabrication of carbon nanosphere super-hydrophobic surface. Appl Surf Sci. 2015;347:535–40.
[274] Kahradeh KH, Saievar-Iranizad E, Bayat A. Electrophoretically deposited carbon micro and nanospheres thin films as superhydrophobic coatings. Surf Coat Technol. 2017;319:318–25.
[275] Mittal N, Kumar R, Mishra G, Deva D, Sharma A. Mesoporous carbon nanocapsules based coatings with multifunctionalities. Adv Mater Interface. 2016;3:1500708.
[276] Mittal N, Deva D, Kumar R, Sharma A. Exceptionally robust and conductive superhydrophobic free-standing films of

mesoporous carbon nanocapsule/polymer composite for multifunctional applications. Carbon. 2015;93:492–501.
[277] Yang N, Luo ZX, Chen SC, Wu G, Wang YZ. Superhydrophobic magnetic hollow carbon microspheres with hierarchical micro/nano-structure for ultrafast and highly-efficient multitasking oil–water separation. Carbon. 2021;174:70–8.
[278] Cui W, Wang T, Yan A, Wang S. Superamphiphobic surfaces constructed by cross-linked hollow SiO_2 spheres. Appl Surf Sci. 2017;400:162–71.
[279] Li X, Wang N, He J, Yang Z, Zhao F, Wang K, et al. One-step preparation of highly durable superhydrophobic carbon nanothorn arrays. Small. 2020;16:1907013.
[280] Wu Y, Zhao M, Guo Z. Robust, heat-resistant and multifunctional superhydrophobic coating of carbon microflowers with molybdenum trioxide nanoparticles. J Colloid Interface Sci. 2017;506:649–58.
[281] Ghosh M, Rao GM. Synthesis of vertically aligned and tree-like carbon nanostructures. Carbon. 2018;133:239–48.
[282] Hu H, Gao L, Chen C, Chen Q. Low-cost, acid/alkaline-resistant, and fluorine-free superhydrophobic fabric coating from onionlike carbon microspheres converted from waste polyethylene terephthalate. Environ Sci Technol. 2014;48:2928–33.
[283] Zhou YB, Yang Y, Liu WM, Ye Q, He B, Zou YS, et al. Preparation of superhydrophobic nanodiamond and cubic boron nitride films. Appl Phys Lett. 2010;97:133110.
[284] Coffinier Y, Galopin E, Szunerits S, Boukherroub R. Preparation of superhydrophobic and oleophobic diamond nanograss array. J Mater Chem. 2010;20:10671–75.
[285] Marcon L, Addad A, Coffinier Y, Boukherroub R. Cell micropatterning on superhydrophobic diamond nanowires. Acta Biomater. 2013;9:4585–91.
[286] Yang Y, Li H, Cheng S, Zou G, Wang C, Lin Q. Robust diamond meshes with unique wettability properties. Chem Commun. 2014;50:2900–3.
[287] Wang Q, Bai J, Dai B, Yang Z, Guo S, Yang L, et al. Robust superhydrophobic diamond microspheres for no-loss transport of corrosive liquid microdroplets. Chem Commun. 2017;53:2355–8.
[288] Deshmukh S, Sankaran KJ, Banerjee D, Yeh CJ, Leou KC, Phase DM, et al. Direct synthesis of electrowettable nanostructured hybrid diamond. J Mater Chem A. 2019;7:19026–36.
[289] Lu F, Neal EA, Nakanishi T. Self-assembled and nonassembled alkylated-fullerene materials. Acc Chem Res. 2019;52:1834–43.
[290] Nakanishi T, Michinobu T, Yoshida K, Shirahata N, Ariga K, Mohwald H, et al. Nanocarbon superhydrophobic surfaces created from fullerene-based hierarchical supramolecular assemblies. Adv Mater. 2008;20:443–6.
[291] Yin G, Xue W, Chen F, Fan X. Self-repairing and superhydrophobic film of gold nanoparticles and fullerene pyridyl derivative based on the self-assembly approach. Colloid Surf A. 2009;340:121–5.
[292] Nakanishi T, Shen Y, Wang J, Li H, Fernandes P, Yoshida K, et al. Superstructures and superhydrophobic property in hierarchical organized architectures of fullerenes bearing long alkyl tails. J Mater Chem. 2010;20:1253–60.
[293] Wei L, Wu Y, Wang L, Fu H, Yao J. Supramolecular synthesis of fullerene/tetracene hybrid flowerlike microstructures of nanoplates via the charge-transfer interactions. J Phys Chem C. 2011;115:21629–34.
[294] Zheng S, Xu M, Lu X. Facile method toward hierarchical fullerene architectures with enhanced hydrophobicity and photoluminescence. ACS Appl Mater Interfaces. 2015;7:20285–91.
[295] Partheeban T, Sathish M. Selective growth of fullerene octahedra and flower-like particles by a liquid–liquid interfacial precipitation method for super-hydrophobic applications. RSC Adv. 2016;6:78791–4.
[296] Pérez-Ojeda ME, Wabra I, Böettcher C, Hirsch A. Fullerene building blocks with tailor-made solubility and new insights into their hierarchical self-assembly. Chem Europ J. 2018;24:14088–100.
[297] Stanmore BR, Brilhac JF, Gilot P. The oxidation of soot: a review of experiments, mechanisms and models. Carbon. 2001;39:2247–68.
[298] Kandjani AE, Sabri YM, Field MR, Coyle VE, Smith R, Bhargava SK. Candle-soot derived photoactive and superamphiphobic fractal titania electrode. Chem Mater. 2016;28:7919–27.
[299] Feng L, Yang Z, Zhai J, Song Y, Liu B, Ma Y, et al. Superhydrophobicity of nanostructured carbon films in a wide range of pH values. Angew Chem Int Ed. 2003;42:4217–20.
[300] Mansurov ZA, Nazhipkyzy M, Lesbayev BT, Prikhodko NG, Auyelkhankyzy M, Puri IK. Synthesis of superhydrophobic carbon surface during combustion propane. ECTJ. 2012;14:19–23.
[301] Mulay MR, Chauhan A, Patel S, Balakrishnan V, Halder A, Vaish R. Candle soot: journey from a pollutant to a functional material. Carbon. 2019;144:684–712.
[302] Sahoo BN, Kandasubramanian B. Photoluminescent carbon soot particles derived from controlled combustion of camphor for superhydrophobic applications. RSC Adv. 2014;4:11331–42.
[303] Sahoo BN, Kandasubramanian B. An experimental design for the investigation of water repellent property of candle soot particles. Mater Chem Phys. 2014;148:134–42.
[304] Esmeryan KE, Castano CE, Bressler AH, Abolghasemibizaki M, Mohammadi R. Rapid synthesis of inherently robust and stable superhydrophobic carbon soot coatings. Appl Surf Sci. 2016;369:341–7.
[305] Smagulova GT, Nazhipkyzy M, Lesbaev BT, Bakkara AE, Prikhod'ko NG, Mansurov ZA. Influence of the type of catalysts on the formation of a superhydrophobic carbon nanomaterial in hydrocarbon flames. J Eng Phys Thermophys. 2018;91:774–83.
[306] Boltaev GS, Ganeev RA, Reyimboyev S, Sobirov BR, Shermatov TY, Kutlimurotov BR, et al. Application of combustion flames for generation of third harmonic and superhydrophobiccoating of glasses by deposited carbon nanoparticle films. J Phys D Appl Phys. 2020;53:75301.
[307] Esmeryan KD, Castanob CE, Fedchenko YI, Mohammadi R, Miloushev IK, Temelkov KA. Adjustable optical transmittance of superhydrophobic carbon soot coatings by in-situ single-step control of their physicochemical profile. Colloid Surf A. 2019;567:325–33.
[308] Xu Y, Zhang G, Li L, Xu C, Lv X, Zhang H, et al. Icephobic behaviors of superhydrophobic amorphous carbon nanofilms synthesized from a flame process. J Colloid Interface Sci. 2019;552:613–21.

[309] Sharma CS, Abhishek K, Katepalli H, Sharma A. Biomimicked superhydrophobic polymeric and carbon surfaces. Ind Eng Chem Res. 2011;50:13012–20.
[310] Sahoo BN, Balasubramanian K. Facile synthesis of nano cauliflower and nano broccoli like hierarchical superhydrophobic composite coating using PVDF/carbon soot particles via gelation technique. J Colloid Interface Sci. 2014;436:111–21.
[311] Mishra P, Balasubramanian K. Nanostructured microporous polymer composite imprinted with superhydrophobic camphor soot, for emphatic oil–water separation. RSC Adv. 2014;4:53291–6.
[312] Esmeryan KD, Castano CE, Mohammadi R. Interactions of superhydrophobic carbon soot coatings with short alkyl chain alcohols and fluorocarbon solutions. Colloid Surf A. 2017;529:715–24.
[313] Sahoo BN, Nanda S, Kozinski JA, Mitra SK. PDMS/camphor soot composite coating: towards a self-healing and a self-cleaning superhydrophobic surface. RSC Adv. 2017;7:15027–40.
[314] Zulfiqar U, Hussain SZ, Subhani T, Hussain I, Rehman HU. Mechanically robust superhydrophobic coating from sawdust particles and carbon soot for oil/water separation. Colloid Surf A. 2018;539:391–8.
[315] Li J, Zhao Z, Kang R, Zhang Y, Lv W, Li M, et al. Robust superhydrophobic candle soot and silica composite sponges for efficient oil/water separation in corrosive and hot water. J Sol-Gel Sci Technol. 2017;82:817–26.
[316] Esmeryan KD, Castano CE, Chaushev TA, Mohammadi R, Vladkovad TG. Ag-doped superhydrophobic carbon soot coatings with enhanced wear resistance and anti-microbial performance. Colloid Surf A. 2019;582:123880.
[317] Sui J, Zhang Y, Ren S, Rinke M, Lu J, Jia J. Carbon coating with combined superhydrophobicand self-lubricating properties on titanium silicon carbide. Carbon. 2009;47:629–34.
[318] Lin Z, Liu Y, Wong CP. Facile fabrication of superhydrophobic octadecylamine-functionalized graphite oxide film. Langmuir. 2010;26:16110–4.
[319] Ostrovskaya LY, Ralchenko VG, Bolshakov AP, Saveliev AV, Dzbanovsky NN, Shmegera SV. Wettability of ultrananocrystalline diamond and graphite nanowalls films: a comparison with their single crystal analogs. J Nanosci Nanotechnol. 2009;9:3665–71.
[320] Nosonovsky M, Hejazi V, Nyong AE, Rohatgi PK. Metal matrix composites for sustainable lotus-effect surfaces. Langmuir. 2011;27:14419–24.
[321] Maruyama J, Maruyama S, Fukuhara T, Chashiro K, Uyama H. Ordered mesoporous structure by graphitized carbon nanowall assembly. Carbon. 2018;126:452–5.
[322] Schutzius TM, Bayer IS, Qin J, Waldroup D, Megaridis CM. Water-based, nonfluorinated dispersions for environmentally benign, large-area, superhydrophobic coatings. ACS Appl Mater Interfaces. 2013;5:13419–25.
[323] Sahoo BN, Balasubramanian K. A nanocellular PVDF-graphite water-repellent composite coating. RSC Adv. 2015;5:6743–51.
[324] Bay HH, Patino D, Mutlu Z, Romero P, Ozkan M, Ozkan CS. Scalable multifunctional ultra-thin graphite sponge: free-standing, superporous, superhydrophobic, oleophilic architecture with ferromagnetic properties for environmental cleaning. Sci Rep. 2016;6:21858.
[325] Li Z, Guo Z. Flexible 3D porous superhydrophobic composites for oil–water separation and organic solvent detection. Mater Des. 2020;196:109144.
[326] Boltaev GS, Khan SA, Ganeev RA, Kim VV, Iqbal M, Alnaser AS. Superhydrophobic and superhydrophilic properties of laser-ablated plane and curved surfaces. Appl Phys A. 2020;126:62.
[327] Beshkar F, Salavati-Niasari M, Amiri O. Superhydrophobic-superoleophilic copper-graphite/styrene-butadiene-styrene based cotton filter for efficient separation of oil derivatives from aqueous mixtures. Cellulose. 2020;27:4691–705.
[328] Gonzales J, Kurihara D, Maeda T, Yamazaki M, Saruhashi T, Kimura S, et al. Novel superhydrophobic surface with solar-absorptive material for improved de-icing performance. Materials. 2019;12:2758.
[329] Chen K, Gou W, Xu L, Zhao Y. Low cost and facile preparation of robust multifunctional coatings with self-healing superhydrophobicity and high conductivity. Compos Sci Technol. 2018;156:177–85.
[330] Sun Y, Cui H, Gong L, Wang J, Wang C. Triple phase boundary induced self-catalyzed growth of Ge-graphite core-shell nanowires: field electron emission and surface wettability. RSC Adv. 2015;5:39310–8.
[331] Zhang Y, Yang S, Wang S, Liu HK, Li L, Dou SX, et al. Engineering high-performance MoO_2-based nanomaterials with supercapacity and superhydrophobicity by tuning the raw materials source. Small. 2018;14:1800480.
[332] Cumont A, Zhang R, Corscadden L, Pan J, Zheng Y, Ye H. Characterisation and antibacterial investigation of a novel coating consisting of mushroom microstructures and HFCVD graphite. Mater Des. 2020;189:108498.
[333] Li RX, Wang Z, Liang SK. Superhydrophobic surface manufacture on pyrolytic carbon via electrostatic spinning method. Appl Mech Mater. 2013;423–426:391–4.
[334] Sansotera M, Navarrini W, Resnati G, Metrangolo P, Famulari A, Bianchi CL, et al. Preparation and characterization of superhydrophobic conductive fluorinated carbon blacks. Carbon. 2010;48:4382–90.
[335] Schutzius TM, Tiwari MK, Bayer IS, Megaridis CM. High strain sustaining, nitrile rubber based, large-area, superhydrophobic, nanostructured composite coatings. Compo A: Appl Sci Manuf. 2011;42:979–85.
[336] Wang W, Li Y, Li Y, Zhou M, Arotiba OA. Electro-Fenton and photoelectro-Fenton degradation of sulfamethazine using an active gas diffusion electrode without aeration. Chemosphere. 2020;250:126177.
[337] Paczosa-Bator B. Ion-selective electrodes with superhydrophobic polymer/carbon nanocomposites as solid contact. Carbon. 2015;95:879–87.
[338] Liu Y, Chen J, Guo D, Cao M, Jiang L. Floatable, self-cleaning, and carbon-black-based superhydrophobic gauze for the solar evaporation enhancement at the air-water interface. ACS Appl Mater Interfaces. 2015;7:13645–52.
[339] Jiao X, Li M, Cheng Z, Yu X, Yang S, Zhang Y. Recyclable superhydrophobic, antimoisture-activated carbon pellets for air and water purification. ACS Appl Mater Interfaces. 2020;12:25345–52.

[340] Sun H, Li A, Zhu Z, Liang W, Zhao X, La P, et al. Superhydrophobic activated carbon-coated sponges for separation and absorption. ChemSusChem. 2013;6:1057–62.
[341] Aljumaily MM, Alsaadi MA, Binti Hashim NW, Mjalli FS, Alsalhy QF, Khan AL, et al. Superhydrophobic nanocarbon-based membrane with antibacterial characteristics. Biotechnol Prog. 2020;36:e2963.
[342] Hu R, Jiang G, Wang X, Xi X, Wang R. Facile preparation of superhydrophobic surface with high adhesive forces based carbon/silica composite films. Bull Mater Sci. 2013;36:1091–5.
[343] Zhou Y, Song X, Yu M, Wang B, Yan H. Superhydrophobic surfaces prepared by plasma fluorination of lotus-leaf-like amorphous carbon films. Surf Rev Lett. 2006;13:117–22.
[344] Tian H, Yang T, Chen Y. Synthesis and characterization of carbon/silica superhydrophobic multi-layer films. Thin Solid Films. 2010;518:5183–7.
[345] Yan Q, Zhou S, Li Q, Liu J, Pu J. Superhydrophobic surface by SiO_2 particle modified SiO_2-Ni/a-C:H film deposition and superior corrosion protection. Surf Topo: Metrol Prop. 2019;7:014003.
[346] Zhou S, Zhu X, Yan Q, Wang S. Corrosion resistance and self-cleaning behaviour of Ni/a-C:H superhydrophobic films. Surf Eng. 2018;34:611–9.
[347] Zhou S, Zhu X, Yan Q. One-step electrochemical deposition to achieve superhydrophobic cobalt incorporated amorphous carbon-based film with self-cleaning and anti-corrosion. Surf Interface Anal. 2018;50:290–6.
[348] Dong S, Li B, Zhang J, Wang A. Superamphiphobic coatings with low sliding angles from attapulgite/carbon composites. Adv Mater Interface. 2018;5:1701520.
[349] Li Y, Gou L, Wang H, Wang Y, Zhang J, Li N, et al. Fluorine-free superhydrophobic carbon-based coatings on the concrete. Mater Lett. 2019;244:31–4.
[350] Conde JJ, Ferreira-Aparicio P, Chaparro AM. Anti-corrosion coating for metal surfaces based on superhydrophobic electrosprayed carbon layers. Appl Mater Today. 2018;13:100–6.
[351] Esmeryan KD, Radeva EI, Avramov ID. Durable superhydrophobic carbon soot coatings for sensor applications. J Phys D: Appl Phys. 2016;49:025309.
[352] Jing Z, Ding J, Zhang T, Yang D, Qiu F, Chen Q, et al. Flexible, versatility and superhydrophobic biomass carbon aerogels derived from corn bracts for efficient oil/water separation. Food Bioprod Process. 2019;115:134–42.
[353] Dai J, Zhang R, Ge W, Xie A, Chang Z, Tian S, et al. 3D macroscopic superhydrophobic magnetic porous carbon aerogel converted from biorenewable popcorn for selective oil–water separation. Mater Des. 2018;139:122–31.
[354] Yang J, Xu P, Xia Y, Chen B. Multifunctional carbon aerogels from typha orientalis for oil/water separation and simultaneous removal of oil-soluble pollutants. Cellulose. 2018;25:5863–75.
[355] Yang J, Chen Y, Xu P, Li Y, Jia X, Song H. Fabrication of compressible and underwater superoleophobic carbon/g-C_3N_4 aerogel for wastewater purification. Mater Lett. 2019;254:210–3.
[356] Xu P, Qian P, Yang J, Li J, Xia Y, Qian W, et al. Superhydrophobic and compressible carbon aerogels derived from platanus orientalis for oil absorption and emulsion separation. J Taiwan Inst Chem Eng. 2019;103:209–16.
[357] Wang N, Deng Z. Synthesis of magnetic, durable and superhydrophobic carbon sponges for oil/water separation. Mater Res Bull. 2019;115:19–26.
[358] Yuan D, Zhang T, Guo Q, Qiu F, Yang D, Ou Z. Superhydrophobic hierarchical biomass carbon aerogel assembled with TiO_2 nanorods for selective immiscible oil/water mixture and emulsion separation. Ind Eng Chem Res. 2018;57:14758–66.
[359] Wang Y, Zhang D, Deng J, Zhou F, Duan Z, Su Q, et al. Mosquito's compound eyes as inspiration for fabrication of conductive superhydrophobic nanocarbon materials from waste wheat straw. ACS Sust Chem Eng. 2019;7:3883–94.
[360] Cheng Y, He G, Barras A, Coffinier Y, Lu S, Xu W, et al. One-step immersion for fabrication of superhydrophobic/superoleophilic carbon felts with fire resistance: fast separation and removal of oil from water. Chem Eng J. 2018;331:372–82.
[361] Zhao Z, Qin S, Wang D, Pu Y, Wang JX, Saczekc J, et al. Multi-stimuli-responsive liquid marbles stabilized by superhydrophobic luminescent carbon dots for miniature reactors. Chem Eng J. 2020;391:123478.
[362] Pang S, Zhang Y, Su Q, Liu F, Xie X, Duan Z, et al. Superhydrophobic nickel/carbon core-shell nanocomposites for the hydrogen transfer reactions of nitrobenzene and N-heterocycles. Green Chem. 2020;22:1996–2010.
[363] Lei S, Zeng M, Huang D, Wang L, Zhang L, Xi B, et al. Synergistic high-flux oil–saltwater separation and membrane desalination with carbon quantum dots functionalized membrane. ACS Sust Chem Eng. 2019;7:13708–16.
[364] Wang Y, Wang L, Wang S, Wood RJK, Xue Q. From natural lotus leaf to highly hard-flexible diamond-like carbon surface with superhydrophobic and good tribological performance. Surf Coat Technol. 2012;206:2258–64.
[365] Jin YN, Yang HC, Huang H, Xu ZK. Underwater superoleophobic coatings fabricated from tannic acid-decorated CNTs. RSC Adv. 2015;5:16112–5.
[366] Machado MM, Lobo AO, Marciano FR, Corat EJ, Corat MAF. Analysis of cellular adhesion on superhydrophobic and superhydrophilic vertically aligned carbon nanotube scaffolds. Mater Sci Eng C. 2015;48:365–71.
[367] Gao X, Zhou J, Du R, Xie Z, Deng S, Liu R, et al. Robust superhydrophobic foam: a graphdiyne-based hierarchical architecture for oil/water separation. Adv Mater. 2016;28:168–73.
[368] Wang F, Zuo Z, Shang H, Zhao Y, Li Y. Ultrafastly interweaving graphdiyne nanochain on arbitrary substrates and its performance as a supercapacitor electrode. ACS Appl Mater Interfaces. 2019;11:2599–607.
[369] Cao N, Guo J, Cai K, Xue Q, Zhu L, Shao Q, et al. Functionalized carbon fiber felts with selective superwettability and fire retardancy: designed for efficient oil/water separation. Sep Purif Technol. 2020;251:117308.
[370] Watanabe H, Kondo H, Sekine M, Hiramatsu M, Hori M. Control of superhydrophobicity and super hydrophilic surfaces of carbon nanowalls using atmospheric pressure plasma treatments. Jap J Appl Phys. 2012;51:01AJ07.
[371] Chen W, Yan L, Bangal PR. Preparation of graphene by the rapid and mild thermal reduction of graphene oxide induced by MWs. Carbon. 2010;48:1146–52.

[372] Stankovich S, Dikin DA, Piner RD, Kohlhaas KA, Kleinhammes A, Jia Y, et al. Synthesis of graphene-based nanosheets via chemical reduction of exfoliated graphite oxide. Carbon. 2007;45:1558–65.
[373] Zhang Y, Guo L, Wei S, He Y, Xia H, Chen Q, et al. Direct imprinting of microcircuits on graphene oxides film by femtosecond laser reduction. Nano Today. 2010;5:15–20.
[374] Zhou Y, Bao Q, Varghese B, Tang LAL, Tan CK, Sow CH, et al. Microstructuring of graphene oxide nanosheets using direct laser writing. Adv Mater. 2010;22:67–71.
[375] Ye R, James DK, Tour JM. Laser-induced graphene. Acc Chem Res. 2018;51:1609–20.
[376] Trusovas R, Račiukaitis G, Niaura G, Barkauskas J, Pauliukaite GVR. Recent advances in laser utilization in the chemical modification of graphene oxide and its applications. Adv Opt Mater. 2016;4:37–65.
[377] Rafiee J, Rafiee MA, Yu ZZ, Koratkar N. A superhydrophobic to superhydrophilic wetting control in graphene films. Adv Mater. 2010;22:2151–4.
[378] Zhou Y, Xu F, Jiang G, Wang X, Hu R, Wang R, et al. Superhydrophobic and high adhesive performance of functionalized graphene films. Powder Technol. 2012;230:247–51.
[379] Shanmugharaj AM, Yoon JH, Yang WJ, Ryu SH. Synthesis, characterization, and surface wettability properties of amine functionalized graphene oxide films with varying amine chain lengths. J Colloid Interface Sci. 2013;401:148–54.
[380] Dong J, Yao Z, Yang T, Jiang L, Shen C. Control of superhydrophilic and superhydrophobic graphene interface. Sci Rep. 2013;3:1733.
[381] Gao JM, Song XF, Hu J, Guo SC, Fang L, Wu F, et al. Superhydrophobic graphenic carbon nanowalls fabricated by one-step PECVD. Mater Lett. 2016;184:273–7.
[382] Liu Y, Zhang J, Li S, Wang Y, Han Z, Ren L. Fabrication of superhydrophobic graphene surface with excellent mechanical abrasion and corrosion resistance on aluminum alloy substrate. RSC Adv. 2014;4:45389–96.
[383] Chen PY, Sodhi J, Qiu Y, Valentin TM, Steinberg RP, Wang Z, et al. Multiscale graphene topographies programmed by sequential mechanical deformation. Adv Mater. 2016;28:3564–71.
[384] Choi MK, Park I, Kim DC, Joh E, Park OK, Kim J, et al. Thermally controlled, patterned graphene transfer printing for transparent and wearable electronic/optoelectronic system. Adv Funct Mater. 2015;25:7109–18.
[385] Wang JN, Shao RQ, Zhang YL, Guo L, Jiang HB, Lu DX, et al. Biomimetic graphene Surfaces with superhydrophobicity and iridescence. Chem Asian J. 2012;7:301–4.
[386] Shi X, Li X, Jiang L, Qu L, Zhao Y, Ran P, et al. Femtosecond laser rapid fabrication of large-area rose-like micropatterns on freestanding flexible graphene films. Sci Rep. 2015;5:17557.
[387] Jiang HB, Zhang YL, Liu Y, Fu XY, Liu YF, Li CH, et al. Bioinspired few-layer graphene prepared by chemical vapor deposition on femtosecond laser-structured Cu foil. Laser Phot Rev. 2016;10:441–50.
[388] Li Y, Luong DX, Zhang J, Tarkunde YR, Kittrell C, Sargunaraj F, et al. Laser-induced graphene in controlled atmospheres: from superhydrophilic to superhydrophobic surfaces. Adv Mater. 2017;29:1700496.
[389] Das SR, Srinivasan S, Stromberg LR, He Q, Garland N, Straszheim WE, et al. Superhydrophobic inkjet printed flexible graphene circuits via direct-pulsed laser writing. Nanoscale. 2017;9:19058–65.
[390] Jiang HB, Liu YQ, Zhang YL, Liu Y, Fu XY, Han DD, et al. Reed leaf-inspired graphene films with anisotropic superhydrophobicity. ACS Appl Mater Interfaces. 2018;10:18416–25.
[391] Wu W, Liang R, Lu L, Wang W, Ran X, Yue D. Preparation of superhydrophobic laser-induced graphene using taro leaf structure as templates. Surf Coat Technol. 2020;393:125744.
[392] Hall LS, Hwang D, Chen B, Belle BV, Johnson ZT, Hondred JA, et al. All-graphene-based open fluidics for pumpless, small-scale fluid transport via laser-controlled wettability patterning. Nanoscale Horiz. 2021;6:24–32.
[393] Zhong H, Zhu Z, Lin J, Cheung CF, Lu VL, Yan F, et al. Reusable and recyclable graphene masks with outstanding superhydrophobic and photothermal performances. ACS Nano. 2020;14:6213–21.
[394] Nasser J, Lin J, Zhang L, Sodano HA. Laser induced graphene printing of spatially controlled super-hydrophobic/hydrophilic surfaces. Carbon. 2020;162:570–8.
[395] Li T, Cao Y, Xue W, Sun B, Zhu D. Self-assembly of graphene-based planar micro-supercapacitor with selective laser etching-induced superhydrophobic/superhydrophilic pattern. SN Appl Sci. 2020;2:206.
[396] Luong DX, Yang K, Yoon J, Singh SP, Wang T, Arnusch CJ, et al. Laser-induced graphene composites as multifunctional surfaces. ACS Nano. 2019;13:2579–86.
[397] Li X, Jiang C, Zhao F, Shao Y, Ying Y, Ping J. A self-charging device with bionic self-cleaning interface for energy harvesting. Nano Energy. 2020;73:104738.
[398] Zhong D, Yang Q, Guo L, Dou S, Liu K, Jiang L. Fusion of nacre, mussel, and lotus leaf: bio-inspired graphene composite paper with multifunctional integration. Nanoscale. 2013;5:5758–64.
[399] Ding G, Jiao W, Wang R, Niu Y, Hao L, Yang F, et al. A biomimetic, multifunctional, superhydrophobic graphene film with self-sensing and fast recovery properties for microdroplet transportation. J Mater Chem A. 2017;5:17325–34.
[400] Samanta S, Singh S, Sahoo RR. Effect of thermal annealing on the physico-chemical and tribological performance of hydrophobic alkylated graphene sheets. New J Chem. 2019;43:2624–39.
[401] Wu J, Li Z, Xie X, Tao K, Liu C, Khor KA, et al. 3D superhydrophobic reduced graphene oxide for activated NO2 sensing with enhanced immunity to humidity. J Mater Chem A. 2018;6:478–88.
[402] Li Z, Tang XZ, Zhu W, Thompson BC, Huang M, Yang J, et al. Single-step process toward achieving superhydrophobic reduced graphene oxide. ACS Appl Mater Interfaces. 2016;8:10985–94.
[403] Lin Z, Wang Z, Zhang X, Diao D. Superhydrophobic, photosterilize, and reusable mask based on graphene nanosheet-embedded carbon (GNEC) film. Nano Res. 2021;14:1110–5.
[404] Jiang HB, Zhang YL, Han DD, Xia H, Feng J, Chen QD, et al. Bioinspired fabrication of superhydrophobic graphene films by two-beam laser interference. Adv Funct Mater. 2014;24:4595–602.

[405] Yan ZX, Zhang YL, Wang W, Fu XY, Jiang HB, Liu YQ, et al. Superhydrophobic SERS substrates based on silver-coated reduced graphene oxide gratings prepared by two-beam laser interference. ACS Appl Mater Interfaces. 2015;7:27059–65.
[406] Tan Y, Hu B, Chu Z, Wu W. Bioinspired superhydrophobic papillae with tunable adhesive force and ultralarge liquid capacity for microdroplet manipulation. Adv Funct Mater. 2019;29:1900266.
[407] Wang P, Zhang D. Superhydrophobic film prepared with reduced graphene sheets and its application as corrosion barrier to copper. Appl Mech Mater. 2013;365–366:1100–5.
[408] Song J, Tan Y, Chu Z, Xiao M, Li G, Jiang Z, et al. Hierarchical reduced graphene oxide ridges for stretchable, wearable, and washable strain sensors. ACS Appl Mater Interfaces. 2019;11:1283–93.
[409] Yun X, Xiong Z, He Y, Wang X. Superhydrophobic lotus-leaf-like surface made from reduced graphene oxide through soft-lithographic duplication. RSC Adv. 2020;10:5478–86.
[410] Wang T, Zheng Y, Raji ARO, Li Y, Sikkema WKA, Tour JM. Passive anti-icing and active deicing films. ACS Appl Mater Interfaces. 2016;8:14169–73.
[411] Abbas R, Elkhoshkhany N, Hefnawy A, Ebrahim S, Rahal A. High stability performance of superhydrophobic modified fluorinated graphene films on copper alloy substrates. Adv Mater Sci Eng. 2017;2017:6197872.
[412] Kim GH, Jang H, Yoon JY, Jeong J, Park SY, Walker B, et al. Fluorine functionalized graphene nano platelets for highly stable inverted perovskite solar cells. Nano Lett. 2017;17:6385–90.
[413] Li H, Hou G, Tian Q, Bi S, Liu Z, Lin Y, et al. Preparation of fluorinated graphene oxide with different oxygen content and its superhydrophobic property. Mater Res Exp. 2019;6:045601.
[414] Zhang L, Zha D, Du T, Mei S, Shi Z, Jin Z. Formation of superhydrophobic microspheres of poly(vinylidene fluoride–hexafluoropropylene)/graphene composite via gelation. Langmuir. 2011;27:8943–9.
[415] Zhang L, Hu N, Yang C, Wei H, Yang Z, Wang Y, et al. Free-standing functional graphene reinforced carbon films with excellent mechanical properties and superhydrophobic characteristic. Comp A: Appl Sci Manuf. 2015;74:96–106.
[416] Geng Y, Li S, Hou D, Zhang W, Jin Z, Li Q, et al. Fabrication of superhydrophobicity on foamed concrete surface by GO/silane coating. Mater Lett. 2020;265:127423.
[417] Chu Z, Jiao W, Huang Y, Yan M, Zheng Y, Wang R, et al. Smart superhydrophobic films with self-sensing and anti-icing properties based on silica nanoparticles and graphene. Adv Mater Interfaces. 2020;7:2000492.
[418] Bharathidasan T, Narayanan TN, Sathyanaryanan S, Sreejakumari SS. Above 170° water contact angle and oleophobicity of fluorinated graphene oxide based transparent polymeric films. Carbon. 2015;84:207–13.
[419] Yan H, Zhou H, Ye Q, Wang X, Cho CM, Tan AYX, et al. Engineering polydimethylsiloxane with two-dimensional graphene oxide for an extremely durable superhydrophobic fabric coating. RSC Adv. 2016;6:66834–40.
[420] Wang P, Yao T, Sun B, Fan X, Dong S, Bai Y, et al. A cost-effective method for preparing mechanically stable anti-corrosive superhydrophobic coating based on electrochemically exfoliated graphene. Colloid Surf A. 2017;513:396–401.
[421] Song Y, Liu Y, Jiang H, Li S, Kaya C, Stegmaier T, et al. A bioinspired structured graphene surface with tunable wetting and high wearable properties for efficient fog collection. Nanoscale. 2018;10:16127–37.
[422] Mo ZH, Luo Z, Huang Q, Deng JP, Wu YX. Superhydrophobic hybrid membranes by grafting arc-like macromolecular bridges on graphene sheets: synthesis, characterization and properties. Appl Surf Sci. 2018;440:359–68.
[423] Saharudin KA, Karim MA, Sreekantan S. Preparation of a polydimethyl siloxane (PDMS)/graphene-based superhydrophobic coating. Mater Today Proc. 2019;17:752–60.
[424] Dinh Le TS, An J, Huang Y, Vo Q, Boonruangkan J, Tran T, et al. Ultrasensitive anti-interference voice recognition by bio-inspired skin-attachable self-cleaning acoustic sensors. ACS Nano. 2019;13:13293–303.
[425] Wang X, Jiao N, Tung S, Liu L. Photoresponsive graphene composite bilayer actuator for soft robots. ACS Appl Mater Interfaces. 2019;11:30290–9.
[426] Ding G, Jiao W, Wang R, Yan M, Chu Z, He X. Superhydrophobic heterogeneous graphene networks with controllable adhesion behavior for detecting multiple underwater motions. J Mater Chem A. 2019;7:17766–74.
[427] Xue Y, Liu Y, Lu F, Qu J, Chen H, Dai L. Functionalization of graphene oxide with polyhedral oligomeric silsesquioxane (POSS) for multifunctional applications. J Phys Chem Lett. 2012;3:1607–12.
[428] Das A, Maji K, Naskar S, Manna U. Facile optimization of hierarchical topography and chemistry on magnetically active graphene oxide nanosheets. Chem Sci. 2020;11:6556–66.
[429] Makowski T, Svyntkivska M, Piorkowska E, Mizerska U, Fortuniak W, Kowalczyk D, et al. Conductive and superhydrophobic cotton fabric through pentaerythritol tetrakis(3-(3,5-di-tert-butyl-4-hydroxyphenyl)propionate) assisted thermal reduction of graphene oxide and modification with methyltrichlorosilane. Cellulose. 2018;25:5377–88.
[430] Lin J, Cai X, Liu Z, Liu N, Xie M, Zhou BP, et al. Anti-liquid-interfering and bacterially antiadhesive strategy for highly stretchable and ultrasensitive strain sensors based on Cassie-Baxter wetting state. Adv Funct Mater. 2020;30:2000398.
[431] Lim CS, Kueh TC, Soh AK, Hung YM. Engineered superhydrophilicity and superhydrophobicity of graphene-nanoplatelet coatings via thermal treatment. Powder Technol. 2020;364:88–97.
[432] Ye TN, Feng WJ, Zhang B, Xu M, Lv LB, Su J, et al. Converting waste paper to multifunctional graphene-decorated carbon paper: from trash to treasure. J Mater Chem A. 2015;3:13926–32.
[433] Nagappan S, Ha CS. In-situ addition of graphene oxide for improving the thermal stability of superhydrophobic hybrid materials. Polymer. 2017;116:412–22.
[434] Wan S, Wan H, Bi H, Zhu J, He L, Yin K, et al. A surface transition of nanoparticle-decorated graphene films from water-adhesive to water-repellent. Nanoscale. 2018;10:17015–20.

[435] Lee JS, Yoon JC, Jang JH. A route towards superhydrophobic graphene surfaces: surface-treated reduced grapheneoxide spheres. J Mater Chem A. 2013;1:7312–5.
[436] Yang S, Chen L, Wang C, Rana M, Ma PC. Surface roughness induced superhydrophobicity of graphene foam for oil–water separation. J Colloid Interface Sci. 2017;508:254–62.
[437] Chu Z, Jiao W, Huang Y, Chen L, Zheng Y, Wang R, et al. Directional rebound control of droplets on low-temperature regular and irregular wrinkled superhydrophobic surfaces. Appl Surf Sci. 2020;530:147099.
[438] Vanithakumari SC, Jena G, Sofia S, Thinaharan C, George RP, Philip J. Fabrication of superhydrophobic titanium surfaces with superior antibacterial properties using graphene oxide and silanized silica nanoparticles. Surf Coat Technol. 2020;400:126074.
[439] Gao J, Li B, Huang X, Wang L, Lin L, Wang H, et al. Electrically conductive and fluorine free superhydrophobic strain sensors based on SiO_2/graphene-decorated electrospun nanofibers for human motion monitoring. Chem Eng J. 2019;373:298–306.
[440] Nine MJ, Cole MA, Johnson L, Tran DNH, Losic D. Robust superhydrophobic graphene-based composite coatings with self-cleaning and corrosion barrier properties. ACS Appl Mater Interfaces. 2015;7:28482–93.
[441] Bai ZG, Zhang B. Fabrication of a mechanically-stable anti-icing graphene oxide-diatomaceous earth/epoxy coating. Mater Res Express. 2019;6:085090.
[442] Wang P, Yao T, Li Z, Wei W, Xie Q, Duan W, et al. A superhydrophobic/electrothermal synergistically anti-icing strategy based on graphene composite. Sci Technol. 2020;198:108307.
[443] Chu Z, Jiao W, Huang Y, Ding G, Zhong X, Yan M, et al. FDTS-modified SiO_2/rGO wrinkled films with a micro-nanoscale hierarchical structure and anti-icing/deicing properties under condensation condition. Adv Mater Interface. 2020;7:1901446.
[444] Fan P, Chen J, Yang J, Chen F, Zhong M. GO@CuSilicate nanoneedle arrays hierarchical structure: a new route to prepare high optical transparent, excellent self-cleaning and anticorrosion superhydrophobic surface. J Nanoparticle Res. 2017;19:36.
[445] Selim MS, El-Safty SA, Abbas MA, Shenashen MA. Facile design of graphene oxide-ZnO nanorod-based ternary nanocomposite as a superhydrophobic and corrosion-barrier coating. Colloid Surf A. 2020;611:125793.
[446] Selim MS, El-Safty SA, Fatthallah NA, Shenashen MA. Silicone/graphene oxide sheet-alumina nanorod ternary composite for superhydrophobic antifouling coating. Prog Org Coat. 2018;121:160–72.
[447] Liu Y, Wang X, Fei B, Hu H, Lai C, Xin JH. Bioinspired, stimuli-responsive, multifunctional superhydrophobic surface with directional wetting, adhesion, and transport of water. Adv Funct Mater. 2015;25:5047–56.
[448] Li Q, Wang Y, Rong C, Zhang F, Liu Y, Chen L, et al. Facile assembly of graphene and titania on micro-structured substrates for superhydrophobic surfaces. Ceram Int A. 2016;42:2829–35.
[449] Naghdi S, Jaleh B, Shahbazi N. Reversible wettability conversion of electrodeposited graphene oxide/titania nanocomposite coating: Investigation of surface structures. Appl Surf Sci. 2016;368:409–16.
[450] Stan MS, Nica IC, Popa M, Chifiriuc MC, Iordache O, Dumitrescu I, et al. Reduced graphene oxide/TiO_2 nanocomposites coating of cotton fabrics with antibacterial and self-cleaning properties. J Ind Textile. 2018;49:277–93.
[451] Mirzadeh S, Asefnejad A, Khonakdar HA, Jafari SH. Improved surface properties in spray-coated PU/TiO_2/graphene hybrid nanocomposites through nonsolvent-induced phase separation. Surf Coat Technol. 2021;405:126507.
[452] Kang Y, Ju S. Superhydrophobic SnO_2 nanowire/graphene heterostructure-based ultraviolet detectors. J Vacuum Sci Technol B. 2020;38:062210.
[453] Huang Y, Jiao W, Chu Z, Wang S, Chen L, Nie X, et al. sensitivity, humidity-independent, flexible NO_2 and NH_3 gas sensors based on SnS_2 hybrid functional graphene ink. ACS Appl Mater Interfaces. 2020;12:997–1004.
[454] Wu M, An R, Yadav SK, Jiang X. Graphene tailored by Fe_3O_4 nanoparticles: low-adhesive and durable superhydrophobic coatings. RSC Adv. 2019;9:16235–45.
[455] Peng C, Wu R, Yang Y, Li C, Lin Y, Chen S, et al. Hydrothermal formation of controllable hexagonal holes and Er_2O_3/Er_2O_3-RGO particles on silicon wafers toward superhydrophobic surfaces. J Colloid Interface Sci. 2020;580:768–75.
[456] Ding S, Xiang T, Li C, Zheng S, Wang J, Zhang M, et al. Fabrication of self-cleaning super-hydrophobic nickel/graphene hybrid film with improved corrosion resistance on mild steel. Mater Des. 2017;117:280–8.
[457] Jena G, Thinaharan C, George RP, Philip J. Robust nickel-reduced graphene oxide-myristic acid superhydrophobic coating on carbon steel using electrochemical codeposition and its corrosion resistance. Surf Coat Technol. 2020;397:125942.
[458] Bai Z, Zhang B. Fabrication of superhydrophobic reduced-graphene oxide/nickel coating with mechanical durability, self-cleaning and anticorrosion performance. Nano Mater Sci. 2020;2:151–8.
[459] Zhu X, Zhou S, Yan Q. Ternary graphene/amorphous carbon/nickel nanocomposite film for outstanding superhydrophobicity. Chem Phys. 2018;505:19–25.
[460] Yan Q, Zhou S, Ma L, Wan S, Zhu X. Approach to excellent superhydrophobicity and corrosion resistance of carbon-based films by graphene and cobalt synergism. Surf Interface Anal. 2019;51:152–63.
[461] Kalgudi S, Pavithra GP, Prabhu KN, Koppad PG, Gowda CV. Effect of surface treatment on wetting behavior of copper. Mater Today: Proc. 2021;35:295–7.
[462] Xie H, Lai X, Li H, Gao J, Zeng X, Huang X, et al. A sandwich-like flame retardant nanocoating for supersensitive fire-warning. Chem Eng J. 2020;382:122929.
[463] Jayaramulu K, Datta KKR, Roesler C, Petr M, Otyepka M, Zboril R, et al. Biomimetic superhydrophobic/superoleophilic highly fluorinated graphene oxide and ZIF-8 composites for oil–water separation. Ang Chem Int Ed. 2016;55:1178–82.
[464] Zhan Y, He S, Hu J, Zhao S, Zeng G, Zhou M, et al. Robust super-hydrophobic/super-oleophilic sandwich-like UIO-66-F4@rGO composites for efficient and multitasking oil/water separation applications. J Hazardous Mater. 2020;388:121752.

[465] Zha D, Mei S, Wang Z, Li H, Shi Z, Jin Z. Superhydrophobic polyvinylidene fluoride/graphene porous materials. Carbon. 2011;49:5166–72.
[466] Wu J, Tao K, Miao J, Norford LK. Three-dimensional hierarchical and superhydrophobic graphene gas sensor with good immunity to humidity. 2018 IEEE micro electro mechanical systems; 21–25 January 2018, Belfast, UK. INSPEC Accession Number 17732966. doi: 10.1109/MEMSYS.2018.8346702.
[467] Choi BC, Park HS. Superhydrophobic graphene/nafion nanohybrid films with hierarchical roughness. J Phys Chem. 2012;116:3207–11.
[468] Stańczyk B, Góra K, Jach K, Dobrzanski L. Evaluation of hydrophobic properties of organic layers modified with graphene flakes. Materialy Elektroniczne. 2017;45:18–24.
[469] Shulga YM, Melezhik AV, Kabachkov EN, Milovich FO, Lyskov NV, Tkachev AG, et al. New approach to creating superhydrophobic surfaces. High Energy Chem. 2019;53:47–9.
[470] Moradi R, Karimi-Sabet J, Shariaty-Niassar M, Koochaki MA. Preparation and characterization of polyvinylidene fluoride/graphene superhydrophobic fibrous films. Polymers. 2015;7:1444–63.
[471] Wang H, Liu Z, Zhang X, Lv C, Yuan R, Zhu Y, et al. Durable self-healing superhydrophobic coating with biomimic "chloroplast" analogous structure. Adv Mater Interface. 2016;3:1600040.
[472] Wang Y, Yu Y, Hu X, Feng A, Jiang F, Song L. p-Phenylenediamine strengthened graphene oxide for the fabrication of superhydrophobic surface. Mater Des. 2017;127:22–9.
[473] Das A, Deka J, Rather AM, Bhunia BK, Saikia PP, Mandal BM, et al. Strategic formulation of graphene oxide sheets for flexible monoliths and robust polymeric coatings embedded with durable bioinspired wettability. ACS Appl Mater Interfaces. 2017;9:42354–65.
[474] Das A, Deka J, Raidongia K, Manna U. Robust and self-healable bulk-superhydrophobic polymeric coating. Chem Mater. 2017;29:8720–8.
[475] Hou TF, Shanmugasundaram A, Kim DS, Lee DW. Highly flexible superhydrophobic poly(urethane acrylate) film for applications requiring high optical transparency. Macromol Mater Eng. 2020;305:2000292.
[476] Wang P, Sun B, Liang Y, Han H, Fan X, Wang W, et al. A stretchable and super-robust graphene superhydrophobic composite for electromechanical sensor application. J Mater Chem A. 2018;6:10404–10.
[477] Wang Y, Zhou Z, Zhang J, Tang J, Wu P, Wang K, et al. Properties of graphene-thermoplastic polyurethane flexible conductive film. Coatings. 2020;10:400.
[478] Li B, Luo j, Huang X, Lin L, Wang L, Hu M, et al. A highly stretchable, super-hydrophobic strain sensor based on polydopamine and graphene reinforced nanofiber composite for human motion monitoring. Composites B: Eng. 2020;181:107580.
[479] Naderizadeh S, Athanassiou A, Bayer IS. Interfacing superhydrophobic silica nanoparticle films with graphene and thermoplastic polyurethane for wear/abrasion resistance. J Colloid Interface Sci. 2018;519:285–95.
[480] Guo KY, Wu Q, Mao M, Chen H, Zhang GD, Zhao L, et al. Water-based hybrid coatings toward mechanically flexible, super-hydrophobic and flame-retardant polyurethane foam nanocomposites with high-efficiency and reliable fire alarm response. Composites B: Eng. 2020;193:108017.
[481] Ye Y, Zhang D, Li J, Liu T, Pu J, Zhao H, et al. One-step synthesis of superhydrophobic polyhedral oligomeric silsesquioxane-graphene oxide and its application in anti-corrosion and anti-wear fields. Corros Sci. 2019;147:9–21.
[482] Liu Y, Xia XC, Zehri A, Ye L, Wang N, Zhmud B, et al. Surface modification of graphene for use as a structural fortifier in water-borne epoxy coatings. Coatings. 2019;9:754.
[483] Zhang X, Liu Z, Li Y, Wang C, Zhu Y, Wang H, et al. Robust superhydrophobic epoxy composite coating prepared by dual interfacial enhancement. Chem Eng J. 2019;371:276–85.
[484] Ye Y, Zhang D, Liu T, Liu Z, Liu W, Pu J, et al. Improvement of anticorrosion ability of epoxy matrix in simulate marine environment by filled with superhydrophobic POSS-GO nanosheets. J Hazardous Mater. 2019;364:244–55.
[485] Feng Y, Peng C, Li Y, Hu J, Deng Q, Wu Q, et al. Superhydrophobic nanocomposite coatings with photoinitiated three-dimensional networks based on reactive graphene nanosheet-induced self-wrinkling patterned surfaces. J Colloid Interface Sci. 2019;536:149–59.
[486] Lu S, Gao H, Wang Q, Xu W, Szunerits S, Boukherroub R. Fabrication of stable homogeneous superhydrophobic HDPE/graphene oxide surfaces on zinc substrates. RSC Adv. 2016;6:29823–9.
[487] Qiu L, Zhang R, Zhang Y, Li C, Zhang Q, Zhou Y. Superhydrophobic, mechanically flexible and recyclable reduced graphene oxide wrapped sponge for highly efficient oil/water separation. Front Chem Sci Eng. 2018;12:390–9.
[488] Ding G, Jiao W, Chen L, Yan M, Hao L, Wang R. A self-sensing, superhydrophobic, heterogeneous graphene network with controllable adhesion behavior. J Mater Chem A. 2018;6:16992–7000.
[489] Zhang Y, Liu Z, Chen A, Wang Q, Zhang J, Zhao C, et al. Fabrication of micro-/submicro-/nanostructured polypropylene/graphene superhydrophobic surfaces with extreme dynamic pressure resistance assisted by single hierarchically porous anodic Al oxide template. J Phys Chem C. 2020;124:6197–205.
[490] Bai Y. Research on hydrophobicity of graphene composites. AIP Conf Proc. 2017;1794:020008.
[491] Chen A, Ding S, Huang J, Zhang J, Dong Y, Fu X, et al. Fabrication of superrepellent microstructured polypropylene/graphene surfaces with enhanced wear resistance. J Mater Sci. 2019;54:3914–26.
[492] Asmatulu R, Ceylan M, Nuraje N. Study of superhydrophobic electrospun nanocomposite fibers for energy systems. Langmuir. 2011;27:504–7.
[493] Zhang P, Lv L, Liang Y, Li J, Cheng H, Zhao Y, et al. A versatile, superelastic polystyrene/graphene capsule-like framework. J Mater Chem A. 2016;4:10118–23.
[494] Uzoma PC, Liu F, Xu L, Zhang Z, Han EH, Ke W, et al. Superhydrophobicity, conductivity and anticorrosion of

robust siloxane-acrylic coatings modified with graphene nanosheets. Prog Org Coat. 2019;127:239–51.
[495] Das A, Sengupta S, Deka J, Rather AM, Raidongia K, Manna U. Synthesis of fish scale and lotus leaf mimicking, stretchable and durable multilayers. J Mater Chem A. 2018;6:15993–6002.
[496] Zhou SY, Yang B, Li Y, Gao XR, Ji X, Zhong GJ, et al. Realization of ultra-high barrier to water vapor by 3D-interconnection of super-hydrophobic graphene layers in polylactide films. J Mater Chem A. 2017;5:14377–86.
[497] Ghosh S, Nitin B, Remanan S, Bhattacharjee Y, Ghorai A, Dey T, et al. A multifunctional smart textile derived from merino wool/nylon polymer nanocomposites as next generation MW absorber and soft touch sensor. ACS Appl Mater Interface. 2020;12:17988–8001.
[498] Liu H, Li Q, Bu Y, Zhang N, Wang C, Pan C, et al. Stretchable conductive nonwoven fabrics with self-cleaning capability for tunable wearable strain sensor. Nano Energy. 2019;66:104143.
[499] Geng Y, Li Z, Zhao H, Chen M, Zhang L. Removal of entrained organic phase from raffinate in spent fuel reprocessing with graphene-based composites. J Radioanal Nucl Chem. 2020;323:1157–65.
[500] T, Sun, S, Hao, R, Fan, et al. MOF Constructs superhydrophobic MOF-rGO aerogel for efficient oil–water separation. ACS Appl Mater Interfaces. 2020;12:56435–44.
[501] Zare FD, Allahdadlalouni M, Baktash MY, Bagheri H. Reduced graphene oxide-melamine formaldehyde as a highly efficient platform for needle trap microextraction of volatile organic compounds. Microchem J. 2020;157:104932.
[502] Zhao Q, Yang W, Li Y, He Z, Li Z, Zhou Y, et al. Multifunctional phase change microcapsules based on graphene oxide Pickering emulsion for photothermal energy conversion and superhydrophobicity. Int J Energy Res. 2020;44:4464–74.
[503] Fang M, Tang Z, Lu H, Nutt S. Multifunctional superhydrophobic composite films from a synergistic self-organization process. J Mater Chem. 2012;22:109–14.
[504] Huang S, Ren L, Guo J, Zhu HT, Zhang C, Liu T. The preparation of graphene hybrid films decorated with poly[2-methoxy-5-(2′-ethyl-hexyloxy)-1,4-phenylene vinylene] particles prepared by non-solvent induced precipitation. Carbon. 2012;50:216–24.
[505] Zhao W, Hou Z, Yao Z, Zhuang X, Zhang F, Feng X. Hypercrosslinked porous polymer nanosheets: 2D RAFT agent directed emulsion polymerization for multifunctional applications. Polym Chem. 2015;6:7171–8.
[506] Mi HY, Jing X, Huang HX, Turng LS. Controlling superwettability by microstructure and surface energy manipulation on three-dimensional substrates for versatile gravity-driven oil/water separation. ACS Appl Mater Interface. 2017;9:37529–35.
[507] Nguyen DD, Tai NH, Lee SB, Kuo WS. Superhydrophobic and superoleophobic properties of graphene-based sponges fabricated using a facile dip coating method. Energy Environ Sci. 2012;5:7908–12.
[508] Fan ZL, Qin XJ, Sun HX, Zhu ZQ, Pei CJ, Liang WD, et al. Superhydrophobic mesoporous graphene for separation and absorption. ChemPlusChem. 2013;78:1282–7.
[509] Singh E, Chen Z, Houshmand F, Ren W, Peles Y, Cheng HM, et al. Superhydrophobic graphene foams. Small. 2013;9:75–80.
[510] Li B, Liu X, Zhang X, Chai W, Ma Y, Tao J. Facile preparation of graphene-coated polyurethane sponge with superhydrophobic/superoleophilic properties. J Polym Res. 2015;22:190.
[511] Lv LB, Cui TL, Zhang B, Wang HH, Li XH, Chen JS. Wrinkled graphene monoliths as superabsorbing building blocks for superhydrophobic and superhydrophilic surfaces. Angew Chem Int Ed. 2015;54:15165–9.
[512] Shiu RF, Lee CL, Hsieh PY, Chen CH, Kang YY, Chin WC, et al. Superhydrophobic graphene-based sponge as a novel sorbent for crude oil removal under various environmental conditions. Chemosphere. 2018;207:110–7.
[513] Zhang L, Li H, Lai X, Su X, Liang T, Zeng X. Thiolated graphene-based superhydrophobic sponges for oil–water separation. Chem Eng J. 2017;316:736–43.
[514] Xu Y, Wang G, Zhu L, Shen L, Zhang Z, Ren T, et al. Multifunctional superhydrophobic adsorbents by mixed-dimensional particles assembly for polymorphic and highly efficient oil–water separation. J Hazardous Mater. 2020;407:124374.
[515] Cai Y, Chen D, Li N, Xu Q, Li H, He J, et al. Self-healing graphene-reinforced composite for highly efficient oil/water separation. Langmuir. 2019;35:13950–7.
[516] Wang H, Wang C, Liu S, Chen L, Yang S. Superhydrophobic and superoleophilic graphene aerogel for adsorption of oil pollutants from water. RSC Adv. 2019;9:8569–74.
[517] Ding G, Jiao W, Wang R, Niu Y, Chen L, Hao L. Ultrafast, Reversible transition of superwettability of graphene network and controllable underwater oil adhesion for oil microdroplet transportation. Adv Funct Mater. 2018;28:1706686.
[518] Gu J, Fan H, Li C, Caro J, Meng H. Robust superhydrophobic/superoleophilic wrinkled microspherical MOF@rGO composites for efficient oil–water separation. Angew Chem Int Ed. 2019;58:5297–301.
[519] Nguyen DD, Hsieh PY, Tsai MT, Lee CY, Tai NH, To BD, et al. Hollow few-layer graphene-based structures from parafilm waste for flexible transparent supercapacitors and oil spill cleanup. ACS Appl Mater Interfaces. 2017;9:40645–54.
[520] Zhang T, Xiao C, Zhao J, Liu X, Ji D, Zhang H. One-step facile fabrication of PVDF/graphene composite nanofibrous membrane with enhanced oil affinity for highly efficient gravity-driven emulsified oil/water separation and selective oil absorption. Sep Purif Technol. 2021;254:117576.
[521] Lin Y, Ehlert GJ, Bukowsky C, Sodano HA. Superhydrophobic functionalized graphene aerogels. ACS Appl Mater Interfaces. 2011;3:2200–3.
[522] Hu H, Zhao Z, Wan W, Gogotsi Y, Qiu J. Polymer/graphene hybrid aerogel with high compressibility, conductivity, and “sticky” superhydrophobicity. ACS Appl Mater Interface. 2014;6:3242–9.
[523] Li R, Chen C, Li J, Xu L, Xiao G, Yan D. A facile approach to superhydrophobic and superoleophilic graphene/polymer aerogels. J Mater Chem A. 2014;2:3057–64.
[524] Xu L, Xiao G, Chen C, Li R, Mai Y, Sun G, et al. Superhydrophobic and superoleophilic graphene aerogel prepared by facile chemical reduction. J Mater Chem A. 2015;3:7498–504.
[525] Zhou S, Zhou X, Jiang W, Wang T, Zhang N, Lu Y, et al. 3-Mercaptopropyl)trimethoxysilane-assisted synthesis of

macro- and mesoporous graphene aerogels exhibiting robust superhydrophobicity and exceptional thermal stability. Ind Eng Chem Res. 2016;55:948–53.
[526] Ren RP, Li W, Lv YK. A robust, superhydrophobic graphene aerogel as a recyclable sorbent for oils and organic solvents at various temperatures. J Colloid Interface Sci. 2017;500:63–8.
[527] Shafiq YM, Cheong WK, Lau EV. Graphene aerogel – recovery of heavy crude oil from contaminated sand. J Environ Chem Eng. 2017;5:1711–7.
[528] Li L, Li B, Zhang J. Dopamine-mediated fabrication of ultralight graphene aerogels with low volume shrinkage. J Mater Chem A. 2016;4:512–8.
[529] Wang X, Nie S, Zhang P, Song L, Hu Y. Superhydrophobic and superoleophilic graphene aerogel for ultrafast removal of hazardous organics from water. J Mater Res Technol. 2020;9:667–74.
[530] Ha H, Shanmuganathan K, Ellison CJ. Mechanically stable thermally crosslinked poly(acrylic acid)/reduced graphene oxide aerogels. ACS Appl Mater Interfaces. 2015;7:6220–9.
[531] Mi HY, Jing X, Huang HX, Peng XF, Turng LS. Superhydrophobic graphene/cellulose/silica aerogel with hierarchical structure as superabsorbers for high efficiency selective oil absorption and recovery. Ind Eng Chem Res. 2018;57:1745–55.
[532] Zu G, Kanamori K, Nakanishi K, Huang J. Superhydrophobic ultraflexible triple-network graphene/polyorganosiloxane aerogels for a high-performance multifunctional temperature/strain/pressure sensing array. Chem Mater. 2019;31:6276–85.
[533] Geng Y, Li J, Li Z, Chen M, Zhao H, Zhang L. Facile preparation of 3D graphene-based/polyvinylidene fluoride composite for organic solvents capture in spent fuel reprocessing. J Porous Mater. 2019;26:1619–29.
[534] Yang S, Shen C, Chen L, Wang C, Rana M, Lv P. Vapor-liquid deposition strategy to prepare superhydrophobic and superoleophilic graphene aerogel for oil–water separation. ACS Appl Nano Mater. 2018;1:531–40.
[535] Qin W, Zhu W, Ma J, Yang Y, Tang B. Carbon fibers assisted 3D N-doped graphene aerogel on excellent adsorption capacity and mechanical property. Colloid Surf A. 2021;608:125602.
[536] Meng Y, Liu T, Yu S, Cheng Y, Lu J, Wang H. A lignin-based carbon aerogel enhanced by graphene oxide and application in oil/water separation. Fuel. 2020;278:118376.
[537] Wang J, Zhang W, Zhang C. Versatile fabrication of anisotropic and superhydrophobic aerogels for highly selective oil absorption. Carbon. 2019;155:16–24.
[538] Baskakov SA, Baskakova YV, Kabachkov EN, Dremova NN, Michtchenko A, Shulga YM. Novel superhydrophobic aerogel on the base of polytetrafluoroethylene. ACS Appl Mater Interfaces. 2019;11:32517–22.
[539] Baskakov SA, Baskakova YV, Kabachkov EN, Dremova NN, Lobach AS, Zakutina EA, et al. Superhydrophobic aerogel of polytetrafluoroethylene/graphene oxide composite. High Energy Chem. 2019;53:407–12.
[540] Volfkovich YM, Sosenkin VE, Mayorova NA, Rychagov AY, Baskakov SA, Kabachkov EN, et al. PTFE/rGO aerogels with both superhydrophobic and superhydrophilic properties for electroreduction of molecular oxygen. Energy Fuels. 2020;34:7573–81.
[541] Zu G, Kanamori K, Wang X, Nakanishi K, Shen J. Superelastic triple-network polyorganosiloxane-based aerogels as transparent thermal superinsulators and efficient separators. Chem Mater. 2020;32:1595–604.
[542] Wu J, Li H, Lai X, Chen Z, Zeng X. Conductive and superhydrophobic F-rGO@CNTs/chitosan aerogel for piezoresistive pressure sensor. Chem Eng J. 2020;386:123998.
[543] Wu S, Zou M, Shi X, Yuan Y, Bai W, Ding M, et al. Hydrophobic, structure-tunable Cu nanowire@graphene core-shell aerogels for piezoresistive pressure sensing. Adv Mater Technol. 2019;4:1900470.
[544] Zu G, Kanamori K, Nakanishi K, Lu X, Yu K, Huang J, et al. Superelastic multifunctional aminosilane-crosslinked graphene aerogels for high thermal insulation, three-component separation, and strain/pressure-sensing arrays. ACS Appl Mater Interface. 2019;11:43533–42.
[545] Xu Z, Zhou H, Tan S, Jiang X, Wu W, Shi J, et al. Ultralight super-hydrophobic carbon aerogels based on cellulose nanofibers/poly(vinyl alcohol)/graphene oxide (CNFs/PVA/GO) for highly effective oil–water separation. Beilstein J Nanotechnol. 2018;9:508–19.
[546] Ren X, Guo H, Ma X, Hou G, Chen L, Xu X, et al. Improved interfacial floatability of superhydrophobic and compressive S, N co-doped graphene aerogel by electrostatic spraying for highly efficient organic pollutants recovery from water. Appl Surf Sci. 2018;457:780–8.
[547] Lu Y, Wang H, Lu Y. An architectural exfoliated-graphene carbon aerogel with superhydrophobicity and efficient selectivity. Mater Des. 2019;184:108134.
[548] Valentin TM, Landauer AK, Morales LC, DuBois EM, Shukla S, Liu M, et al. Alginate-graphene oxide hydrogels with enhanced ionic tunability and chemomechanical stability for light-directed 3D printing. Carbon. 2019;143:447–56.
[549] Ge B, Zhang Z, Zhu X, Men X, Zhou X, Xue Q. A graphene coated cotton for oil/water separation. Comp Sci Technol. 2014;102:100–5.
[550] Shateri-Khalilabad M, Yazdanshenas ME. Preparation of superhydrophobic electroconductive graphene-coated cotton cellulose. Cellulose. 2013;20:963–72.
[551] Sun H, Zhu Z, Liang W, Yang B, Qin X, Zhao X, et al. Reduced graphene oxide-coated cottons for selective absorption of organic solvents and oils from water. RSC Adv. 2014;4:30587–91.
[552] Li X, Jiang T, Wang X, Zhang Z, Li Y, Gui J, et al. superhydrophobic graphene-decorated mesh gauze: recycling oils and organic solvents enhanced by large-diameter capillary action. Sci China Mater. 2016;59:581–8.
[553] Hoai NT, Sang NN, Hoang TD. Thermal reduction of graphene-oxide-coated cotton for oil and organic solvent removal. Mater Sci Eng B. 2017;216:10–5.
[554] Dashairya L, Rout M, Saha P. Reduced graphene oxide-coated cotton as an efficient absorbent in oil–water separation. Adv Compo Hybrid Mater. 2018;1:135–48.
[555] Guo G, Liu L, Zhang Q, Pan C, Zou Q. Solution-processable, durable, scalable, fluorine-grafted graphene-based superhydrophobic coating for highly efficient oil/water separation under harsh environment. New J Chem. 2018;42:3819–27.

[556] Liu S, Wang S, Wang H, Lv C, Miao Y, Chen L, et al. Gold nanoparticles modified graphene foam with superhydrophobicity and superoleophilicity for oil–water separation. Sci Total Environ. 2020;758:143660.
[557] Nabipour H, Wang X, Song L, Hu Y. Graphene oxide/zeolitic imidazolate frameworks-8 coating for cotton fabrics with highly flame retardant, self-cleaning and efficient oil/water separation performances. Mater Chem Phys. 2020;256:123656.
[558] Jiang G, Hu R, Wang X, Xi X, Wang R, Wei Z, et al. Preparation of superhydrophobic and superoleophilic polypropylene fibers with application in oil/water separation. J Textile Inst. 2013;104:790–7.
[559] Liao X, Li H, Zhang L, Su X, Lai X, Zeng X. Superhydrophobic mGO/PDMS hybrid coating on polyester fabric for oil/water separation. Prog Org Coat. 2018;115:172–80.
[560] Avila AF, Munhoz VC, de Oliveira AM, Santos MCG, Lacerda GRBS, Gonçalves CP. Nano-based systems for oil spills control and cleanup. J Hazardous Mater. 2014;272:20–7.
[561] Chen C, Li R, Xu L, Yan D. Three-dimensional superhydrophobic porous hybrid monoliths for effective removal of oil droplets from the surface of water. RSC Adv. 2014;4:17393–400.
[562] Wang Y, Wang B, Wang J, Ren Y, Xuan C, Liu C, et al. Superhydrophobic and superoleophilic porous reduced graphene oxide/polycarbonate monoliths for high-efficiency oil/water separation. J Hazardous Mater. 2018;344:849–56.
[563] Liu HD, Liu ZY, Yang MB, He Q. Surperhydrophobic polyurethane foam modified by graphene oxide. J App Polym Sci. 2013;130:3530–6.
[564] Liu Y, Zhou J, Zhu E, Tang J, Liu X, Tang W. Covalently intercalated graphene oxide for oil–water separation. Carbon. 2015;82:264–72.
[565] Liu C, Yang J, Tang Y, Yin L, Tang H, Li C. Versatile fabrication of the magnetic polymer-based graphene foam and applications for oil–water separation. Colloid Surf A. 2015;468:10–6.
[566] Li B, Liu X, Zhang X, Zou J, Chai W, Xu J. Oil-absorbent polyurethane sponge coated with KH-570-modified graphene. J Appl Polym Sci. 2015;132:41821.
[567] Rahmani Z, Samadi MT, Kazemi A, Rashidi AM, Rahmani AR. Nanoporous graphene and graphene oxide-coated polyurethane sponge as a highly efficient, superhydrophobic, and reusable oil spill absorbent. J Envir Chem Eng. 2017;5:5025–32.
[568] Xia C, Li Y, Fei T, Gong W. Facile one-pot synthesis of superhydrophobic reduced graphene oxide-coated polyurethane sponge at the presence of EtOH for oil–water separation. Chem Eng J. 2018;345:648–58.
[569] Luo Y, Jiang S, Xiao Q, Chen C, Li B. Highly reusable and superhydrophobic spongy graphene aerogels for efficient oil/water separation. Sci Rep. 2017;7:7162.
[570] Zhou S, Hao G, Zhou X, Jiang W, Wang T, Zhang N, et al. One-pot synthesis of robust superhydrophobic, functionalized graphene/polyurethane sponge for effective continuous oil–water separation. Chem Eng J. 2016;302:155–62.
[571] Oribayo O, Feng X, Rempel GL, Pan Q. Synthesis of lignin-based polyurethane/graphene oxide foam and its application as an absorbent for oil spill clean-ups and recovery. Chem Eng J. 2017;323:191–202.
[572] Cao N, Guo JY, Boukherroub R, Shao QG, Zang XB, Li J, et al. Robust superhydrophobic polyurethane sponge functionalized with perfluorinated graphene oxide for efficient immiscible oil/water mixture, stable emulsion separation and crude oil dehydration. Sci China Technol Sci. 2019;62:1585–95.
[573] Ma J, Zhu W, Lartey PO, Qin W. Ultra fast oil–water separation for different viscous oil using fluorine-free, reusable, superhydrophobic polyurethane sponge. J Nanosci Nanotechnol. 2020;20:1540–53.
[574] Jamsaz A, Goharshadi EK. Flame retardant, superhydrophobic, and superoleophilic reduced graphene oxide/orthoaminophenol polyurethane sponge for efficient oil/water separation. J Mol Liq. 2020;307:112979.
[575] Khalilifard M, Javadian S. Magnetic superhydrophobic polyurethane sponge loaded with Fe_3O_4@oleic acid@graphene oxide as high performance adsorbent oil from water. Chem Eng J. 2021;408:127369.
[576] Joy J, Abraham J, Sunny J, Mathew J, George SC. Hydrophobic, superabsorbing materials from reduced graphene oxide/MoS_2 polyurethane foam as a promising sorbent for oil and organic solvents. Polym Test. 2020;87:106429.
[577] Cai AJ, Yan XR, Liu J. Preparation of high-strength magnetically controlled superhydrophilic/oleophobic graphene-based sponges. AIP Adv. 2019;9:095032.
[578] Wei Q, Oribayo O, Feng X, Rempel GL, Pan Q. Synthesis of polyurethane foams loaded with TiO_2 nanoparticles and their Modification for enhanced performance in oil spill cleanup. Ind Eng Chem Res. 2018;57:8918–26.
[579] Cho EC, Hsiao YS, Lee KC, Huang JS. Few-layer graphene based sponge as a highly efficient, recyclable and selective sorbent for organic solvents and oils. RSC Adv. 2015;5:53741–48.
[580] Qin Y, Li S, Li Y, Pan F, Han L, Chen Z, et al. Mechanically robust polybenzoxazine/reduced graphene oxide wrapped-cellulose sponge towards highly efficient oil/water separation, and solar-driven for cleaning up crude oil, Comp. Sci Technol. 2020;197:108254.
[581] Liu T, Zhao G, Zhang W, Chi H, Hou C, Sun Y. The preparation of superhydrophobic graphene/melamine composite sponge applied in treatment of oil pollution. J Porous Mater. 2015;22:1573–80.
[582] Ren H, Shi X, Zhu J, Zhang Y, Bi Y, Zhang L. Facile synthesis of N-doped graphene aerogel and its application for organic solvent adsorption. J Mater Sci. 2016;51:6419–27.
[583] Zhu H, Chen D, An W, Li N, Xu Q, Li H, et al. A robust and cost-effective superhydrophobic graphene foam for efficient oil and organic solvent recovery. Small. 2015;11:5222–9.
[584] Song S, Yang H, Su C, Jiang Z, Lu Z. Ultrasonic-microwave assisted synthesis of stable reduced graphene oxide modified melamine foam with superhydrophobicity and high oil adsorption capacities. Chem Eng J. 2016;306:504–11.
[585] Liu W, Jiang H, Ru Y, Zhang X, Qiao J. Conductive graphene-melamine sponge prepared via MW irradiation. ACS Appl Mater Interfaces. 2018;10:24776–83.

[586] Ji C, Zhang K, Li L, Chen X, Hu J, Yan D, et al. High performance graphene-based foam fabricated by a facile approach for oil absorption. J Mater Chem A. 2017;5:11263–70.
[587] Han L, Bi H, Xie X, Su S, Mao P, Sun L. Superhydrophobic graphene-coated sponge with microcavities for high efficiency oil-in-water emulsion separation. Nanoscale. 2020;12:17812–20.
[588] Chen C, Zhu X, Chen B. Durable superhydrophobic/superoleophilic graphene-based foam for high-efficiency oil spill cleanups and recovery. Environ Sci Technol. 2019;53:1509–17.
[589] Zhang Z, Liu H, Qiao W. Reduced graphene-based superhydrophobic sponges modified by hexadecyltrimethoxysilane for oil adsorption. Colloid Surf A. 2020;589:124433.
[590] Lv X, Tian D, Peng Y, Li J, Jiang G. Superhydrophobic magnetic reduced graphene oxide-decorated foam for efficient and repeatable oil–water separation. Appl Surf Sci. 2019;466:937–45.
[591] Peng M, Chen G, Zeng G, Chen A, He K, Huang Z, et al. Superhydrophobic kaolinite modified graphene oxide-melamine sponge with excellent properties for oil–water separation. Appl Clay Sci. 2018;163:63–71.
[592] Saha P, Dashairya L. Reduced graphene oxide modified melamine formaldehyde (rGO@MF) superhydrophobic sponge for efficient oil–water separation. J Porous Mater. 2018;25:1475–88.
[593] Mirhosseinian NS, Anbia M, Salehi S. Preparation and characterization of superhydrophobic melamine and melamine-derived carbon sponges modified with reduced graphene oxide-TiO_2 nanocomposite as oil absorbent materials. J Mater Sci. 2020;55:1536–52.
[594] Pethsangave DA, Wadekar PW, Khose RV, Some S. Superhydrophobic carrageenan cross-linked graphene sponge for recovery of oil and organic solvent from their water mixtures. Polym Test. 2020;90:106743.
[595] Qiu L, Zhang R, Zhang Y, Li C, Zhang Q, Zhou Y. Superhydrophobic, mechanically flexible and recyclable reduced graphene oxide wrapped sponge for highly efficient oil/water separation. Front Chem Sci Eng. 2018;12:390–9.
[596] Zhang X, Wang C, Chai W, Liu X, Xu Y, Zhou S. Kapok fiber as a natural source for fabrication of oil absorbent. J Chem Technol Biotechnol. 2017;92:1613–9.
[597] Luo Z, Li D, Huang L, Tan S, Huang J. Flexible and superhydrophobic aerogel based on an interpenetrating network of konjac glucomannan and reduced graphene oxide for efficient water–oil separation. J Mater Sci. 2020;55:12884–96.
[598] Jaleh B, Shariati K, Khosravi M, Moradi A, Ghasemi S, Azizian S. Uniform and stable electrophoretic deposition of graphene oxide on steel mesh: Low temperature thermal treatment for switching from superhydrophilicity to superhydrophobicity. Colloid Surf A. 2019;577:323–32.
[599] Lu H, Sha S, Yang S, Wu J, Ma J, Hou C, et al. The coating and reduction of graphene oxide on meshes with inverse wettability for continuous water/oil separation. Appl Surf Sci. 2021;538:147948.
[600] Chen J, Li K, Zhang H, Liu J, Wu S, Fan Q, et al. Highly efficient and robust oil/water separation materials based on wire mesh coated by reduced graphene oxide. Langmuir. 2017;33:9590–7.
[601] Tang W, Sun D, Liu S, Li B, Sun W, Fu J, et al. One step electrochemical fabricating of the biomimetic graphene skins with superhydrophobicity and superoleophilicity for highly efficient oil–water separation. Sep Purif Technol. 2020;236:116293.
[602] Wang X, Han Z, Huang S. Fabrication of superhydrophobic surface on stainless steel meshes for oil–water separation. IOP Conf Ser: Mater Sci Eng. 2019;612:032136.
[603] Bao Z, Chen D, Li N, Xu Q, Li H, He J, et al. Superamphiphilic and underwater superoleophobic membrane for oil/water emulsion separation and organic dye degradation. J Membrane Sci. 2020;598:117804.
[604] Du J, Zhou C, Chen L, Cheng J, Pi P, Zuo J, et al. Gate-embedding strategy for pore size manipulation on stainless steel mesh: toward highly efficient water-in-oil nanoemulsions separation. Ind Eng Chem Res. 2019;58:15288–96.
[605] Yu ZP, Zhan B, Dong LM, Jiang W, Song YY, Hu SA. Self-healing structured graphene surface with reversible wettability for oil–water separation. ACS Appl Nano Mater. 2019;2:1505–15.
[606] Zhu H, Chen D, Li N, Xu Q, Li H, He J, et al. Dual-layer copper mesh for integrated oil–water separation and water purification. Appl Catal B. 2017;200:594–600.
[607] Liu YQ, Han DD, Jiao ZZ, Liu Y, Jiang HB, Wu XH, et al. Laser-structured Janus wire mesh for efficient oil–water separation. Nanoscale. 2017;9:17933–8.
[608] Bi Y, Han L, Zheng Y, Guan Y, Zhang H, Ge S, et al. Lotus-seedpod-bioinspired 3D superhydrophobic diatomite porous ceramics comodified by graphene and carbon nanobelts. ACS Appl Mater Interfaces. 2018;10:27416–23.
[609] Mai VC, Das P, Ronn G, Zhou J, Lim TT, Duan H. Hierarchical graphene/metal-organic framework composites with tailored wettability for separation of immiscible liquids. ACS Appl Mater Interfaces. 2020;12:35563–71.
[610] Yang S, Sha S, Lu H, Wu J, Ma J, Wang D, et al. Graphene oxide and reduced graphene oxide coated cotton fabrics with opposite wettability for continuous oil/water separation. Sep Purif Technol. 2021;259:118095.
[611] Gong T, Kim J, Woo JW, Jang JH, Lee SE, Han CS. Fabrics coated with hot-iron-treated graphene oxide for a self--cleaning and mechanically robust water-oil separation material. RSC Adv. 2017;7:25796–802.
[612] Cheng Y, Barras A, Lu S, Xu W, Szunerits S, Boukherroub R. Fabrication of superhydrophobic/superoleophilic functionalized reduced graphene oxide/polydopamine/PFDT membrane for efficient oil/water separation. Sep Purif Technol. 2020;236:116240.
[613] Ma W, Li Y, Zhang M, Gao S, Cui J, Huang C, et al. Biomimetic durable multifunctional self-cleaning nanofibrous membrane with outstanding oil/water separation, photodegradation of organic contaminants, and antibacterial performances. ACS Appl Mater Interface. 2020;12:34999–5010.
[614] Tittle CM, Yilman D, Pope MA, Backhouse CJ. Robust superhydrophobic laser-induced graphene for desalination applications. Adv Mater Technol. 2018;3:1700207.
[615] Liu W, Li M, Jiang H, Zhang X, Qiao J. High performance graphene-melamine sponge prepared via eco-friendly and cost-effective process. J Nanoparticle Res. 2019;21:36.

[616] Gontarek E, Macedonio F, Militano F, Giorno L, Lieder M, Politano A, et al. Adsorption-assisted transport of water vapour in super-hydrophobic membranes filled with multilayer graphene platelets. Nanoscale. 2019;11:11521–9.
[617] Zhang T, Xiao C, Zhao J, Cheng J, Chen K, Huang Y. Graphene-coated poly(ethylene terephthalate) nonwoven hollow tube for continuous and highly effective oil collection from the water surface. ACS Omega. 2019;4:7237–45.
[618] Liu D, Tai T, He Y. Solar heated graphene-melamine foam for absorbing oil and organic solvents. Energy Proc. 2019;158:490–6.
[619] Tabish TA, Memon FA, Gomez DE, Horsell DW, Zhang S. A facile synthesis of porous graphene for efficient water and wastewater treatment. Sci Rep. 2018;8:1817.
[620] Woo YC, Tijing LD, Shim WG, Choi JS, Kim SH, He T, et al. Water desalination using graphene-enhanced electrospun nanofiber membrane via air gap membrane distillation. J Membr Sci. 2016;520:99–110.
[621] Feng C, Yi Z, She F, Gao W, Peng Z, Garvey CJ, et al. Superhydrophobic and superoleophilic micro-wrinkled reduced graphene oxide as a highly portable and recyclable oil sorbent. ACS Appl Mater Interfaces. 2016;8:9977–85.
[622] Saji VS, Cook R. Corrosion control and prevention using nanomaterials. Cambridge: Woodhead Publishing, ISBN 1 84569 949 1; Elsevier Science, ISBN: 978-1-84569-949-9; 2012.
[623] Saji VS, Umoren SA. Corrosion inhibitors in the oil and gas industry. Weinheim, Germany: Wiley-VCH Verlag GmbH & Co. KGaA; 2020. ISBN 978-3-527-34618-9.
[624] Saji VS, Meroufel AA, Sorour AA. Corrosion and fouling control in desalination industry. Cham, Switzerland: Springer Nature; 2020. ISBN 978-3-030-34284-5.
[625] Saji VS, Lopatin SI. Molybdenum and its compounds – applications, electrochemical properties and geological implications. Nova Science Publishing; 2014. ISBN: 978-1-63321-210-7.
[626] Saji VS. Organic conversion coatings for magnesium and its alloys. J Ind Eng Chem. 2019;75:20–37.
[627] Saji VS. Review of rare-earth-based conversion coatings for magnesium and its alloys. J Mater Res Technol. 2019;8:5012–35.
[628] Saji VS. Supramolecular concepts and approaches in corrosion and biofouling prevention. Corro Rev. 2019;37:187–230.
[629] Saji VS. Progress in rust converters. Prog Org Coat. 2019;127:88–99.
[630] Saji VS. Rust preventives – a retrospective. Prog Org Coat. 2020;140:105511.
[631] Saji VS. Research advancements in sulfide scavengers. Rev Chem Eng. 2020. doi: 10.1515/revce-2019-0049.
[632] Saji VS. Photoelectrochemical cathodic protection in the dark: a review of nanocomposite and energy-storing photoanodes. J Electrochem Soc. 2020;167:121505.
[633] Saji VS. Contemporary developments in corrosion inhibitors – review of patents. Innov Corros Mater Sci. 2011;1:63–71.
[634] Arunima SR, Deepa MJ, Geethanjali CV, Saji VS, Shibli SMA. Tuning of hydrophobicity of WO_3-based hot-dip zinc coating with improved self-cleaning and anti-corrosion properties. Appl Surf Sci. 2020;527:146762.
[635] Wang H, Wang E, Liu Z, Gao D, Yuan R, Sun L, et al. A novel carbon nanotubes reinforced superhydrophobic and superoleophilic polyurethane sponge for selective oil–water separation through a chemical fabrication. J Mater Chem A. 2015;3:266–73.
[636] Liu Y, Peng Y, Zhang T, Qiu F, Yuan D. Superhydrophobic, ultralight and flexible biomass carbon aerogels derived from sisal fibers for highly efficient oil–water separation. Cellulose. 2018;25:3067–78.
[637] Cortese B, Caschera D, Federici F, Ingoc GM, Giglia G. Superhydrophobic fabrics for oil–water separation through a diamond like carbon (DLC) coating. J Mater Chem A. 2014;2:6781–9.
[638] Yang S, Chen L, Liu S, Hou W, Zhu J, Zhang Q, et al. Robust bifunctional compressed carbon foam for highly effective oil/water emulsion separation. ACS Appl Mater Interfaces. 2020;12:44952–60.
[639] Du L, Quan X, Fan X, Chen S, Yu H. Electro-responsive carbon membranes with reversible superhydrophobicity/superhydrophilicity switch for efficient oil/water separation. Sep Purif Technol. 2019;210:891–9.
[640] Song Y, Lang J, Guo J, Zhang Q, Han Q, Fan H, et al. Preparation of carbon cloth membrane with visible light induced self-cleaning performance for oil–water separation. Surf Coat Technol. 2020;403:126372.
[641] Tseng HH, Wu JC, Lin YC, Zhuang GL. Superoleophilic and superhydrophobic carbon membranes for high quantity and quality separation of trace water-in-oil emulsions. J Membr Sci. 2018;559:148–58.
[642] Cho E, Kim SH, Kim M, Park JS, Lee SJ. Super-hydrophobic and antimicrobial properties of Ag-PPFC nanocomposite thin films fabricated using a ternary carbon nanotube-Ag-PTFE composite sputtering target. Surf Coat Technol. 2019;370:18–23.
[643] Washe AP, Lozano-Sánchez P, Bejarano-Nosas D, Teixeira-Dias B, Katakis I. Electrochemically actuated passive stop–go microvalves for flow control in microfluidic systems. Microelectr Eng. 2013;111:416–20.
[644] Yan KK, Jiao L, Lin S, Ji X, Lu Y, Zhang L. Superhydrophobic electrospun nanofiber membrane coated by carbon nanotubes network for membrane distillation. Desalination. 2018;437:26–33.
[645] Aljumaily MM, Alsaadi MA, Hashim NA, Alsalhy QF, Mjalli FS, Atieh MA, et al. PVDF-co-HFP/superhydrophobic acetylene-based nanocarbon hybrid membrane for seawater desalination via DCMD. Chem Eng Res Design. 2018;138:248–59.
[646] Huang XH, Li B, Wang L, Lai X, Xue H, Gao J. Superhydrophilic, underwater superoleophobic, and highly stretchable humidity and chemical vapor sensors for human breath detection. ACS Appl Mater Interfaces. 2019;11:24533–43.
[647] Zhao Q, An J, Wang S, Qiao Y, Liao C, Wang C, et al. Superhydrophobic air-breathing cathode for efficient hydrogen peroxide generation through two-electron pathway oxygen reduction reaction. ACS Appl Mater Interface. 2019;11:35410–9.
[648] Shen Y, Reparaz JS, Wagner MR, Hoffmann A, Thomsen C, Lee JO, et al. Assembly of carbon nanotubes and alkylated fullerenes: nanocarbon hybrid towards photovoltaic applications. Chem Sci. 2011;2:2243–50.
[649] Su Y, Kravets VG, Wong SL, Waters J, Geim AK, Nair RR. Impermeable barrier films and protective coatings based on reduced graphene oxide. Nat Commun. 2014;5:4843.

[650] Schriver M, Regan W, Gannett WJ, Zaniewski AM, Crommie MF, Zettl A. Graphene as a long-term metal oxidation barrier: worse than nothing. ACS Nano. 2013;7:5763–8.
[651] Hsieh YP, Hofmann M, Chang KW, Jhu JG, Li YY, Chen KY, et al. Complete corrosion inhibition through graphene defect passivation. ACS Nano. 2014;8:443–8.
[652] Nine MJ, Cole MA, Tran DNH, Losic D. Graphene: a multipurpose material for protective coatings. J Mater Chem A. 2015;3:12580–602.
[653] Cui G, Bi Z, Zhang R, Liu J, Yu X, Li Z. A comprehensive review on graphene-based anti-corrosive coatings. Chem Eng J. 2019;373:104–21.
[654] Saji VS. Electrodeposition in bulk metallic glasses. Materialia. 2018;3:1–11.
[655] Yang Z, Wang L, Sun W, Li S, Zhu T, Liu W, et al. Superhydrophobic epoxy coating modified by fluorographene used for anti-corrosion and self-cleaning. Appl Surf Sci. 2017;401:146–55.
[656] Xing LB, Hou SF, Zhang JL, Zhou J, Li Z, Si W, et al. Nitrogen-doped graphene aerogels with 3D architectures for multifunctional applications in supercapacitor and absorption. J Nanosci Nanotechnol. 2016;16:8451–9.
[657] Chen M, Li Z, Geng Y, Zhao H, He S, Chen A, et al. A modular process for the treatment of high level liquid waste (HLLW) using solvent-impregnated graphene aerogel. Hydrometallurgy. 2018;179:167–74.
[658] Cao N, Lyu Q, Li J, Wang Y, Yang B, Szunerits S, et al. Facile synthesis of fluorinated polydopamine/chitosan/reduced graphene oxide composite aerogel for efficient oil/water separation. Chem Eng J. 2017;326:17–28.
[659] Chen M, Li Z, Geng Y, Zhao H, He S, Li Q, et al. Adsorption behavior of thorium on N,N,N',N'-tetraoctyldiglycolamide (TODGA) impregnated graphene aerogel. Talanta. 2018;181:311–7.
[660] Li X, Jiang T, Wang X, Zhang Z, Li Y, Gui J, et al. Superhydrophobic graphene-decorated mesh gauze: recycling oils and organic solvents enhanced by large-diameter capillary action. Sci China Mater. 2016;59:581–8.
[661] Mao J, Ge M, Huang J, Lai Y, Lin C, Zhang K, et al. Constructing multifunctional MOF@rGO hydro-/aerogels by the self-assembly process for customized water remediation. J Mater Chem A. 2017;5:11873–81.
[662] Zhang R, Cao J, Liu Y, Guan J, He M, Jiang Z. Metal-organic framework-intercalated graphene oxide membranes for highly efficient oil/water separation. Ind Eng Chem Res. 2020;59:16762–71.
[663] Zheng Y, Zheng S, Xue H, Pang H. Metal-organic frameworks/graphene-based materials: preparations and applications. Adv Funct Mater. 2018;28:1804950.
[664] Mi HY, Jing X, Politowicz AL, Chen E, Huang HX, Turng LS. Highly compressible ultra-light anisotropic cellulose/graphene aerogel fabricated by bidirectional freeze drying for selective oil absorption. Carbon. 2018;132:199–209.
[665] Xiao J, Lv W, Song Y, Zheng Q. Graphene/nanofiber aerogels: performance regulation towards multiple applications in dye adsorption and oil/water separation. Chem Eng J. 2018;338:202–10.
[666] Long S, Feng Y, He F, He S, Hong H, Yang X, et al. An ultralight, supercompressible, superhydrophobic and multifunctional carbon aerogel with a specially designed structure. Carbon. 2020;158:137–45.
[667] Yan T, Meng H, Hu W, Jiao F. Superhydrophilicity and underwater superoleophobicity graphene oxide-micro crystalline cellulose complex-based mesh applied for efficient oil/water separation. Desalin Water Treat. 2018;111:155–64.
[668] Podila R, Moore T, Alexis F, Rao AM. Graphene coatings for enhanced hemo-compatibility of nitinol stents. RSC Adv. 2013;3:1660–5.
[669] Li J, Wang G, Geng H, Zhu H, Zhang M, Di Z, et al. CVD growth of graphene on NiTi alloy for enhanced biological activity. ACS Appl Mater Interfaces. 2015;7:19876–81.
[670] Akhtar N, Anemone G, Farias D, Holst B. Fluorinated graphene provides long lasting ice inhibition in high humidity. Carbon. 2019;141:451–6.
[671] Wang Y, Guo Y, Guo W. Screening effect of monolayer van der Waals crystals on surface deicing: a molecular simulation study. Phys Chem Chem Phys. 2020;22:27873–81.
[672] Wang WT, Lu LS, Xie YX, Li ZH, Wu WB, Liang RX, et al. One-step laser induced conversion of a gelatin-coated polyimide film into graphene: tunable morphology, surface wettability and microsupercapacitor applications. Sci China: Technol Sci. 2021;64:1030–40.
[673] Qian H, Zhu M, Song H, Wang H, Liu Z, Wang C. Anti-scaling of superhydrophobic poly(vinylidene fluoride) composite coating: tackling effect of carbon nanotubes. Prog Org Coat. 2020;142:105566.
[674] Li G, Hong G, Dong D, Song W, Zhang X. Multiresponsive graphene-aerogel-directed phase-change smart fibers. Adv Mater. 2018;30:1801754.